CLEAN WATER WATER POLLUTION CONTROL RESEARCH SERIES • 15040 EJZ 12/70

Selective Withdrawal From A Stratified Reservoir

ENVIRONMENTAL PROTECTION AGENCY • WATER QUALITY OFFICE

WATER POLLUTION CONTROL RESEARCH SERIES

The Water Pollution Control Research Reports describe the results and progress in the control and abatement of pollution in our Nation's waters. They provide a central source of information on the research, development, and demonstration activities in the Environmental Protection Agency, Water Quality Office, through inhouse research and grants and contracts with Federal, State, and local agencies, research institutions, and industrial organizations.

A tripilicate abstract card sheet is included in the report to facilitate information retrieval. Space is provided on the card for the user's accession number and for additional uniterms.

Inquiries pertaining to Water Pollution Control Research Reports should be directed to the Head, Project Reports System, Office of Research and Development, Environmental Protection Agency, Water Quality Office, Washington, D. C. 20242.

Selective Withdrawal From A Stratified Reservoir

by

Jorg Imberger
and
Hugo B. Fischer

University of California
Berkeley, California 94720

for the

Environmental Protection Agency

Project Number 15040 E J Z

December 1970

For sale by the Superintendent of Documents, U.S. Government Printing Office
Washington, D.C., 20402 - Price $1

EPA Review Notice

This report has been reviewed by the Environmental Protection Agency and approved for publication. Approval does not signify that the contents necessarily reflect the views and policies of the Environmental Protection Agency, nor does mention of trade names or commercial products consitute endorsement or recommendation for use.

ABSTRACT

This study describes both theoretically and experimentally the flow into a line sink in a linearly density stratified reservoir. The geometry of the boundaries is simplified to a parallel walled duct with the line sink at the center of the fluid. The primary focus is on partitioning the flow into distinct flow regimes, and predicting the withdrawal layer thickness as a function of the distance from the sink.

For fluids with a Schmidt number of order unity, the withdrawal layer is shown to be composed of distinct regions in each of which a definite force balance prevails. The outer flow, where inertia forces are neglected, changes from a parallel uniform flow upstream to a symmetric self similar withdrawal layer near the sink. Inertia becomes a force of equal importance to buoyancy and viscosity for distances from the sink smaller than $x_c = (q/\nu)^{3/2}(\nu D/\varepsilon g)^{1/4}$. When viewed from the outer coordinates, this is a small distance, but in physical terms it may be equal to, or longer than, the length of the reservoir, depending on the sink discharge. The equations valid in this inner region, and which have solutions capable of being matched to the outer flow, are derived. Using the inner limit of the outer flow as the upstream boundary condition, these inner equations are approximately solved for the withdrawal layer thickness by an integral method. The inner and outer variations of δ , the withdrawal layer thickness, are combined to yield a composite solution, and it is seen that inclusion of the inertia forces yields layers thicker than a strict buoyancy-viscous force balance. Also in terms of the inner variables, the equations, their solutions and any experimental data are shown to be dependent only on the Schmidt number.

Experimental laboratory experiments were carried out to verify the conclusions reached from the theoretical considerations. The observed withdrawal layer thicknesses were shown to be closely predicted by the integral solution. Furthermore, the data could be represented in terms of the inner variables by a single curve verifying the independence of any parameter other than the Schmidt number.

Prototype data is still sparse, but comparison with the measurements made by the Tennessee Valley Authority indicates that in a reservoir the withdrawal layers are approximately one and a half times as large as predicted. The difference in thickness is probably explained by the presence of a certain amount of turbulence in the reservoir, and interference by the rear boundary of the reservoir.

This report was submitted in fulfillment of Grant No. 15040 E.J.Z. between the Environmental Protection Agency and the University of California, Berkeley.

CONTENTS

FIGURES

TABLES

CONCLUSIONS

The long term objective of this research is to provide an operational technique for managing the quality of reservoir outflow. This objective requires a complete understanding of the details of stratified flow and mixing in a prototype reservoir. In recent years a number of bulk management schemes have been devised and tested. These schemes are encouraging, but their predictions are usually restricted to the reservoir for which they have been calibrated. This failing is predominantly due to their primitive description of the reservoir mechanics.

The present report describes a detailed mathematical and experimental investigation of one aspect of the management problem, the withdrawal layer which forms at the level of the exit.

The following summarizes the conclusions drawn from a critical study of previous work and the conclusions derived from the present study.

Prior Knowledge

Previous work on the steady flow problem may be divided into the following two categories:

(i) The fluid is inviscid and the upstream boundary condition is given by $\rho_T U^2$ = constant. The layers corresponding to this class have been designated as type (b) in Chapter 2; or

(ii) The inertia forces are completely neglected and the fluid is assumed to be of infinite extent. The layers corresponding to this class have been designated as type (c) in Chapter 2.

The weakness of the solutions of class (i), when applied to reservoir flow, is that in a reservoir the upstream condition is supplied by a solution of type (c) or by a solid vertical or sloping wall, and not by the rather special constant head condition $\rho_T U^2$ = constant. It is therefore not clear where and how well this solution approximates the flow.

The solutions of class (ii) have generally been thought to be valid at large distances from the sink. In Section 2 it is shown, however, that both the diffusive and non-diffusive solutions corresponding to this class have a physically unrealistic behavior at infinity. In both cases the work done on the fluid at infinity by the pressure anomaly is infinite. Furthermore, the validity of neglecting the inertia terms in any part of the reservoir must be established.

Both classes of solution yield withdrawal layer thicknesses much smaller than obtained from experimental or prototype observations.

Koh's (1966a) analysis may be used to estimate the time taken for steady withdrawal layer to form. In Section 6 a comparison with some prototype data showed that this yields good results.

Contributions of the Present Study to the Unsteady Problem

The solution by Koh (1966a) predicts, as mentioned above, times for the development of a withdrawal layer which are in good agreement with prototype and experimental observations. However, the method of solution involved a non-uniformity for small times and for large distances from the sink, the effects of which were uncertain. This inconsistency in the method of solution was removed by:

(a) considering flow confined in a duct of finite depth,

(b) by not making the Boussinesq assumption, but leaving the domain infinite.

In both cases the time taken for the flow to reach a thickness δ_s was the same as predicted by Koh (1966a) and is given by

$$t = \frac{\pi}{\sqrt{\epsilon g}} \frac{x}{\delta_s} .$$

Contributions of the Present Study for the Steady Withdrawal Layer

The withdrawal layer in a duct was analyzed and partitioned into different flow regions. Each region is characterized by a particular force balance summarized in Fig. 3.6. By matching the region where inertia may be neglected to the thin layer zone nearer the sink, a form of non-dimensionalization was derived, which leaves the layer dynamics dependent only on a single parameter - the square root G of the Schmidt number. The magnitude of the withdrawal layer thickness, determined by an integral method applied to the dimensionless equations, and the observation that G is the only parameter remaining when the flow is viewed from the dimensionless coordinates, was in good agreement with experimental data.

(a) Flow Regions: In Section 3 a partial answer has been found to the intricacies of the flow structure of the withdrawal layer for Schmidt numbers of order unity. The limit used to derive the structure shown in Fig. 3.6 was that the Froude number and the Rayleigh number tend to zero, but the Reynolds number q/ν tends to infinity. The outer flow, where inertia forces are neglected, changes from a parallel uniform flow upstream to a symmetric withdrawal layer near the sink. In the limit of zero x, the outer flow pattern asymptotes to the similarity solution found by Koh (1966b) for a withdrawal layer in a fluid of infinite extent. Thus, even though the problem in an infinite domain, considered by Koh (1966b), is not well set, its solution approximates the correct solution

in a region near the sink, but sufficiently far away to avoid the influence of inertia.

Inertia is shown to become a force of equal importance to buoyancy and viscosity for distances from the sink, smaller than

$$x_c = \left(\frac{q}{\nu}\right)^{3/2} \left(\frac{\nu D}{\varepsilon g}\right)^{1/4}.$$

This is referred to as the inner region. When the flow reaches a distance of Order $(q/\sqrt{\varepsilon g})$ from the sink, an inviscid core of thickness of $O(q/\sqrt{\varepsilon g})$ forms. To be able to meet the edge boundary conditions it is probable that a further zone, consisting of a buoyancy-viscous force balance, forms at the perimeter of the inviscid core.

(b) Integral Solution: The equations valid in the inner region, and which have solutions capable of being matched to the outer flow, are derived in Section 3. Using the inner limit of the outer flow as the upstream boundary condition, these inner equations were approximately solved for the withdrawal layer thickness by an integral method. The inner and outer variations of δ, the withdrawal layer thickness, were then combined to yield a composite solution. This is shown graphically for different Froude and Schmidt numbers in Figs. 3.7 and 3.8.

(c) G as a parameter: When the outer region was matched to the inner region it was noticed that the inner equations, in terms of the inner stretched variables $(x/x_c, z/F_m^{\frac{1}{2}})$, were only dependent on the parameter G. Hence any experimental data, or solution of these equations, when represented in terms of the stretched variables will depend only on G. So far, G has been assumed to be of order unity. The flow structure, developed for Schmidt number of order unity could, however, be quite different when the Schmidt number is large. Extra regions in which viscosity is important, but diffusion is not, would be introduced. The new domains would, however, be governed by equations which are special cases of the present inner equations. Hence even if G is not of order unity, the conclusion that the flow, in terms of the inner variables, is only dependent on the parameter G, is still valid. The integral solution and any experimental withdrawal layer thicknesses may therefore quite generally be represented non-dimensionally with G being the only remaining parameter.

(d) Physical properties of water: If s(z) is the variation with depth of the concentration of a dissolved substance, for example O_2, then the outlet concentration will be given by the weighted mean over the depth of the hypolimnion;

$$\frac{1}{q}\int_{-\ell}^{\ell} u(z)\, s(z)\, dz$$

If the reservoir is long enough, so that the outer region is well established in the upper reaches of the reservoir, then this simplifies to

$$\frac{1}{2\ell}\int_{-\ell}^{\ell} s(z)\, dz \ .$$

(e) Comparison with experimental data: Fig. 5.1 shows the experimental variation of δ/F_m^2 with $(x/x_c)^{1/3}$. The scatter in the data is small, indicating the independence of the results from any parameter other than G. Comparison with the integral curve is good everywhere except near the sink. The assumption that the velocity profile is self similar, made in the integral method, is verified in Fig. 5.2. Koh (1966b) had noticed this similarity for each individual discharge q, but this is now seen to be true more generally in terms of the inner coordinates. The data in Fig. 5.2 shows that the velocity profile remained self similar, except for small changes in the back flow, for a variation of (x/x_c) from 0.008 to 64.

(f) Comparison with prototype data: The available prototype data are reproduced in Fig. 6.1. Included are the composite integral solution, the linear solution, and the withdrawal layer thickness obtained from the inviscid model. It is seen that the integral solution is an improvement over the other two, especially as x/x_c increases, but the increase in the withdrawal layer thickness, gained by the inclusion of the inertia terms, is still not sufficient to fully explain the observed prototype values of δ .

It is further noteworthy that in the prototype studies the value of x_c , when based on molecular transport coefficients, is usually greater than the length of the reservoir. With eddy transport coefficients which have been adjusted so that the T.V.A. (1969(a),(b)) data fits the integral solution, x_c becomes roughly equal to the length of a typical reservoir. This means that the flow in the reservoir, in either case, is predominantly characterized by the inner solution and that insufficient length is available for the outer solution, to which Koh's (1966b) solution is an approximation, to form. Of course, the inner solution depends on the existence of the outer solution, so that the presence of the reservoir end may be expected to invalidate the inner solution to some extent, and may be responsible for the discrepancy with prototype measurements. Nevertheless even in relatively short reservoirs the inner solution appears to be a reasonably correct description of the flow. The reasons for a larger layer in the prototype, than predicted by the integral method, have therefore been restricted to the presence of small amounts of effective eddy viscosity or the presence of a rear boundary; probably a combination of both is needed for the full explanation.

RECOMMENDATIONS

In the process of this research the following natural extensions became apparent:

(a) The analysis in Section 3 was carried out for the simplest geometry. This work should be extended to include the following:

(i) end walls and a free surface
(ii) a more realistic bottom geometry
(iii) different sink positions
(iv) no slip walls.

(b) The unsteady outer flow should be reanalyzed to include viscous and diffusive effects. This would make the patching suggested in Section 3.2 unnecessary.

(c) The structure of the withdrawal layer flow should be examined for large values of the Schmidt number.

(d) The matching of the inviscid core IV near the sink, to the inner boundary layer flow III, should be further studied. This will, however, require an understanding of the behavior of the solutions of the non-linear Euler equation.

(e) More experimental data are needed on the values of the transport coefficients in actual reservoirs.

(f) The flow changes caused by a sudden decrease in discharge are still unknown and should be investigated.

(g) The reverse problem, a jet moving into a stratified reservoir, appears to have received little theoretical attention. The river inflow at the upper end of the reservoir is such a jet, and its solution is required for a better understanding of the overall reservoir dynamics.

1. INTRODUCTION

For centuries surface water reservoirs have been constructed as a means of storing water for flood control and water supply. As such their function is well understood and their design is no longer a field of new research. Only in the past few decades, however, have engineers become aware of a major, sometimes helpful and sometimes deleterious side effect of reservoirs, namely their effect on water quality. A surface reservoir represents not only a given number of cubic feet of stored water, but also an inventory of dissolved oxygen, heat, nutrients, minerals, turbidity, plants, and animals, all distributed in an uneven manner throughout the reservoir in a delicate balance whose maintenance is vital to the health of the reservoir environment and the river downstream. Engineers know a great deal about managing the amount of water in a reservoir, but very little about managing its quality. Properly managed, reservoirs can provide a useful means of regulating the quality of water in a stream, including its temperature, dissolved oxygen, and other constituents, in whatever way will be most beneficial to the downstream users. Improperly managed a reservoir can contribute to the destruction of a river environment by permanently changing its temperature, oxygen content, and turbidity, with disastrous effects on the downstream ecology. Much remains to be learned about how the flow in a reservoir can be controlled to produce the desired quality of outflow. This report presents a contribution to our understanding of one aspect of the problem, namely prediction of the thickness of the withdrawal layer when the reservoir is stratified.

Most large surface reservoirs are density stratified throughout most or all of the year. The surface, or epilimnion water, consisting of the upper 15 feet or so, is heated by the sun and becomes lighter than the water beneath. Below this there is a sharp drop in temperature, called the thermocline. The deep water, called the hypolimnion, has a slight, nearly linear stable temperature gradient, meaning that the density of the water increases continuously as one goes down in the reservoir. The effects of this slight stratification are profound, because the flow patterns found in stratified water are totally different from those found in water of constant density. In stratified systems flow in the vertical direction requires the expenditure of energy, whereas flow in the horizontal direction does not; hence flows in stratified waters tend to extend over great horizontal distances, while being confined to narrow vertical layers. When water is taken out of a stratified reservoir the discharge tends to come only from the level of the exit, flowing in a layer which extends over the entire length of the reservoir but only over a fraction of the depth. The temperature of the outflow, as well as the concentration of dissolved constituents such as oxygen and nutrients, is that of the water in the reservoir at the exit level. Management of the temperature and quality of water downstream of the reservoir can be achieved by varying the level of the exit to select the desired quality.

The long-term objective of this research is to provide an operational technique for managing the quality of reservoir outflow. This objective, a substantial undertaking, will require a complete understanding of the details of stratified flow and mixing in an arbitrarily shaped reservoir. The complexities are enormous, and may never be understood in complete detail. Nevertheless, in recent years several bulk management schemes have been put into use, for instance those described by Orlob and Selna (1970) and Beard and Wiley (1970). In these schemes a computer is told as much as is presently known about reservoir mechanics, that the incoming river water sinks till it reaches its level of buoyancy, that the outflow comes from the level of the exit, that solar energy is supplied at the water surface, and that some type of vertical mixing takes place. The computer is given an historical sequence of in and outflows and is programmed to keep track of temperature and water quality as a function of depth in the reservoir. These schemes have considerable promise, their only failing being in the primitiveness of their description of the reservoir mechanics. Thus Beard and Wiley (1970) find that the coefficients required for their program vary from reservoir to reservoir by a substantial factor, and that the variation cannot be predicted within the present state of knowledge. Improvement in the accuracy of schemes such as this one will come only by improving our understanding of the basic mechanics of the processes involved.

The present report describes a mathematical and experimental investigation of one aspect of the management problem, the withdrawal layer which forms at the level of the exit. Even in this detail the mathematical difficulties are so formidable that the reservoir must be idealized to obtain a solution. Mathematically the reservoir is considered to be infinitely long and of constant width and depth, and the density profile is taken to be linear. The exit is assumed to be located halfway from the surface to the bottom, and all walls are assumed to be stress-free. Within these limitations a mathematical solution can be obtained; the details of the derivation are described in Section 3. Sections 4 and 5 describe a laboratory experiment and compare the results of the experiment to the analysis of Section 3; the comparison is extremely good. In Section 6 the theory is compared with the few available measurements in prototype reservoirs; the thickness of the predicted layer is less than is observed, but not by a large amount, and the result is much closer than those of previous theories. The most important reason for the error is believed to be the mathematical assertion of an infinitely long reservoir; indeed, one significant result of the mathematics is that prototype reservoirs are in general short compared to the length required for complete development of the withdrawal layer. A major recommendation for further research is study of the influence of the sloping bottom of the reservoir on the formation of the layers.

The major analytical technique used in this report is the method of matched asymptotic expansions, a method developed by applied

mathematicians only within the past approximately 20 years for the solution of problems in boundary layer theory. The method has proved a powerful tool in many branches of fluid mechanics, and appears to be of significant usefulness in many civil engineering problems, even though it obviously will not be familiar to many practicing engineers. The authors hope that a detailed understanding of the mathematics will not be essential to understanding the results of the study; those less interested in the mathematics may skip directly to the description of the discussion of the experiments, and their results on the comparison of the theoretical predictions with field observations.

2. A REVIEW OF PREVIOUS WORK

The following is a review of previous work on selective withdrawal by a line sink. The physical limitations of the various solutions are investigated and their applicability to experimental work is discussed. The comments here complement the recent survey article by Brooks and Koh (1969).

A Physical Discussion

A sink placed in a homogeneous fluid of infinite extent induces a radial motion. When the same sink is placed in a stably stratified fluid a thin layer of fluid is observed to move, from both the left and the right, towards the sink. It is this layer which is of interest here. Before proceeding, however, to discuss specific known solutions of the above phenomenon it is perhaps helpful to look at the general implications of a variable density.

Let

$$\rho_T = \rho_o + \rho_e(z) + \rho(x,z,t),$$

where

ρ_T = total density

ρ_o = mean over the depth of the density

$\rho_e(z)$ = density above ρ_o when motion is absent

$\rho(x,z,t)$ = density changes induced by the motion

then a measure of the scale of the density gradients is given by

$$\epsilon = \frac{1}{\rho_o} \frac{d\,\rho_e}{dz} .$$

The principal flow modification a variable density induces, concerns the creation of a non-trivial body force. The main force, gravity acting on ρ_o, leads only to a passive hydrostatic pressure which may be removed from the equations of motion. However, if say a particle of volume δv moves a vertical distance of order L, then its density anomaly with the surroundings will be of order $\epsilon L \rho_o$. This induces a body force, in the direction of the particle's original level, of order $\epsilon L\ \rho_o\ g\delta v$. This force, which now actively enters any vertical momentum balance, tends to inhibit vertical motion. If the stratification is strong this force will dominate the other prevailing forces, and the flow will be layered or jet like.

Moment of momentum considerations may be used to show that the above force not only inhibits vertical motion, but also induces a vorticity in the fluid motion. Consider again a sphere δv of a stratified fluid. The pressure force acts, to first order, through the center of volume, but the body force vector passes through the center of gravity. In general, as the sphere has more of its mass concentrated in the lower half, the two centers will not coincide and the sphere will tend to rotate. The production of vorticity by this applied moment yields baroclinic motion and the usual notions about inviscide fluids executing irrotational motion must be discarded.

If this buoyancy force is important in an unsteady fluid motion, the time scale will be fixed by the period of the internal waves present. The natural period of the fundamental oscillation may be found by analyzing the motion of the model sphere after it is displaced a vertical distance z from its original position, in a linear density field. The net force experienced by this particle is of the order $\delta v \epsilon \rho_o gz$ towards its original position. Disregarding other forces, the equation of motion governing the particle is,

$$g\delta v\epsilon\rho_o z = \rho_o \delta v \frac{d^2z}{dt^2}$$

or

$$\frac{d^2z}{dt^2} = \epsilon g z ,$$

and the solution is given by

$$z = Ae^{-i\sqrt{\epsilon g}\, t} + Be^{+i\sqrt{\epsilon g}\, t} .$$

Hence the time scale T of the internal oscillations is $1/\sqrt{\epsilon g}$. The frequency $\sqrt{\epsilon g}$ is generally known as the Brunt-Väisällä frequency. If the fluid is forced to respond at a much faster rate, then the buoyancy forces may be overwhelmed and the fluid will respond as a homogeneous mass. The equations of motion are then elliptic.

The other modification a variable density causes is that the inertial resistance of the fluid is now a function of the vertical height. Two particles separated by a vertical distance L will have a density difference of the order ϵL. If both of these particles are placed under a similar pressure gradient, their inertial resistance will be correspondingly different; the lighter particle will accelerate faster than its heavier counterpart. The importance of this effect is related directly to the magnitude of ϵL. In a reservoir L is bounded by 2ℓ, the depth of hypolimnion, making $2\ell\epsilon$ of $O(10^{-3})$. The smallness of ϵL implies that the percentage difference in the inertial resistance is small, which in turn means that the term $\rho_T \frac{D\vec{u}}{Dt}$ in the equations of motion may be approximated by $\rho_o \frac{D\vec{u}}{Dt}$. This is what is generally known

as the Boussinesq approximation and it will be used throughout this report.

The above discussion shows that the pressure gradient induced by switching on a sink, meets only a small viscous resistance in the horizontal direction, but it is counteracted by viscosity and buoyancy in the vertical direction. As the horizontal velocity at the level of the sink increases, the velocity everywhere else will decrease, since the discharge q remains constant. This results in a thin horizontal velocity jet, with an associated vorticity concentration at the level of the sink. As the layer narrows, the velocity and velocity gradients increase and inertia and viscous forces become important.

In contrast to boundary layer theory in a homogeneous fluid, the thin vorticity concentrations in a stratified fluid may be sustained by three distinct mechanisms:

(a) Cross stream diffusion of vorticity is balanced by longitudinal convection (ordinary boundary layer).

(b) Production of vorticity by the baroclinicity is balanced by downstream convection (inviscide buoyancy layer).

(c) Cross stream diffusion of vorticity is balanced by the creation of vorticity of opposite sign by the baroclinicity (creeping flow layer).

A layer of type (a) is usually relevant only when a wall is present and the velocity of the fluid is high enough to overcome any buoyancy effects. Redekopp (1970) has shown how this type of layer may, however, form an obstruction with its displacement thickness, for flow in which buoyancy is important. The other two layers both involve an active participation of the buoyancy forces; they are the ones which constitute the withdrawal layer considered here.

The existence of these layers requires, as already mentioned, that the buoyancy forces be strong enough to make vertical displacements within the layer small compared to the reservoir depth. Dimensionally this means that when assessed with respect to the reservoir depth, the buoyancy forces should be larger than either the inertial or viscous forces, but that also there be a scale present, smaller than the depth, based on which the forces balance. The quotient of the relevant forces to the buoyancy forces, when all are assessed with respect to the reservoir depth, then form the small parameters usually associated with a thin layer theory. For layers of type (b), this yields the quotient

$$\frac{\text{inertia forces}}{\text{buoyancy forces}} = \frac{\delta v\ \rho_o \frac{\vec{Du}}{Dt}}{\delta v\ \varepsilon\, \ell\, \rho_o\, g} = \frac{U^2}{\varepsilon g \ell^2} = \frac{q^2}{\varepsilon g \ell^4} = F^2 \ ,$$

where F is called the densimetric Froude number. Similarly for layers of type (c) the parameter becomes

$$\frac{\text{viscous forces}}{\text{buoyancy forces}} = \frac{\mu U \delta v}{\ell^2} \frac{1}{\delta v \epsilon \ell \rho_o g} = \frac{\nu U}{\epsilon g \ell^3} = \frac{F^2}{R_e} ,$$

where $R_e = \frac{\ell U}{\nu}$ = Reynolds number.

When diffusion of the stratifying species is non-zero, then the speed of propagation of the species is of order D/ℓ. If U is of the same order or smaller than this, the adjustment in density by diffusion is important and the relevant number becomes the Rayleight number R, where

$$R^2 = \frac{\nu}{\epsilon g \ell^3} \cdot \frac{D}{\ell} .$$

In general there are thus three independent parameters F, R_e and R which are important in the study of withdrawal layers. The internal Froude number F is the relevant parameter for layers of type (b), while F^2/R_e and R are the parameters governing the non-diffusive and diffusive layers of type (c). Sometimes it is more convenient to deal with the alternative triplet of parameters F, R, and G, where $G = (\nu/D)^{\frac{1}{2}}$. Known solutions may be categorized into one of the following classes:

$$F \to 0 \; ; \; R = 1/G = 0$$

$$F = 0 \; ; \; F^2/R_e \to 0 \; ; \; 1/G = 0$$

$$F = 0 \; ; \; R \to 0 \; ; \; G = 0(1) ,$$

where the arrow $\to 0$ indicates that the parameter is small, but non-zero, and the solution is the limiting solution as the parameter approaches zero.

Unsteady Flow

The unsteady flow development appears to have received very little attention. The analysis by Koh (1966a) seems to be the only one on the subject. Koh (1966a) deals with the unsteady flow due to a variable sink strength q(t) in a fluid of infinite extent and linear stratification. The analysis neglects all forces except the unsteady inertia force, $\rho_o \frac{\partial \vec{u}}{\partial t}$, pressure and buoyancy, and from above it may be anticipated that the time taken for the flow to reach steady state is $k/\sqrt{\epsilon g}$, where k is a constant to be determined.

For the case where the sink is suddenly brought to full strength q, the solution for small time is near radial flow, while for large time

$$u(x,z,t) \sim q \frac{\cos\theta}{\pi r}\sqrt{1-\beta^2}\ \frac{\sin \beta t^*}{\beta} \sim q\ \delta(z)\ ,$$

where $\theta = \arctan \frac{z}{x}$, $\beta = \sin\theta$ and $t^* = t\sqrt{\epsilon g}$. The solution, for large time, thus collapses to a thin line moving with infinite speed towards the sink. This may be expected as all the forces which could counteract buoyancy have been neglected. Koh (1966a) evaluated the constant k by defining the layer thickness to be given by the 1st velocity reversal and patching the above solution onto a steady layer thickness δ_s. The velocity u is zero when

$$\beta t^* = \pi$$

hence let

$$\frac{\delta_s t^*}{x} = \pi$$

or

$$t = \frac{1}{\sqrt{\epsilon g}} \frac{x}{\delta_s} \ .$$

In assuming that $\frac{\partial \vec{u}}{\partial t}$ is multiplied by ρ_o, rather than ρ_T , (1966a) assumed a Boussinesq approximation. However the solution is radial for small times and thus the scale of the motion L becomes infinite a large distance from the sink. This means that ϵL is not small and the Boussinesq approximation should not have been made. To see the effect of this non-uniformity, the full problem was analyzed by Imberger (1970). Although the flow pattern obtained by him was different, the time estimate for the withdrawal layer formation was insensitive to the non-uniformity and is the same as that found by Koh (1966a). Another way to overcome the non-uniformity is to put the sink between parallel walls of finite spacing - this is done in Section 3.

Type (b) Layers: $F \to 0$; $R = 1/G = 0$

The fluid is inviscid and non diffusive and the depth of the fluid is large enough so that F is small, causing the flowing layer to separate from the walls. With $R = 1/G = 0$, the equations of motion reduce to the Euler equations for a stratified fluid and $\frac{D\rho_T}{Dt} = 0.0$; the density is conserved along streamlines. The equations may be rearranged to form a single equation for the streamfunction ψ (Yih (1965), p. 76).

$$\nabla^2 \psi' = \frac{gz}{\rho_o} \frac{d\rho_T}{d\psi'} + \frac{dH}{d\psi'} = f(\psi') \ , \qquad (2.1)$$

where $\psi' = \sqrt{\frac{\rho_T}{\rho_o}}\ \psi$ and H is the total head. The flow is inviscid and

the only generation of vorticity is by the baroclinicity effect. The equation really states:

$$\nabla^2 \psi' = \text{Pseudo vorticity} = \text{Pseudo vorticity generated in the particles flow history} + \text{Pseudo vorticity inherited by the flow from any upstream shear.}$$

For the case $\frac{d\rho_T}{d\psi} = 0$, Fraenkel (1961) and Childress (1966) have deduced some general results regarding the formation of vorticities in corners, but otherwise little is known about a general solution of this equation.

Yih (1965), pp. 75-140, discusses the case when $\frac{d\rho_T}{d\psi}$ and $\frac{dH}{d\psi}$ are linear functions of ψ. For a sink between parallel walls, the following two upstream conditions meet this requirement.

(a) Upstream density has a linear variation and $\rho U_\infty^2 = \text{constant}$.

(b) Upstream flow velocity and density are parabolic.

In case (a), the solution depends on the Froude number $F = u/\sqrt{\epsilon g\, \ell^2}$. For F larger than $1/\pi$ the solution indicates a motion towards the sink over the complete depth of the channel, the only exception to this being a large eddy in the corner above the sink. This eddy grows as F decreases and when $F = 1/\pi$ it extends to infinity thus violating the assumed upstream boundary condition. List (1970) has investigated the corresponding problem in three dimensions and found that no solution satisfying the above upstream boundary condition exists for any value of $F = q/\sqrt{\epsilon g\, \ell^2}$. This may be explained simply by noting that for a finite q, $u \to 0$ as $r \to \infty$, hence $F = u/\sqrt{\epsilon g\, \ell^2} \to 0$, and by the two dimensional result, no solution exists. Case (b) always falls into the category $F > 1/\pi$ and therefore is only relevant for large discharges where no separate layer forms and the fluid dynamics is only slightly dependent on the buoyancy forces.

In an effort to extend the above work to layered flow, that is where $F \leq \frac{1}{\pi}$, Trustrum (1964) linearized the convective acceleration term about the upstream uniform velocity. This may be compared with the Oseen approximation in slow viscous flow. She then investigated the time dependent problem for suddenly switching on the sink. For $F > \frac{1}{\pi}$ the solution converges in the limit $t \to \infty$, to flows which are very similar to those found by Yih (1965). However, as $F \to 1/\pi$ or $F < 1/\pi$, the eddies in the upstream corner extend to $x = \infty$ as $t \to \infty$ and the original assumption involved in the linearization is violated everywhere. Thus, the analysis suggests uniqueness for $F > 1/\pi$, but nothing is learned for the case $F \leq 1/\pi$.

The fact that the corner eddy extends in both Yih's (1965) and Trustrum's (1964) solutions to infinity, has led Kao (1965 and 1970) to postulate a slip line within the flow field, separating the flowing fluid from a stagnant upper layer. The results of Kao's work, especially the later paper, suggests that the Froude number, based on the flowing depth, remains constant and equal to $1/\pi$, independent of the discharge q.

Two serious questions remain to be answered. Firstly, what happens to the corner eddies as F decreases below $1/\pi$? To say that these are statically unstable is rather vague at best. They are the result of a dynamic force balance in which the centrifugal force plays an important part. To suddenly neglect this in the eddy cannot be justified. What is required is an analysis of their stability to small (or large) disturbances. Segur (1970) has recently carried out such an analysis and he found the flow to be stable if

$$gz \frac{\partial \rho_T}{\partial r} - \frac{\partial H}{\partial r} < 0 \ ,$$

where r is the local radius of curvature. By this criterion the slow moving eddies are in fact stable and it is not clear how they degenerate into a stagnant fluid as the Froude number decreases below $1/\pi$. It could be that viscous forces predominate within the eddy, but this does not appear to have received any attention.

The second question concerns the non-uniformity of the flow as $x \to \infty$ when viscosity is included. The hope in solving any inviscid problem is that the solution so obtained is in fact the solution of the full Navier-Stokes equations in the limit as $\nu \to 0$. However, in the slipline solution, viscosity would be important around the vortex sheets and the two viscous layers (top and bottom of the inviscid layer) would coalesce at some x. For x greater than this, viscosity would be important throughout the whole layer. This in turn could lead to a different upstream boundary condition for the inviscid core, which if Fraenkel's (1961) work is a guide could have first order effects on the slipline solution. What is therefore needed is that these three layers be matched in the sense of matched asymptotic expansions. The difficulty here is that this requires not only a general solution of the equation governing the inviscid core, but also a solution to the coalesced flow. So far, neither is known. In Section 3, an approximate procedure is suggested.

The experiments of Debler (1959) are tailored to the slipline solution, in that the upstream boundary condition was not allowed to develop naturally but was forced in the manner suggested by Yih (1965), to be of the form $\rho_T U^2$ = constant. Hence, although the experiments were in excellent check of Kao's (1970) solution, they do not throw any light on whether the slip line solution with $\rho_T U^2$ =

constant upstream, is the correct limiting solution close to the sink for a long withdrawal layer. Long here means one in which viscous forces are important upstream.

Type (c) Layer : $\frac{F^2}{R_e} \to 0$; $F = 0 = 1/G$.

The fluid is non diffusive and the discharge is small enough so that the inertia terms may be neglected completely. This results in a linear equation, which for the case $\frac{F^2}{R_e} \to 0$, possesses a thin layer like solution.

Gelhar and Mascolo (1966) investigated such a layer imbedded in a fluid of infinite extent, by making a boundary layer assumption. Further, as the fluid is non diffusive, $\frac{D\rho_T}{Dt} = 0$ and ρ_T is not determined until it is specified somewhere in the flow field. The authors assumed

$$- \frac{g}{\rho_o} \frac{d\rho_T}{d\psi} = f \ , \tag{2.2a}$$

where f is a constant. This leads to a single equation for ψ, viz.

$$\frac{\partial^4 \psi}{\partial z^4} + \frac{f}{\nu} \frac{\partial \psi}{\partial x} = 0 \ . \tag{2.2b}$$

The thickness of the layer, in terms of F^2/R_e, may be deduced from the following argument. When $z \to \infty$, the vertical velocity $w \to 0$, which means that for conservation of mass

$$\int_{-\infty}^{\infty} u dz = \psi(\infty) - \psi(-\infty) = - q \tag{2.3}$$

Hence let

$$\psi^* = \frac{\psi}{q} \ ; \ z^* = \frac{z}{L} \quad \text{and} \quad x^* = \frac{x}{L} \ ,$$

where L is taken, in the absence of a duct width, as the distance of the point of consideration from the sink. Then

$$\frac{\nu}{fL^3} \frac{\partial^4 \psi^*}{\partial z^{*4}} + \frac{\partial \psi^*}{\partial x^*} = 0 \tag{2.4}$$

Also $\frac{q}{2} \geq 4 \geq \frac{-q}{2}$ which implies $\frac{-\Delta\rho}{2} \leq \rho \leq \frac{\Delta\rho}{2}$ and f is constant.

$$f = \frac{g}{\rho_o}\frac{\Delta\rho}{q} ,$$

where $\Delta\rho$ is the density jump across the layer. Hence Eq. (2.4) becomes

$$\frac{F^2}{R_e} \cdot \frac{\partial^4\psi^*}{\partial z^{*4}} + \frac{\partial\psi^*}{\partial x^*} = 0$$

where $F^2 = \rho_o q^2/g\Delta\rho L^3$ and $R_e = \frac{q}{\nu}$. Now rescaling z^*, such that

$$z^{**} = \frac{z^*}{\delta}$$

and $\delta = \left(\frac{F^2}{R_e}\right)^{\frac{1}{4}}$ leads to a single parameter free equation

$$\frac{\partial^4\psi^*}{\partial z^{**4}} + \frac{\partial\psi^*}{\partial z^*} = 0 . \qquad (2.5)$$

Gelhar and Mascolo (1966) found the solution to this equation by postulating a similarity solution

$$\psi^* = x^{*m}\, f\left(\frac{z^{**}}{x^{*n}}\right) \qquad (2.6)$$

The condition $\psi^*(\infty) - \psi^*(-\infty) = -1$ implies $m = 0$ and to satisfy Eq. (2.5) n must be equal to 1/4 and the function f must satisfy the equation

$$4f^{(iv)} - \eta f' = 0 , \qquad (2.7)$$

where

$$\eta = \frac{z^{**}}{x^{*\frac{1}{4}}} .$$

The solution was evaluated numerically, with the help of basic power series and the reader is referred to the author's paper for further details. The solution showed a large center line jet moving towards the sink, with a small amount of backflow at the edges.

In a recent paper, Gill and Smith (1970) have given analytic solutions for the more general equation

$$4f^{(iv)} - \eta f' + mf = 0 . \qquad (2.8)$$

They found that

$$f_{m,k} = \int_{C_k} p^{-m-1} e^{p\eta - p^4} dp \ , \qquad (2.9)$$

where C_k are four different paths in the complex plane, yielding four independent solutions. For the sink flow m = 0 and the appropriate real solution reduce to

$$f = A J_o(\eta) \qquad (2.10)$$

where J_o is defined in the paper, and A is a constant adjusted so that $\psi(\infty) - \psi(-\infty) = 1$. For the asymptotic properties and a plot of J_o, the reader is referred to the original paper.

It is important to note that as well as $\psi(\infty) - \psi(-\infty) = 1$ being satisfied, the integral form of the x momentum equation must hold:

$$\rho_o \int_{-\infty}^{\infty} (uu_x + wu_z)\, dz + \int_{-\infty}^{\infty} p_x\, dz = \mu \int_{-\infty}^{\infty} (u_{xx} + u_{zz})\, dz \ .$$

Integration by parts, interchanging the x differentiation and the integration, and using Eq. (2.3) yields

$$\frac{d}{dx} \int_{-\infty}^{\infty} (-\rho_o u^2 + p)\, dz = \mu(u_z(x, \infty) - u_z(x, -\infty))$$
$$= 0 \ .$$

In the present limit, inertia is neglected, so that

$$\int_{-\infty}^{\infty} p dz = J \ , \qquad (2.11)$$

where J is a constant. Substituting the similarity solution into Eq. (2.11) yields

$$J = x^{\frac{1}{2}} \int_{-\infty}^{\infty} p(\eta)\, d\eta \ . \qquad (2.12)$$

Hence for J to be constant $\int_{-\infty}^{\infty} p(\eta) d\eta$ must be equal to zero. That this is indeed so, is not difficult to show. From the momentum equation, with $p = x^{\frac{1}{4}} p(\eta)$

$$p - \eta p' = 4f''' \tag{2.13}$$

Integrating this between $\eta = -\infty$ and ∞ yields

$$2\int_{-\infty}^{\infty} p\,d\eta - \eta p \Big|_{-\infty}^{\infty} = 4(f''(-\infty) - f''(-\infty)) = 0$$

i.e.

$$\int_{-\infty}^{\infty} p\,d\eta = 0 \ .$$

[Conversely, in the problem of a wake in front of a plate, Long (1959) and others assume $J \neq 0$, i.e. $m = -\frac{1}{2}$. This means that $q = 0$, which again is evident from an examination of their solutions.]

Although $\int_{-\infty}^{\infty} p\,dz = 0$ implies that $\int_{-\infty}^{\infty} \rho g\,dz$ = potential energy = 0 i.e. the potential energy of the flow is zero, the energy balance of the flow reads; the work done by the pressure is equal to the loss in unit potential energy $\int_{v} \rho w\,dz\,dx$ plus the work done against viscous dissipation. The pressure work is porportional to

$$\int_{-\infty}^{\infty} up\big|_{x=x_1}\,dz - \int up\big|_{x=x_2}\,dz = (x_1^{\frac{1}{4}} - x_2^{\frac{1}{4}}) \int_{-\infty}^{\infty} f'(\eta)\, p(\eta)\, d\eta \tag{2.14}$$

If $x_1 = 0$ and $x_2 \to \infty$ then an infinite amount of work must be done on the flow at infinity rather than at the sink. In other words, the flow is being pushed from infinity rather than being sucked towards the sink.

Another difficulty with the solution is the matter of how this sort of flow gets started. Gelhar and Mascolo (1966) assume that

$$\frac{g\Delta\rho}{\rho_o} = g\varepsilon t \tag{2.15}$$

where t is the width of the opening. This has no physical basis. Further, assuming that the flow started from an abrupt density variation, with the sink at the density discontinuity is not valid either, as with no diffusion the density profile could not adjust

to a smooth variation.

These didfficulties are crystalized somewhat by noting that as the layer grows, since q is constant, the velocity u will decrease. At some point u will be small enough to be of O(D/L) and then diffusion will modify the solution. Hence, the above non diffusive solution may be regarded as a solution for intermediate x. But again matching is absent.

Type (c) Layer in a Diffusive Fluid: F = 0; G = O(1), R → 0

The flow is slow enough so that inertia may be neglected, and the diffusion of the species is important. From the previous discussion this may be seen to be a limit of the full equations very far from the sink. In Section 3 a rigorous matching is carried out.

Koh (1966b) has investigated the sink flow in this limit, in an infinite domain with linear stratification. (He also considers the axi-symmetric case.) In a similar way to the above the equations of motion may be reduced to a single equation for the stream function $\psi^* = \frac{\psi}{q}$

$$\frac{\partial^6 \psi^*}{\partial z^{**6}} + \frac{\partial^2 \psi^*}{\partial x^{*2}} = 0 \tag{2.16}$$

where $z^{**} = \frac{z^*}{R^{1/3}}$. Hence $\delta = O(R^{1/3})$. Koh (1966b) investigated the solution of the above equation by postulating a similarity solution

$$\psi^* = x^{*m} f(\eta) \; ; \; \eta = \frac{z^{**}}{x^{*1/3}} \tag{2.17}$$

and again m = 0 to satisfy $\int_{-\infty}^{\infty} u^* dz^{**} = -1$. The resulting ordinary differential equation is

$$f^{(vi)} + \frac{1}{9}\eta^2 f'' + \frac{4}{9}\eta f' = 0 \tag{2.18}$$

or if $g = f'$

$$g^{(v)} + \frac{1}{9}\eta^2 g' + \frac{4}{9}\eta g = 0 \tag{2.19}$$

Koh (1966b) obtained the solution by a numerical integration from $\eta = \eta_o \gg 1$ to $\eta = 0$. He obtained the value of g, at the point η_o, by noting that for large η the differential Eq. (2.19) reduces to

$$\eta^2 g' + 4\eta g = 0 \; . \tag{2.20}$$

The solution to this equation is $g = \frac{A}{\eta^4}$. However, this variation for the velocity implies that the density $\rho \sim \frac{1}{z} \to \infty$. This means that an infinite amount of salt would have to be transferred from below the level of the sink to above it. List (1968) in a similar problem for sink flow in a porous media obtained:

$$\rho \sim - \text{ sgn } z \qquad \text{as } z \to \pm \infty$$

- an even worse singularity. He reasoned that the flow could therefore not develop unless this singularity is already present in the fluid before the motion is started.

In an effort to resolve these difficulties, the five solutions of Eq. (2.19) were determined analytically. A detailed discussion of the properties of these solutions is given by Imberger (1970). It is found that of the five solutions two are exponentially large, two exponentially small, and one decays as $1/\eta^4$, as $\eta \to \infty$. By symmetry, the stream function must be an odd function of z, and it is shown that this is only possible if g contains the algebraically decaying solution - as well as the two exponentially small functions. The physical interpretation of the $1/\eta^4$ decaying solution is that the pressure associated with it grows logarithmically as $x \to \infty$. But as J = 0, this is not acceptable. This unpleasant behavior is not due to assuming the Boussinesq approximation, which is quite valid as it makes little sense to keep the variation of inertia, when inertia itself is completely neglected, but rather it is due to posing the infinite problem with a linear density profile.

In addition, when the solution is substituted into the neglected inertia terms, it is seen that near the sink they dominate the retained viscous terms. Hence the solution has non uniformities both far and near the sink. These shortcomings are investigated in Section 3.

Numerical Studies

In an effort to obtain a solution which includes both the effects of inertia and viscosity, Koh (1964) applied an integral technique to the boundary layer form of the Navier-Stokes equations. The fluid was assumed to be non-diffusive and of infinite extent. Assuming the fluid to be non-diffusive means that the density distribution must be specified somewhere. Koh (1964) postulated a relation similar to Eq. (2.2a):

$$\rho_T = \rho_o(1 - \varepsilon\eta) \ , \qquad (2.21)$$

where $\eta = z/\delta(x)$. This leads, however, to the same difficulty in the interpretation of ε, encountered by Gelhar and Mascolo (1966).

In recent years a number of numerical algorithms have been written for solving the full Navier-Stokes equation when diffusion is absent. Slotta et al. (1969) have used what is generally known as the Marker-Cell technique to study withdrawal from a stratified fluid. They show only results for a two layer stratification - a case for which analytic solutions are available for inviscid fluids. They claim that the height of the withdrawing layer d_2 yields a Froude number

$$F = \frac{u_\infty}{\sqrt{gd_2 \frac{\rho_2-\rho_1}{\rho_2}}} = 0.293 \ . \qquad (2.22)$$

This is then compared with Kao's (1965) result $F_c = \frac{1}{\pi}$. However, the latter is derived for the blocked flow in a linearly stratified fluid and is really not relevant to a two layered flow. It is surprising that d_2 is not an independent parameter as in the analytic solutions. Until these discrepancies are explained, comparison with other work is difficult.

Experimental Studies

Koh (1966b) appears to be the only one who has studied selective withdrawal experimentally in a continuously stratified reservoir. A discussion of his results is left to Section 4, as his data was replotted to conform with the theory developed in Section 3. The Tennessee Valley Authority have over the last few years begun investigating withdrawal in actual reservoirs. The data is still sparse, but a full discussion and comparison is given in Section 6.

Summary

A withdrawal layer forms when a sink is placed into a density stratified fluid, because the buoyancy force inhibits vertical fluid motion. The solution, obtained by Koh (1966a), for the transient switch on problem, clearly shows how a density gradient causes a withdrawal layer to form. Since there is no resistance to horizontal motion, the horizontal velocity at the level of the sink increases at the expense of the motion elsewhere, and a layer forms the thickness of which decreases with time. The non-uniformity associated with Koh's (1966a) solution at large distances from the sink, due to the use of Boussinesq approximation, was shown not to be serious, but for completeness it is remedied in Section 3, by a slight modification of the boundary conditions.

If viscous and convective inertia forces are included, then layers of finite thickness form for which the available theories fall into two classes. Firstly, there is the work of Kao (1965, 1970), in which the fluid is assumed to be inviscid and non-diffusive and secondly, similarity solutions have been found by Gelhar and Mascolo

(1965) and Koh (1966b) when the fluids inertia is neglected. For selective withdrawal in a long reservoir the flow changes, as the fluid moves towards the sink, from one in which inertia may be neglected to one in which viscosity and diffusion can be assumed zero. Hence, the known solutions appear to cover the two extremes of the withdrawal layer; the flow very close and the flow very far from the sink. For this to be so the solutions must, however, correspond in the language of matched asymptotic expansions to the inner and outer expansions of the problem with respect to the variable x. In the above review it is shown that this is not so, and further that the inertia free solutions have physically unrealistic pressure distributions at large distances from the sink.

What is therefore required is an analysis of the overall structure of the layer with proper matching of the different regions. This subject is treated in detail in Section 3.

3. ANALYTIC CONSIDERATIONS

In Section 2 it was discussed how a density gradient inhibits vertical motion and causes the fluid to flow in a thin horizontal layer towards the sink. This layer is, within the Boussinesq approximation, symmetric about the x and the z axis and is present not because the Reynolds number is high, but because the overall Froude number is small.

In actual reservoirs the stratification is usually due to a temperature variation with depth. Hence G is of order one. Also the parameters F and R, when the length is based on the half depth ℓ (Fig. 3.1), are always very small. Typical values are of the order 10^{-2} and 10^{-5}, respectively. However, the value of the Reynolds number is usually very high. Hence in what follows, the symmetric problem shown in Fig. 3.1 is analyzed in the limit $F \to 0$, $R \to 0$, $R_e \to \infty$.

First a simplified unsteady problem, similar to the one considered by Koh (1966a) is analyzed for the present geometry. The results here are a substantiation of Koh's (1966a) solution and they have been included mainly for completeness.

Following this the structure of a steady withdrawal layer is analyzed. For simplicity the horizontal walls are assumed to be stress free and the density along them is assumed to be constant ($\rho = 0$). This approximates a well mixed free surface. More complex boundary conditions could be treated in a similar way, but boundary layers at a no-slip wall would further complicate the analysis. Flow in a duct was chosen primarily to overcome the logarithmic rise in pressure at infinity in Koh's (1966b) solution.

The analysis assumes that at large distances from the sink, the flow is uniform and the density varies linearly with depth. The method of matched asymptotic expansions shows that the structure of the flow changes progressively from a slow uniform flow at infinity, to a layer of type (c) closer in, which in turn develops into a jet flow in which inertia is important. There is some evidence that very close to the sink a type (b) layer forms.

The outside flow, where the influence of inertia is neglected, is solved in closed-form and in the limit as x and z tend to zero the solution approaches a similarity solution. The inner equations are solved approximately by Galerkin's method and composite solution for the withdrawal layer thickness is derived.

The Governing Equations

Changes of density in the reservoir water are either caused by temperature differences or by a variable concentration of a denser substance such as salt. In the first case, the basic equations governing the motion will be the Navier-Stokes equation with the energy equation describing the influence of the temperature gradients on the motion. When

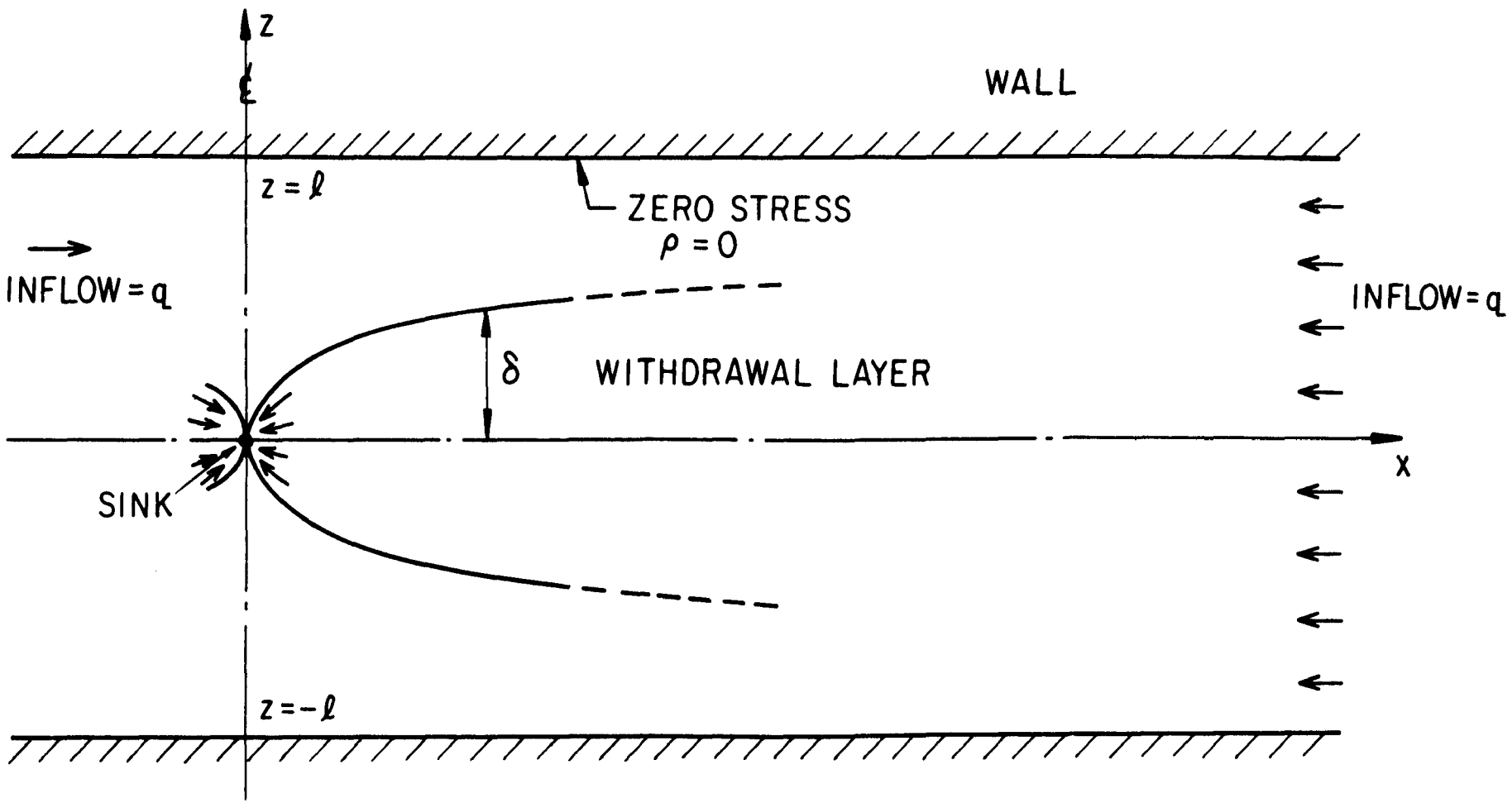

FIG. 3.1 THEORETICAL MODEL

the background stratification is the result of a varying concentration of a second species the governing equations are those of a mixture (Green and Naghdi (1969)). The water in a reservoir can be assumed to be incompressible and if a second species such as salt is present, its concentration will be small. Under these circumstances, Müller (1968) has shown that the equations of motion reduce to the Navier Stokes equations for a single compound species, the density of which is governed by Fick's law. Since the vertical motion is bounded by the duct width 2ℓ , and as $\epsilon\ell \ll 1$, the Boussinesq approximation can be used to further simplify the equations. The derivation of the simplified equations under this assumption is given by Redekopp (1969) and the equations are as follows:

$$\nabla \cdot \vec{u} = 0 \tag{3.1}$$

$$\rho_o \frac{\vec{Du}}{Dt} + \nabla p = - \rho g \hat{k} + \mu \nabla^2 u \tag{3.2}$$

$$\frac{D\rho}{Dt} + \frac{d\rho_e}{dz} w = D\nabla^2 \rho \tag{3.3}$$

$$\vec{\tau}(x, \pm\ell) = 0 \tag{3.4}$$

$$\rho(x, \pm\ell) = 0 \tag{3.5}$$

$$\vec{u}(\infty, z) = - \frac{q}{2\ell} \hat{i} H(t), \tag{3.6}$$

$$u(o,z) = - q\delta(z) H(t), \tag{3.7}$$

where

$$\rho_T = \rho_o + \rho_e(z) + \rho(x,z,t)$$

D = diffusion coefficient

$$p_T = p_e(z) + p(x,z,t)$$

$$\frac{dp_e}{dz} = - (\rho_o + \rho_e(z)) g$$

$\vec{\tau}$ = wall stress

$H(t)$ = unit step function

$\delta(z)$ = Dirac delta function.

Finally, within the Boussinesq assumption, the flow will be symmetric about the line $z = 0$.

The Initial Value Problem

The aim of this section is to investigate the error induced by the Boussinesq assumption in Koh's (1966a) estimate of the time taken for a steady withdrawal layer to establish itself. It is shown below, within the framework of linear inviscid theory, that the finite duct problem is really only a slight extension of Koh's (1966a) work and that to this accuracy, the time taken to achieve steady conditions is independent of the wall spacing and insensitive to the Boussinesq assumption.

Within the framework of Eqs. (3.1-3.7), when the sink is opened, the pressure field will be equivalent to one in a homogeneous fluid. Only when the fluid begins to move will it experience the buoyancy force. Assumed here of course, is that the pressure at the sink is not so low, discharge so high, that inertia completely dominates the buoyancy forces, and the flow is only a slight modification of motion in a homogeneous fluid. Once the fluid begins to move, buoyancy tends to restore any vertical displacement and the resulting motion is an oscillatory adjustment towards the final flow. In this phase of the flow, viscous forces play only a minor role and the flow is essentially governed by a balance of pressure, buoyancy and inertia. The time scale is thus $1/\sqrt{\epsilon g}$ as discussed in the introduction.

Let

$$\rho^* = \frac{\rho}{\Lambda} \; ; \; u^* = \frac{u}{q/\ell} \; ; \; w^* = \frac{w}{q/\ell}$$

$$t^* = \sqrt{\epsilon g}\; t \quad \text{and} \quad p^* = \frac{p}{P} \; ,$$

where

$$P = \Lambda g \; \ell$$

and

$$\Lambda = \epsilon \ell \; \rho_o \quad q/\sqrt{\epsilon g} \; \ell^2 \; .$$

Equations (3.1) to (3.7) then become:

$$\nabla \cdot \vec{u}^* = 0 \tag{3.8}$$

$$\frac{\partial \vec{u}^*}{\partial t^*} + F\,\vec{u}^*\nabla\vec{u}^* + \nabla p^* = -\,\rho^*\hat{k} + R.G.\;\nabla^2\vec{u}^* \tag{3.9}$$

$$\frac{\partial \rho^*}{\partial t^*} + F\,\vec{u}^*\nabla\rho^* - w^* = \frac{R}{G}\,\nabla^2\rho^* \tag{3.10}$$

where

$$-1 \le z^* \le 1 \quad \text{and} \quad 0 \le x^* \le \infty$$

$$F = \frac{q}{\sqrt{\epsilon g}\;\ell^2}\ ,$$

$$R = \sqrt{\frac{\nu D}{\epsilon g}}\;\frac{1}{\ell^2}\ ,$$

and

$$G = \sqrt{\frac{\nu}{D}}\ .$$

In a reservoir $F \ll 1$ and $R \ll 1$ and thus to the zeroth order†.

$$\nabla \cdot \vec{u} = 0 \tag{3.11}$$

$$\frac{\partial \vec{u}}{\partial t} + \nabla p = -\,\rho\hat{k} \tag{3.12}$$

$$\frac{\partial \rho}{\partial t} - w = 0 \tag{3.13}$$

$$x,z \in \{x,z \,|\, -1 \le z \le 1 \quad \text{and} \quad 0 \le x \le \infty\}$$

$$u(\infty,\ z,\ t) = \tfrac{1}{2}H(t)$$

and

$$u(0,\ z,\ t) = \delta(z)\ H(t)\ .$$

(The constant density boundary condition becomes redundant as $D\nabla^2\rho = 0$.)

† The asterisks have been dropped for convenience.

Equations (3.11) - (3.13) are identical to the ones solved by Koh (1966a) for the infinite domain, and his method of solution is adopted here. The solution in terms of the Laplace Transform of the streamfunction ψ is shown by Imberger (1970) to be given by:

$$\bar{\psi} = \frac{1}{\pi p} \operatorname{artan} \left(\coth \frac{\pi x p}{2\sqrt{1+p^2}} \cdot \tan \frac{\pi \eta p}{2\sqrt{1+p^2}} \right) \tag{3.14}$$

The complete solution is now given by the Laplace inverse of Eq. (3.14). This inversion is simplified by noting that there exist a positive number M such that

$$\left| \sqrt{\frac{p^2}{1+p^2}} \right| < M$$

for all p with $\mathrm{Rel}(p) = c > 1$.

Hence for small x and z

$$\bar{\psi} = \frac{1}{\pi p} \operatorname{artan} \frac{\eta}{x} \tag{3.15}$$

which is uniformly valid in p . This is the solution for the infinite domain and Koh (1966a) has given the solution for u , viz.

$$u(x,z,t) = \frac{\cos\theta}{\pi r} \left(J_o(t) + \frac{1-\beta^2}{\beta} \int_o^t J_o(\omega) \sin \beta(t-\omega) d\omega \right), \tag{3.16}$$

where

$$\beta = \sin\theta , \quad \theta = \tan^{-1} z/x,$$

and J_o is the Bessel function of zero order.

Consider x and z fixed, then as $t \to \infty$

$$u(x,zt) \sim \frac{\cos\theta}{\pi r} \frac{1-\beta^2}{\beta} \int_o^\infty J_o(\omega) \sin \beta(t-\omega) \, d\omega$$

$$= \frac{\cos^2\theta}{r} \frac{\sin \beta t}{\beta} \approx \delta(z) . \tag{3.17}$$

The layer thickness, defined to be the distance to where $u = 0$, is therefore given for large t by the equation

$$\beta t = \pi .$$

In terms of the layer thickness this means

$$2\delta = \frac{2\pi x}{t} \tag{3.18}$$

(2π is obtained instead of the graphical value of 6.4 in Koh's 1966 work.)

The finite duct problem has thus the same time response as the infinite domain. The solution is, however, seen to be non-uniform in both time and space. The space non-uniformity is dealt with in the next section for the steady problem and is due to the large velocities near the sink for all times. But also as $t \to \infty$, the vertical scale of motion tends to zero, thus $\partial/\partial z \gg 1/\ell$, the assumed scale of the gradients. A rational approach must again involve a matching procedure, but this is not attempted here. The physical time required for a layer to form can be obtained by patching the above result (see Koh (1966a) also) onto a steady solution. This yields,

$$t = \frac{\pi}{\sqrt{\epsilon g}} \quad \frac{x}{\delta_s} \tag{3.19}$$

where δ_s is the steady withdrawal layer thickness derived in the next section.

Structure of the Withdrawal Layer - Outer Solution

The discussion in the introduction showed that the Boussinesq assumption is valid when $\epsilon L \ll 1$. Here L was a typical vertical scale of the motion. It will become clear from later details of this analysis that inertia is only important close to the sink. Anywhere else inertia is completely neglected so that the Boussinesq approximation automatically applies. Near the sink the thickness of the layer will be shown to be of order $q/\sqrt{g\epsilon}$, hence the Boussinesq approximation is valid provided $q\sqrt{\epsilon/g} \ll 1$. For typical reservoir operation this is of $O(.01)$.

Consider first the flow equation valid far from the sink where inertia may be neglected. Define the new variables

$$x^* = \frac{x}{\rho}, \quad z^* = \frac{z}{\ell}; \quad p^* = \frac{p}{P}; \quad \rho^* = \frac{\rho}{\Lambda}; \quad u^* = \frac{u}{q/\ell}; \quad w^* = \frac{w}{q/\ell};$$

where

$$P = \Lambda g \ell \ ;$$

$$\Lambda = F \ \epsilon \ \ell \ \rho_o \ .$$

In terms of these new variables Eqs. (3.1) - (3.5) become

$$F(u^* u^*_{x^*} + w^* u^*_{z^*}) + p^*_{x^*} = R.G. \ u^*_{z^* z^*} + R \ G \ u^*_{x^* x^*} \tag{3.20}$$

$$F(u^* w^*_{x} + w^* w^*_{z^*}) + p^*_{z^*} = - \ \rho^* + R \ G \ w^*_{z^* z^*} + R \ G \ \ w^*_{x^* x^*} \tag{3.21}$$

$$F(u^* \rho^*_{x^*} + w^* \ \rho^*_{z^*}) - w^* = \frac{1}{G} \ R \ \rho^*_{z^* z^*} + \frac{1}{G} \ R \ \rho^*_{x^* x^*} \tag{3.22}$$

where

$$F = \frac{q}{\sqrt{\epsilon g} \ \ell^2} \ ; \ R = \sqrt{\frac{\nu D}{\epsilon g}} \cdot \frac{1}{\ell^2} \ ; \ G = \sqrt{\frac{\nu}{D}}$$

The outer region is defined as that part of the flow field in which the inertia forces may be neglected. By an order of magnitude analysis Imberger (1970) has shown that the inertia forces may be neglected everywhere except near the origin. The equations governing this outer flow are given by

$$p^*_{x^*} = R.G. \ u^*_{z^* z^*} \tag{3.23}$$

$$p^*_{z^*} = - \ \rho^* \tag{3.24}$$

$$-w^* = \frac{1}{G} \ R \ \rho^*_{z^* z^*} \ , \tag{3.25}$$

which must now be solved in the finite duct. The "inner region" is then that part of the flow where the solution to Eqs. (3.23) - (3.25) no longer describes the flow. This will be near the sink.

The solution is most easily found by taking a finite Fourier Transform in the z^* direction. But first define ψ^* such that

$$u^* = \psi^*_{z^*} \tag{3.26}$$

and

$$w^* = - \ \psi^*_{x^*} \ . \tag{3.27}$$

Then Eqs. (3.23) - (3.25) yield, on the elimination of the pressure,

$$R^2 \frac{\partial^6 \psi^*}{\partial z^{*6}} + \frac{\partial^2 \psi^*}{\partial x^{*2}} = 0 \tag{3.28}$$

The presence of the factor R^2 implies a layer thickness of the order $R^{1/3}$ and the appropriate scaling is given by

$$z^{**} = \frac{\pi}{R^{1/3}} z^* \tag{3.29}$$

and

$$x^{**} = \pi^3 x^* \ . \tag{3.30}$$

Although this scaling is used in the next subsection, the solution to the outer problem is more conveniently represented in terms of the scaling

$$\tilde{z} = \pi z^* \tag{3.31}$$

and

$$\tilde{x} = \pi^3 x^* R \ . \tag{3.32}$$

This also accomplishes the removal of the dependence of R of Eq.(3.27), with the additional advantage that the wall spacing remains independent of R. In terms of these variables the boundary value problem becomes,

$$\frac{\partial^6 \psi^*}{\partial \tilde{z}^6} + \frac{\partial^2 \psi^*}{\partial \tilde{x}^2} = 0 \tag{3.33}$$

$$-\pi \le \tilde{z} \le \pi \quad \text{and} \quad 0 \le \tilde{x} \le \infty$$

with boundary conditions given by

$$\psi^* = \mp \tfrac{1}{2} \qquad \tilde{z} = \pm \pi \qquad \text{(a)}$$

$$\frac{\partial^2 \psi^*}{\partial \tilde{z}^2} = 0 \qquad \tilde{z} = \pm \pi \qquad \text{(b)}$$

$$\frac{\partial^4 \psi^*}{\partial \tilde{z}^4} = 0 \qquad \tilde{z} = \pm \pi \qquad \text{(c)} \tag{3.34}$$

$$\psi(o,\tilde{z}) = -\tfrac{1}{2} \operatorname{sgn} \tilde{z} \qquad \text{(d)}$$

The solution of Eq. (3.33) satisfying Eq. (3.34) and which is bounded at $\tilde{x} = +\infty$ was found by Imberger (1970) to be given by,

$$\psi(\tilde{x},\tilde{z}) = \frac{1}{\pi}\sum_{n=1}^{\infty}\left(-\frac{1}{n}e^{-n^3\tilde{x}}\sin n\tilde{z} - \frac{(-1)^n}{n}\sin n\tilde{z}\right)$$

$$= \frac{1}{\pi}\sum_{n=1}^{\infty} -\frac{1}{n}e^{-n^3\tilde{x}}\sin nz - \frac{\tilde{z}}{2\pi} \qquad (3.35)$$

Convergence of the series is very rapid everywhere, except at the origin where it diverges. This is the singularity corresponding to the sink. The solution given by Eq. (3.35) is shown in Fig. 3.2.

Figure 3.3 is a log-log plot of two streamlines within the forward flowing layer. It is seen that as $\tilde{x} \to 0$ the slope tends to 1/3, which may be compared with Koh's (1966b) solution for the infinite domain.

To study the non-uniformity at the sink, it is necessary to know the limiting solution of $\psi(\tilde{x},\tilde{z})$ as $\tilde{x} \to 0$ and $\tilde{z} \to 0$. The above indicates that this is given by Koh's (1966b) solution. A more formal proof is obtained by noting that the same limit is achieved by fixing $\tilde{x}$ and $\tilde{z}$ and letting the duct walls move apart. This process yields

$$\psi = \int_0^{\infty}\frac{1}{p}e^{-p^3\tilde{x}}\sin p\tilde{z}\,d\tilde{z}$$

$$= \int_0^{\infty}\frac{1}{q}e^{-q^3}\sin q\tilde{\eta}\,dq \qquad (3.36)$$

where $\tilde{\eta} = \tilde{z}/\tilde{x}^{1/3}$. Imberger (1970) has shown that the above is the solution to the corresponding problem in the infinite domain.

The outer flow therefore changes from a uniform channel flow far from the sink to a self similar motion as the sink is approached.

Before turning to the inner flow, it should be noted that although the simplified mass flux condition (3.1) has been used, the solution does not imply an accumulation of mass in the duct. The rate of mass leaving the duct at the sink is, by symmetry, equal to

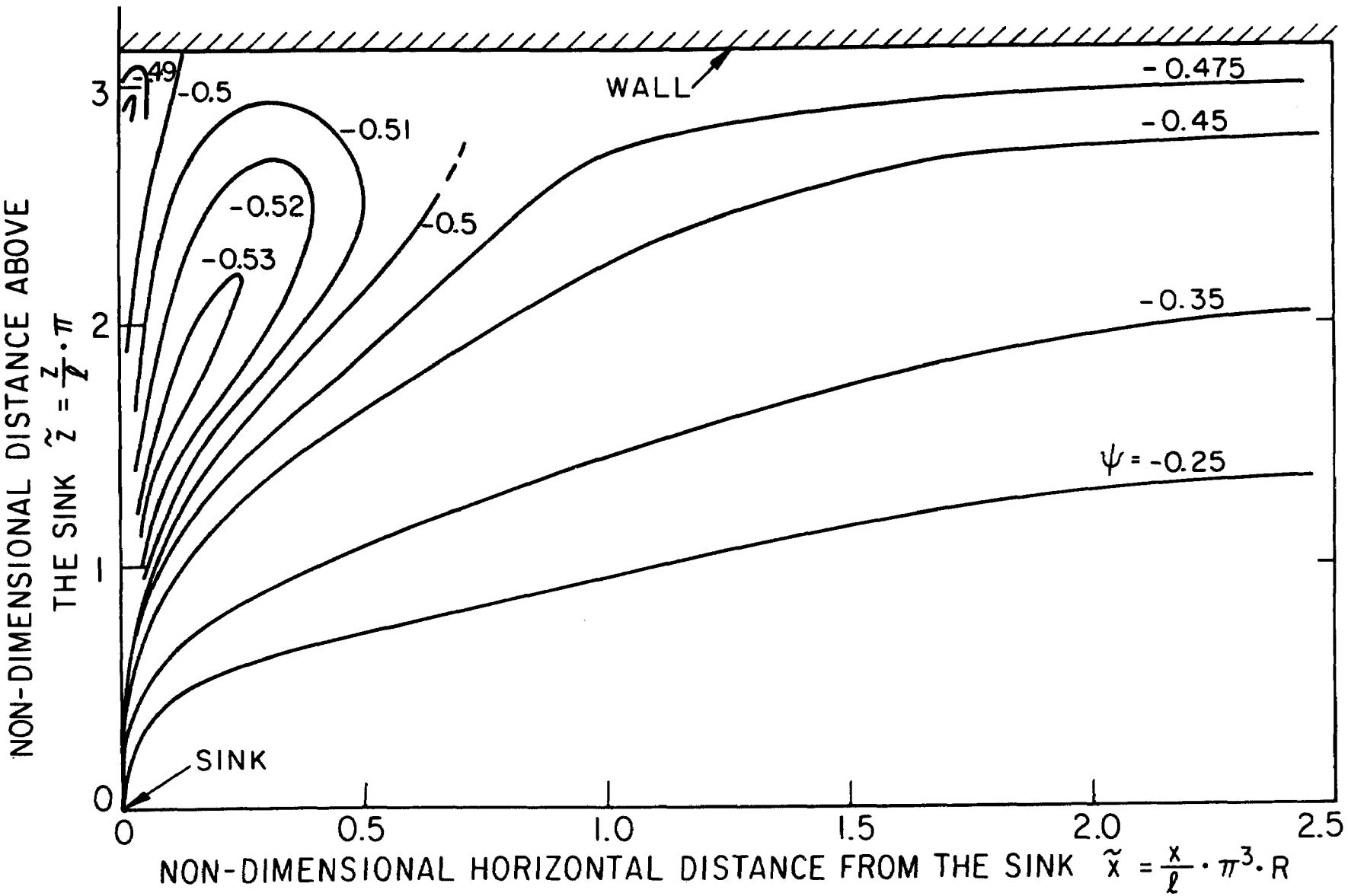

FIG. 3.2 OUTER SOLUTION

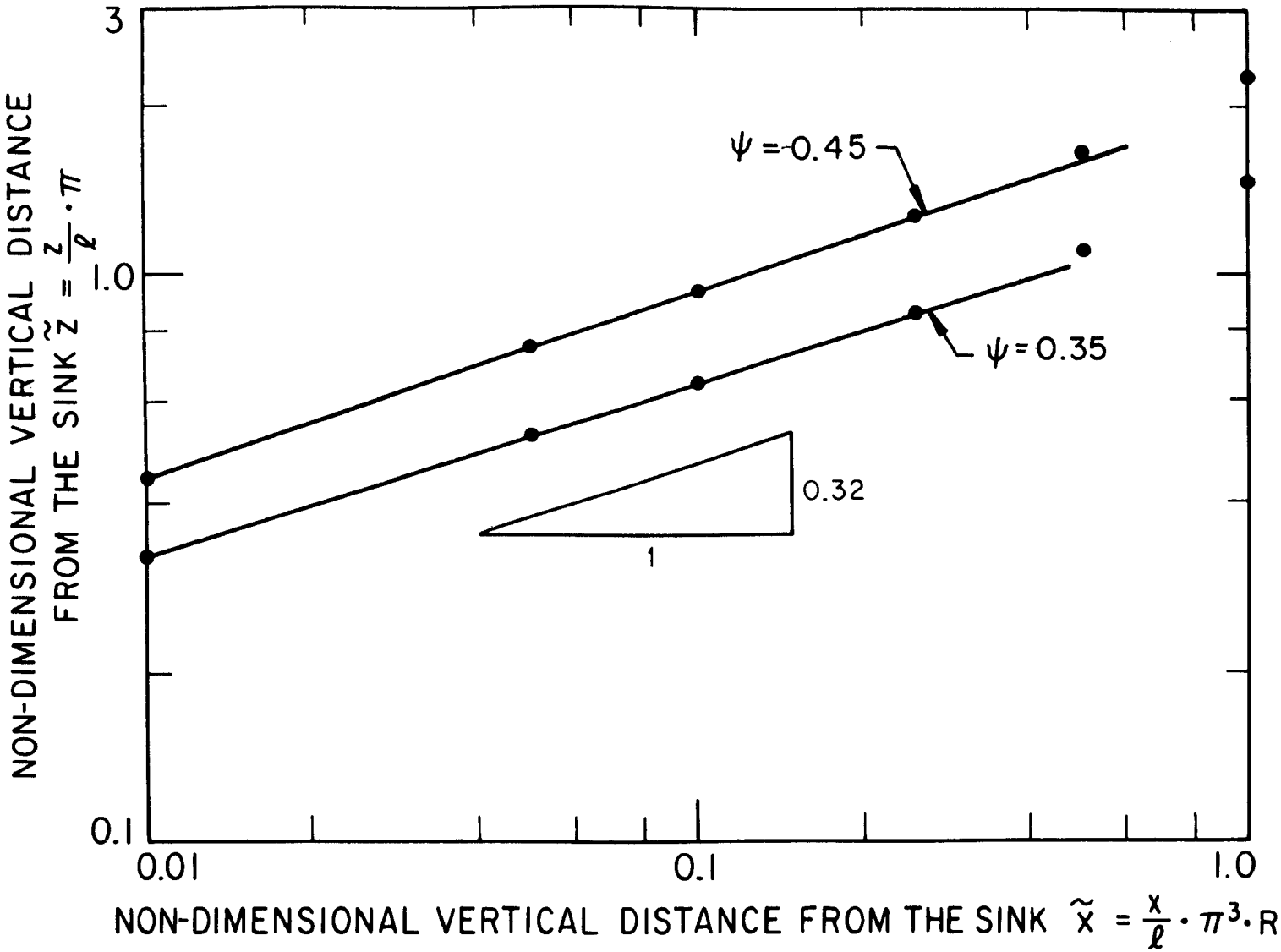

FIG. 3.3 OUTER SOLUTION

$$(\rho_e(o) + \rho_o)\ q\ .$$

The rate of which mass enters the duct at infinity is given by

$$\int_{-\ell}^{\ell} \rho_T\ u\ dz$$

$$= u_\infty \int_{-\ell}^{\ell} \rho_T\ dz$$

$$= (\rho_e(o) + \rho_o)\ q\ ,$$

the same as that leaving at the sink. Similarly if $s(z)$ is the concentration distribution of a passive substance, such as O_2, then the concentration s_o at the sink is given by the mass balance:

$$s_o\ q = \int_{-\ell}^{\ell} s(z)\ u(z)\ dz$$

$$= q\ \frac{1}{2\ell} \int_{-\ell}^{\ell} s(z)\ dz \qquad (3.37)$$

and

$$s_o = \frac{1}{2\ell} \int_{-\ell}^{\ell} s(z)\ dz$$

Structure of the Withdrawal Layer - Inner Equations

The inner region is that part of the flow in which Eq. (3.35) fails to yield the proper description of the flow.

In the above subsection it was shown that the governing equations within the layer in the outer region are obtained by scaling the z^* coordinate with respect to $R^{1/3}$. Carrying this out for the full

Eqs. (3.20) - (3.22) yields

$$\frac{F}{R^{2/3}} \left(\psi^*_{z^{**}} \psi^*_{z^{**}x^*} - \psi^*_{x^*} \psi^*_{z^{**}z^{**}}\right) + p^*_{x^*} = G \psi^*_{z^{**}z^{**}z^{**}}$$

$$+ GR^{2/3} \psi^*_{z^{**}x^*x^*} \tag{3.38}$$

$$F(-\psi^*_{z^{**}} \psi^*_{x^*x^*} + \psi^*_{x^*} \psi^*_{x^*z^{**}}) + p^*_{z^{**}} = - \rho^{**}$$

$$- GR^{4/3} \psi^*_{x^*x^*x^*} - GR^{2/3} \psi^*_{x^*z^{**}z^{**}} \tag{3.39}$$

$$\frac{F}{R^{2/3}} \left(\psi^*_{z^{**}} \rho^{**}_{x^*} - \psi^*_{x^*} \rho^{**}_{z^{**}}\right) - \psi^*_{x^*} = \frac{R^{2/3}}{G} \rho^{**}_{x^*x^*} + \frac{1}{G} \rho^{**}_{z^{**}z^{**}} \tag{3.40}$$

where the new density $\rho^{**} = R^{1/3} \rho^*$. The outer layer flow equations are obtained as the limit $R \to 0$ and $F/R^{2/3} \to 0$.

One method (Koh (1966b)) to compute the influence of the nonlinear convection near the sink would be to expand the stream function ψ^* in a regular series in the small parameter $F/R^{2/3}$. However, an inspection of the second term of this series shows that the series diverges when x becomes smaller than

$$\left(\frac{q}{\nu}\right)^{3/2} \left(\frac{\nu D}{\varepsilon g \ell^4}\right)^{1/4} = \left(\frac{F}{R^{2/3}}\right)^{3/2} \cdot G^{-3/2} = x^*_c \, G^{-3/2} ,$$

where

$$x^*_c = (F/R^{2/3})^{3/2} . \tag{3.41}$$

In other words, for distances smaller than x^*_c the influence of inertia is not merely a correction to the outer flow, but it is the prime force. This means that near the sink $\delta = 0(F^{\frac{1}{2}})$ and new stretched variables are needed.

Let

$$x^{**} = \frac{x^*}{\left(\frac{F}{R^{2/3}}\right)^{3/2}}$$

and

$$z^{***} = \frac{z^{**}}{F^{1/2}/R^{1/3}} \tag{3.42}$$

The outer solution $\psi^*(x^*, z^{**})$ when rewritten in terms of the inner variables is

$$\psi^*\left(\left(\frac{F}{R^{2/3}}\right)^{3/2} x^{**} \ , \ \left(\frac{F}{R^{2/3}}\right)^{1/2} z^{***}\right) .$$

Now as $F/R^{2/3} \to 0$, this becomes $\psi^*(\eta^{**})$, where

$$\eta^{**} = \frac{z^{***}}{x^{**1/3}} \ ,$$

hence the inner stream-function remains unscaled. Also to be able to match ρ^{**} , it must be rescaled

$$\rho^{***} = \frac{1}{R^{1/3}/F^{1/2}} \rho^{**}$$

as

$$\rho^{**} = \frac{1}{x^{*1/3}} h(\eta^*) \ .$$

The equations in terms of these inner variables may thus be written:

$$\psi^*_{z^{***}} \psi^*_{z^{***}x^{**}} - \psi^*_{x^{**}} \psi^*_{z^{***}z^{***}} + p^*_{x^{**}} = G \psi^*_{z^{***}z^{***}z^{***}}$$

$$\frac{1}{R_e^2} G \psi^*_{z^{***}x^{**}x^{**}} \tag{3.43}$$

$$\frac{1}{R_e^2}(- \psi^*_{z^{***}} \psi^*_{x^{**}x^{**}} + \psi^*_{x^{**}} \psi^*_{x^{**}z^{***}}) + p^*_{z^{***}} = - \rho^{***}$$

$$- \frac{G}{R_e^4} \psi^*_{x^{**}x^{**}x^{**}} - \frac{G}{R_e^2} \psi^*_{x^{**}z^{***}z^{***}} \tag{3.44}$$

$$\psi^*_{z***}\ \rho^{***}_{x**} - \psi^*_{x**}\ \rho^{***}_{z***} + \psi^*_{x**} = \frac{1}{R_e^2}\ \rho^{***}_{x**x**} + \frac{1}{G}\ \rho^{***}_{z***z***} \tag{3.45}$$

where $R_e = q/\nu$.

In the limit as $R_e \to \infty$ Eqs. (3.43) - (3.45) reduce to:†

$$\psi_z\ \psi_{zx} - \psi_x\ \psi_{zz} + p_x = G\ \psi_{zzz} \tag{3.46}$$

$$p_z = -\ \rho \tag{3.47}$$

$$\psi_z\ \rho_x - \psi_x\ \rho_z - \psi_x = \frac{1}{G}\ \rho_{zz} \tag{3.48}$$

which constitute the required inner equations for the limit $R \to 0$, $F \to 0$, $R_e \to \infty$ and $F/R^{2/3} \to 0$. Equations (3.46) - (3.48) must now be solved with the solution (3.35) as the upstream boundary condition.

It is interesting to note that Eqs. (3.46) - (3.48) include the outer equations, and hence for those regions in which the wall influence is absent, the flow only depends on the parameter G. Any experimental flow at a given value of G is therefore self similar with respect to the coordinates (x^{**}, z^{***}). The experiments described in Section 5 verify this result very well (Fig. 5.1).

The reason why R_e should be large for the above equations to be valid is perhaps best seen by examining the width-to-length ratio of the region of nonuniformity. The physical width of the region δ is of order $F^{1/2}\ell$ and the physical length x_c is of order $F^{3/2}\ell/R$. Hence

$$\frac{\delta}{x_c} = \frac{F^{1/2}R}{F^{3/2}} = \frac{R}{F} = \left(\frac{D}{\nu}\right)^{1/2} \cdot \frac{\nu}{q} = \frac{1}{G}\ \frac{1}{R_e}$$

and hence $\delta/x_c \ll 1$ only if R_e is large. It should be noted that with respect to the outside scale x^*, z^{**} this region is very small as $F/R^{2/3} \to 0$. However, in an actual reservoir

$$x_c = \left(\frac{q}{\nu}\right)^{3/2}\ \left(\frac{\nu D}{eg}\right)^{1/4} = 0(10^6)\ \text{ft.}$$

† Asterisks have been dropped for convenience.

and the inertial region may occupy the whole of the reservoir. When R_e is small, Eqs. (3.46) - (3.48) are nowhere valid, and the flow near the sink is governed by the full Navier Stokes equations.

As in the case of flow at the leading edge of a flat plate, Eqs. (3.46) - (3.48) cannot be expected to hold very near the sink. For large R_e this non-uniformity may be examined without actually solving Eqs. (3.46) - (3.48). Consider distances closer than $0(F^{1/2})$. Let

$$x^{***} = \frac{x^*}{F^{1/2}} = \frac{Fx^{**}}{R} \tag{3.49}$$

then Eqs. (3.43) - (3.45) become

$$\psi^*_{z^{***}}\ \psi^*_{z^{***}x^{***}} - \psi^*_{x^{***}}\ \psi^*_{z^{***}z^{***}} + p^*_{x^{***}}$$

$$= \frac{G}{R_e}\left\{\psi^*_{z^{***}x^{***}x^{***}} + \psi^*_{z^{***}z^{***}z^{***}}\right\} \tag{3.50}$$

$$- \psi^*_{z^{***}}\ \psi^*_{x^{***}x^{***}} + \psi^*_{x^{***}}\ \psi^*_{x^{***}z^{***}} + p^*_{z^{***}}$$

$$= - \rho^{***} - \frac{G}{R_e}\left\{\psi^*_{x^{***}x^{***}x^{***}} + \psi^*_{x^{***}z^{***}z^{***}}\right. \tag{3.51}$$

$$\psi^*_{z^{***}}\ \rho^{***}_{x^{***}} + \psi^*_{x^{***}}\ \rho^{***}_{z^{***}} - \psi^*_{x^{***}}$$

$$= \frac{1}{GR_e}\left\{\rho^{***}_{x^{***}x^{***}} + \rho^{***}_{z^{***}z^{***}}\right\} \tag{3.52}$$

Hence the flow at the origin is inviscide to 1st order in $1/R_e$ and the equations are given by†

$$\psi_z\ \psi_{zx} - \psi_x\ \psi_{zz} + p_x = 0 \tag{3.53}$$

$$- \psi_z\ \psi_{xx} + \psi_x\ \psi_{xz} + p_z = - \rho \tag{3.54}$$

$$\psi_z\ \rho_x + \psi_x\ \rho_z - \psi_x = 0 \tag{3.55}$$

† Asterisks have been omitted.

The solution of Eqs. (3.53) - (3.55) depends on the solution of Eqs. (3.46) - (3.48) and vice versa. Neither admits a similarity solution, nor are they tractable by linear methods. For the very special upstream condition of uniform flow Kao (1970) has solved Eqs. (3.53) - (3.55). Here a slip line is required at the edge of the layer. The velocity along this slip line remains constant and of order $q^{\frac{1}{2}}/(\varepsilon g)^{\frac{1}{4}}$ which means that around this slip line there is a backward growing viscous-buoyancy layer of thickness $O(R^{1/3})$. However, at the moment it is a matter of speculation whether these two layers could be matched onto a solution of Eqs. (3.46) - (3.48).

Below, Eqs. (3.46) - (3.48) are solved approximately by an integral method. For $x^{**} = \infty$, the withdrawal layer thickness δ is matched to the inner limit of the outer solution, and at $x^{**} = 0$ the boundary condition chosen is $\delta^{***} = 1$, consistent with the above speculations. This is further discussed in Section 5, but as long as the solution is not very sensitive to the exact numerical value at $x^{**} = 0$, this procedure should lead to satisfactory results.

Structure of the Withdrawal Layer - Inner Solution

In the previous section it was shown that for the flow near the sink, Eqs. (3.46) - (3.48) must be solved using Koh's (1966b) similarity solution as the upstream boundary condition at $x^{**} = \infty$. For convenience the equations are reproduced below, omitting the asterisks.

$$u_x + w_z = 0 \tag{3.56}$$

$$u\,u_x + w\,u_z + p_x = G\,u_{zz} \tag{3.57}$$

$$p_z = -\rho \tag{3.58}$$

$$u\,\rho_x + w\,\rho_z - w = \frac{1}{G}\,\rho_{zz} \tag{3.59}$$

$$\int_{-\infty}^{\infty} u\,dz = -1 \tag{3.60}$$

where $G = (\nu/D)^{\frac{1}{2}}$.

This set of equations does not appear to possess a similarity solution satisfying the required boundary conditions, so to obtain at least an approximation of the layer growth, the above equations are solved using an integral method.

Examination of the experimental data obtained by Koh (1966b) shows that for a particular discharge, the velocity profiles are self similar even in the inner region. In Section 5 this is confirmed in the more general coordinates (x^{**}, z^{***}). This suggests postulating a velocity variation given by

$$u(x,z) = a(x)\ f\left(\frac{z}{\delta(x)}\right)$$

as is done in the Polhausen technique, and obtaining f from the upstream flow. However, in that solution $\rho \sim 1/z^{***}$ for large z^{***}, which is non-integrable. To be able to apply an integral method the equations must therefore be premultiplied by a weighting function. This is more easily done if f is an analytic function expressed in terms of elementary functions. It is therefore convenient to let

$$u(x,z) = \frac{-a(x)}{\pi}\ \frac{(1-k\ z^2\delta^{-2})}{(1+z^2\delta^{-2})^3} \tag{3.61}$$

$$\rho(x,z) = \frac{-b(x)}{\pi}\ \frac{z\delta^{-1}}{(1+z^2\delta^{-2})} \tag{3.62}$$

and by continuity

$$w = \frac{-\delta' z a}{\pi\delta}\ \frac{1-k\ z^2\delta^{-2}}{(1+z^2\delta^{-2})^3} \tag{3.63}$$

The value of k is then chosen to yield the best fit to Koh's (1966b) solution. The unknown functions are $a(x)$, $b(x)$ and $\delta(x)$.

Equations (3.61) - (3.63) are now substituted into the following integral form of Eqs. (3.57) - (3.60):

$$\int_0^\infty \frac{1}{(1+z^2\delta^{-2})}\ \{(uu_x + wu_z)_z - \rho_x - G\ u_{zzz}\}\ dz = 0 \tag{3.64}$$

$$\int_0^\infty \{u\rho_x + w\rho_z - w - \frac{1}{G}\ \rho_{zz}\}\ dz = 0 \tag{3.65}$$

$$\int_0^\infty u\,dz = -1 \tag{3.66}$$

The factor $1/1+z^2\delta^{-2}$ is included in Eq. (3.64) to make ρ_x integrable. Carrying out the integration yields two ordinary differential equations and one algebraic equation for a, b and δ, viz.

$$\frac{-aa'}{\pi}\left(\frac{6}{7}+\frac{k}{21}-\frac{k^2}{105}\right)+\frac{1}{2}\,\delta b' = \frac{-Ga}{5\delta^2}\,(11k+32) \tag{3.67}$$

$$\frac{a\delta b'}{\pi}\left(\frac{1}{6}-\frac{k}{12}\right)+\frac{a\delta\delta'}{4}\,(1-k) = \frac{1}{G}\,\frac{b}{\delta} \tag{3.68}$$

$$a\delta = \frac{8}{3-k} \tag{3.69}$$

The prime interest is to determine the growth of the layer, that is, to find δ as a function of x. Elimination of a and b from Eq. (3.67) - (3.69) yields one second order equation for δ viz.

$$(\alpha_1\,\delta^5-\alpha_2\,\delta)\,\delta''+(\alpha_1\,\delta^4+3\alpha_2)\,(\delta')^2+\alpha_3\,\delta'+\alpha_4 = 0 \tag{3.70}$$

where

$$\alpha_1 + \frac{(1-k)}{(3-k)}$$

$$\alpha_2 = \frac{128}{3}\,\frac{1}{\pi^2}\,\frac{(2-k)}{(3-k)^2}\left(\frac{6}{7}+\frac{k}{21}-\frac{k^2}{105}\right)$$

$$\alpha_3 = \frac{64}{\pi}\,\frac{1}{(3-k)^2}\left(\frac{6}{7}+\frac{k}{21}-\frac{k^2}{105}\right)\frac{1}{G}+\frac{16}{5\pi}\,\frac{(2-k)}{(3-k)^2}\,(11k+32)G$$

$$\alpha_4 = \frac{8}{5}\,\frac{11k+32}{3-k}\,.$$

The boundary condition is that $\delta = 1$ when $x = 0$, and that δ asymptotes to the solution of Eq. (3.70) with the inertia terms set to

zero. The method of solution was to reduce this boundary value problem to an initial value problem with the initial values of δ, specified at some large x, being evaluated from an asymptotic solutions of Eq. (3.70). The equation was then integrated with a standard fifth order Runga Kutta algorithm available in the computer center library under the call name RK5.

To shorten the numerical integration the asymptotic series for large x of $\delta(x)$ was computed by Imberger (1970) to the fifth term. The series he found is given by

$$\delta = K_1 x^{1/3} + K_2 x^{-1/3} + K_3 x^{-2/3} + K_4 x^{-1} + K_5 x^{-4/3} + \text{---} \qquad (3.71)$$

where

$$K_1 = \left(\frac{9\alpha_4}{\alpha_1}\right)^{1/6}$$

$$K_2 = \frac{3\alpha_3}{4\alpha_1 K_1^4}$$

$$K_3 = \text{arbitrary}$$

$$K_4 = \frac{2}{3\alpha_1 K_1^5}\left\{\frac{1}{9}\alpha_1 K_1^4 K_2^2 + \frac{K_2 \alpha_3}{3} - \frac{5}{9} K_1^2 \alpha_2\right\}$$

$$K_5 = \frac{1}{14 K_1^5 K_2}\left\{6K_3 \alpha_3 - 22\alpha_1 K_1^4 K_2 K_3\right\} .$$

The similarity of the series (3.71) with that proposed by Koh (1966b) should be noted. However, the above contains extra terms which are all dependent on the arbitrary constant K_3. This free parameter is necessary as nothing has been said about the behavior of the solution at $x = 0$. Similarly Koh's (1966b) proposed series should have an equivalent arbitrary coefficient. An analogous problem is encountered in rotating flow problems (Smith (1969)).

That this arbitrary coefficient must be present can also be inferred by noting that the independent variable x is absent from Eq. (3.70). Hence if $\delta = g(x)$ is a solution then so is $\delta = g(x + c)$. A formal

substitution of $x^* = x + c$ into the series (3.71) yields the same series with K_3 replaced by $K_3 - cK_1/3$, but K_1 and K_2 remain unchanged.

The arbitrary constant K_3 was used to convert the boundary value problem into an initial value problem. In other words, K_3 was fixed, δ and δ' were computed from the series (3.71) for a sufficiently large value of x, and the Eq. (3.70) was integrated numerically to zero. The constant K_3 was adjusted until $\delta = 1$ at $x = 0$.

Inspection of Eq. (3.70) shows that the equation has a singular point when

$$\delta = \delta_c = \left(\frac{\alpha_2}{\alpha_1}\right)^{1/4} .$$

The slope of δ becomes infinite at this value of δ and the assumption of a similar profile can no longer adequately describe the flow here.

The value of k was chosen to make $\delta_c = 1$ and $K_1 = 3.2$ the value obtained by Koh (1966b) for the present definition of δ. With $k = 1/3$ the values K_1 and δ_c are 3.15 and 1.17.

Figure 3.4 shows a comparison of the velocity profile given by the integral curve (3.61) and that obtained by Koh (1966b). The variation of δ with x for $G = 29.0$ and $G = 2.34$ is shown in Fig. 3.5. This corresponds to a salt and heat stratification, respectively.

Summary of the Layer Structure - Composite Solution for δ

The overall layer structure is summarized in Fig. 3.6. The solutions to region I, II and VI have been found explicitly. In region III an integral method was used to obtain the layer thickness. The solutions to regions IV and V are not known and further work is required.

The composite expansion δ was obtained by adding the inner and outer solution and subtracting $K_1 x^{1/3}$, the part which is common to both. This is shown in Fig. 3.7 and Fig. 3.8 for heat and salt stratification. Unfortunately the wall spacing in the outer problem does not scale with $F^{1/2}$, so that the wall "moves," as F changes in an inner (x^{**}, z^{***}) coordinate system. The advantage of this coordinate system, however, is that near the sink the solution only depends on G.

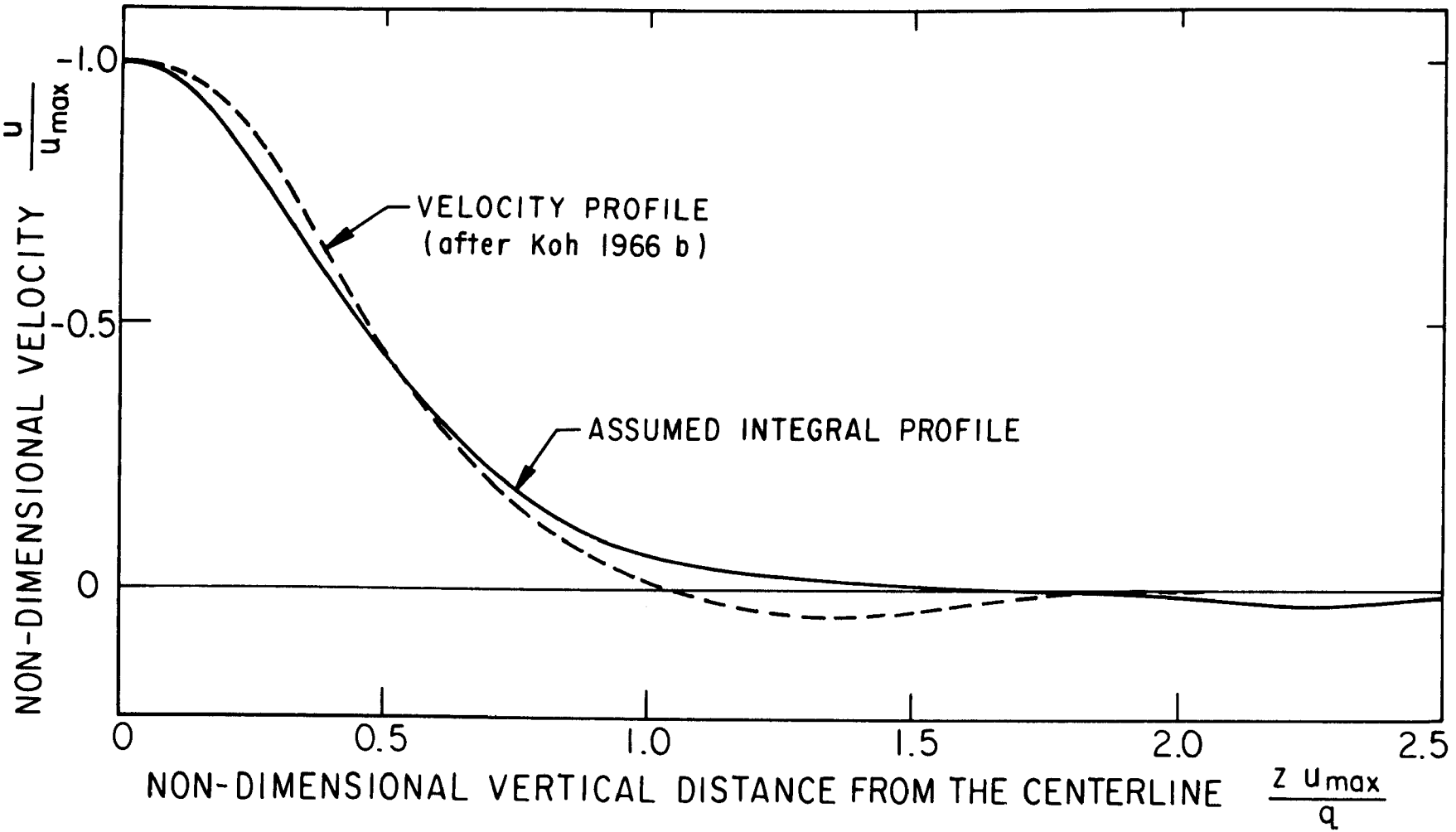

FIG. 3.4 INTEGRAL SOLUTION VELOCITY PROFILE

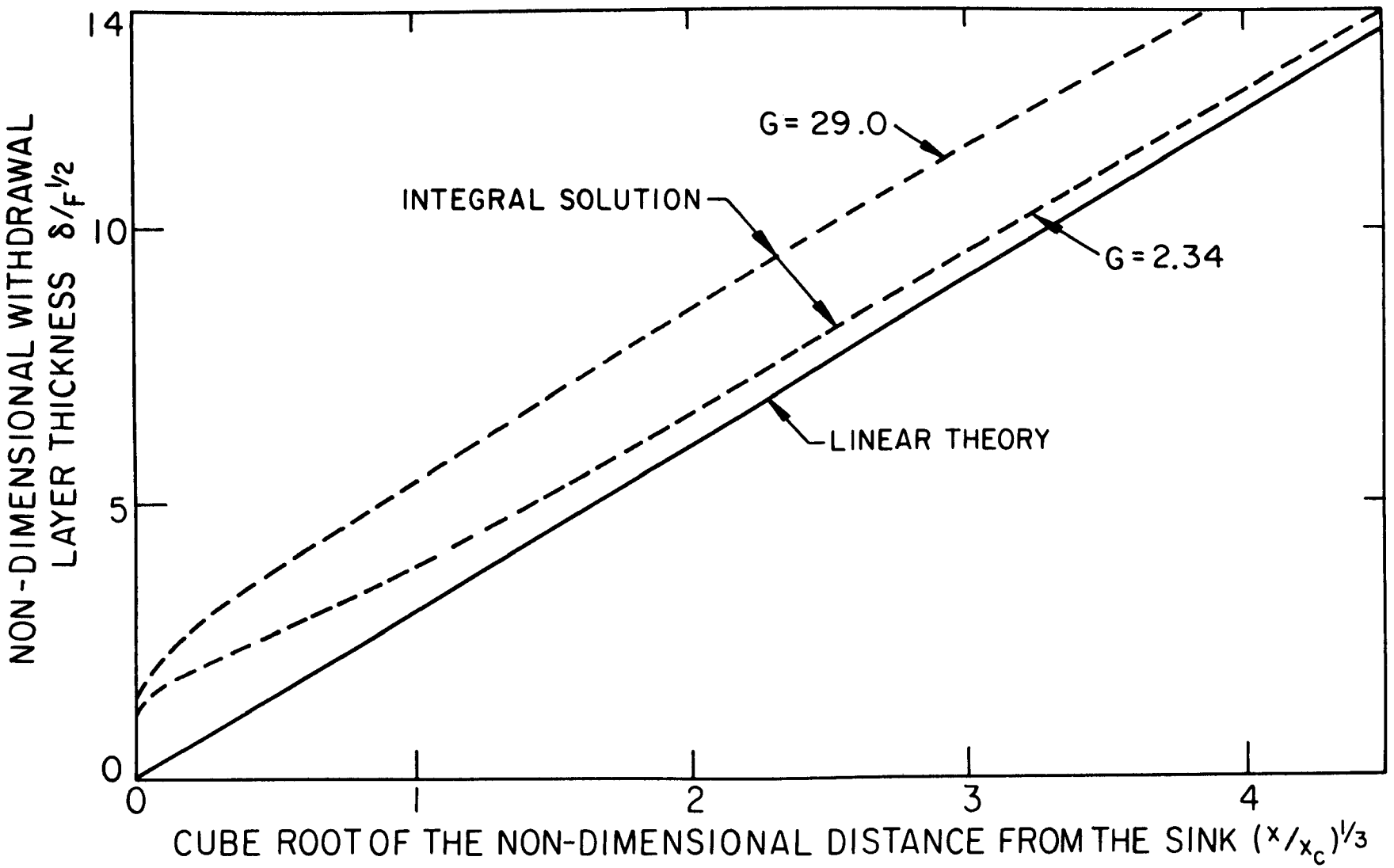

FIG. 3.5 THEORETICAL WITHDRAWAL LAYER THICKNESS

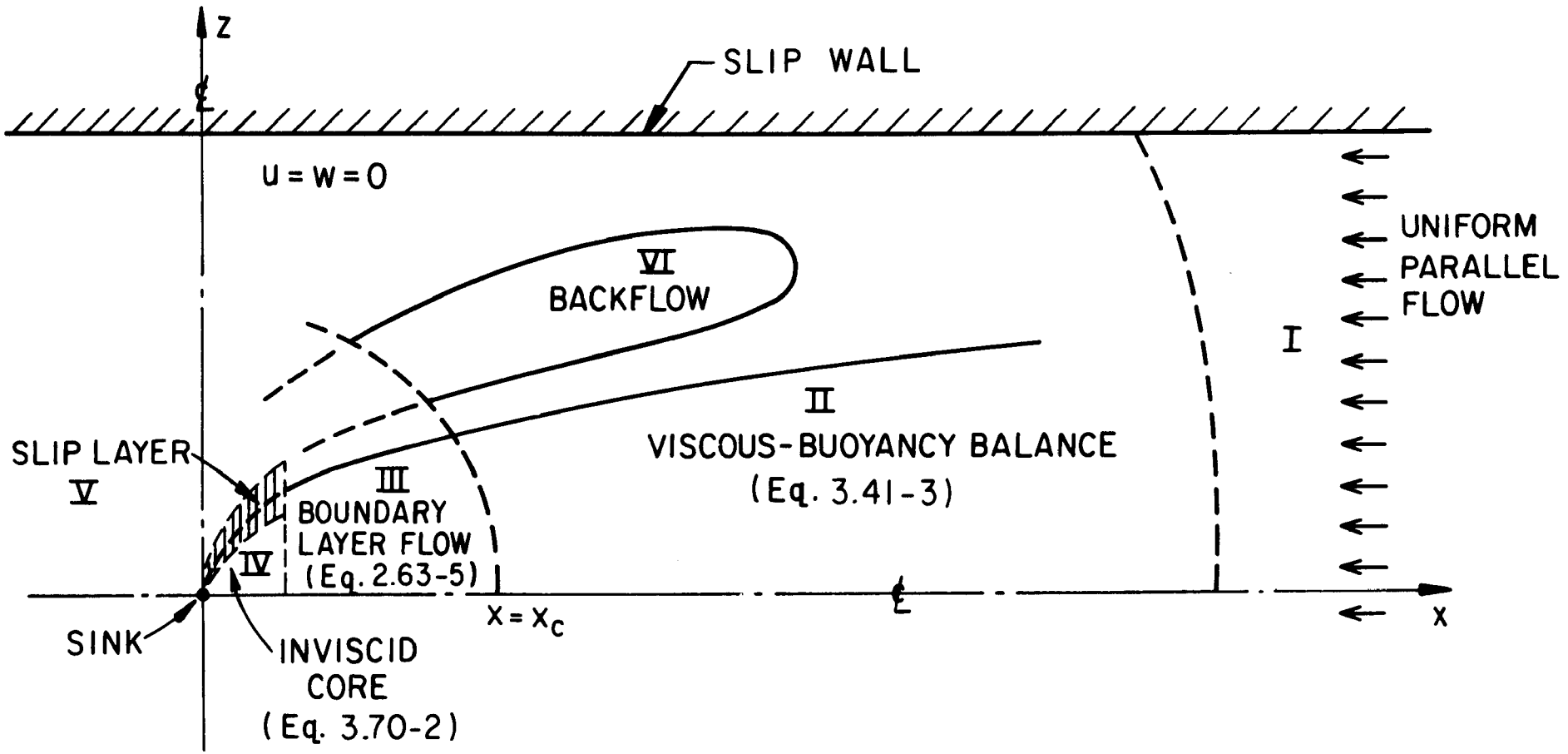

FIG. 3.6 STRUCTURE OF THE WITHDRAWAL LAYER

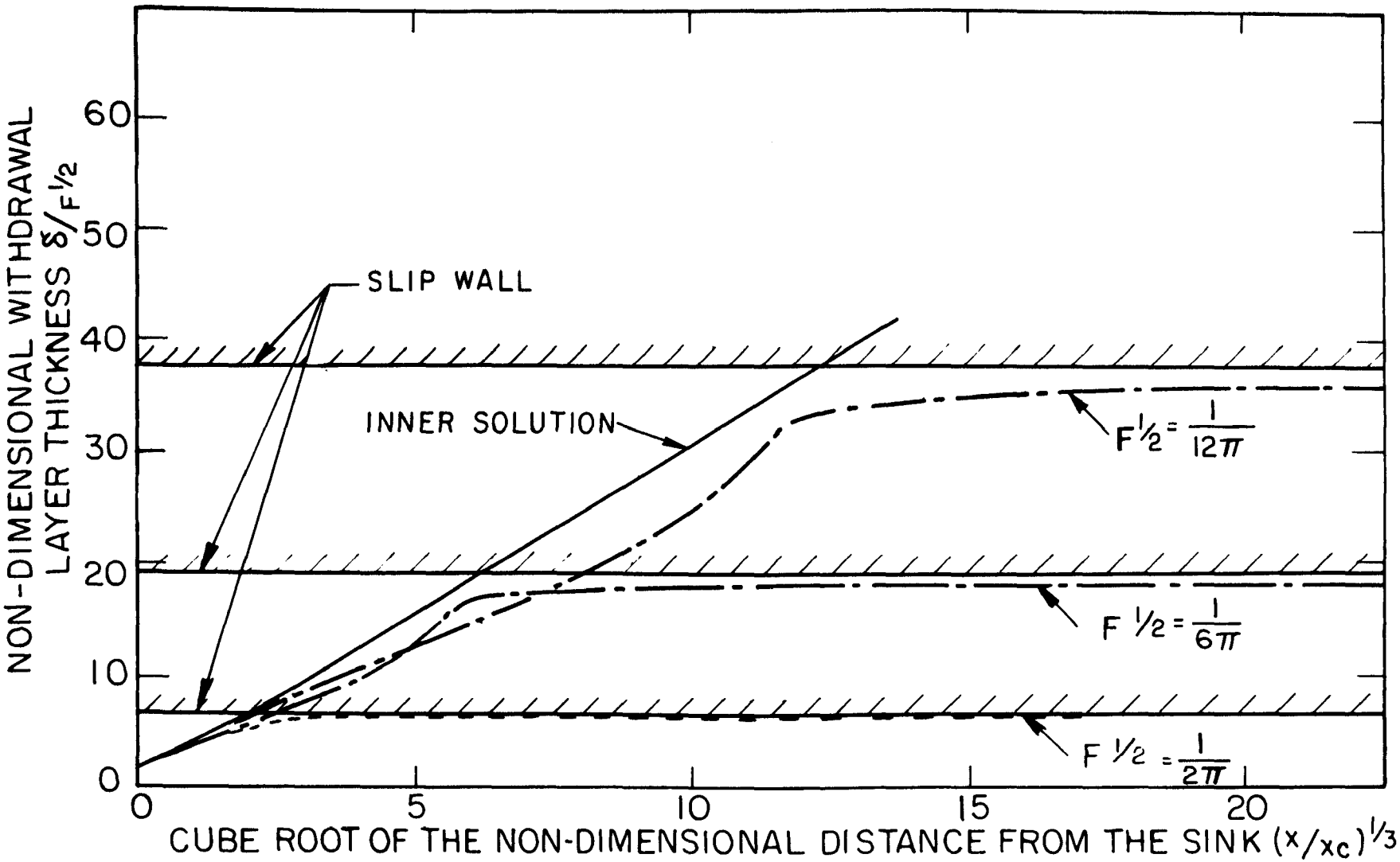

FIG 3.7 THE COMPOSITE SOLUTION G = 2.34

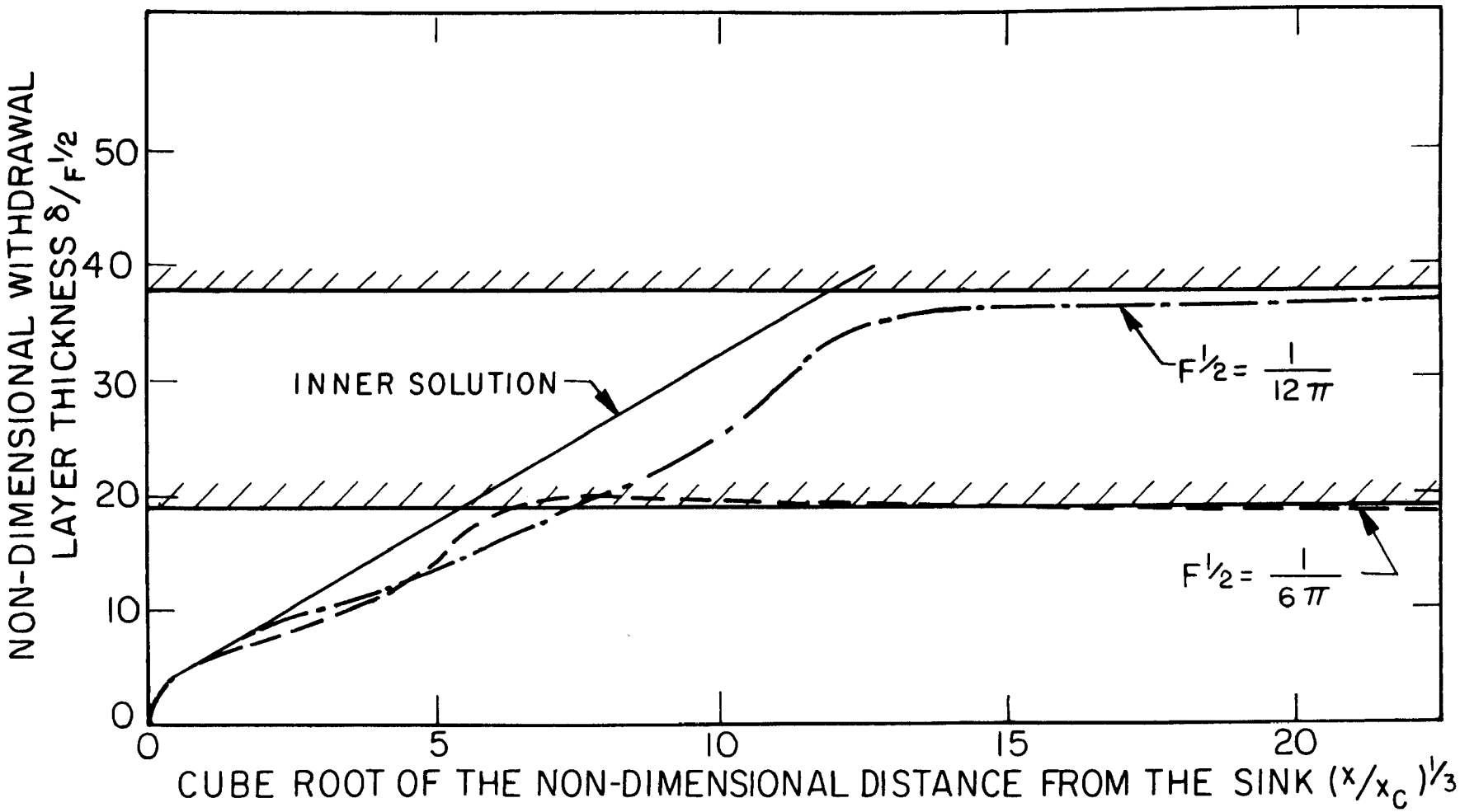

FIG 3.8 THE COMPOSITE SOLUTION G = 2 9.0

4. EXPERIMENTAL OBJECTIVES AND APPARATUS

The analytic considerations of the previous chapter showed that the dynamics of the flow due to a withdrawal from a stratified fluid may be represented in a scaled coordinate system. In this coordinate system the only parameters remaining are the square root of the Schmidt number and the depth of the tank. Hence, when viewed from this reference axes all flows in a fluid of constant Schmidt number are dynamically similar.

Review of Previous Experimental Data

The experimental results obtained by Koh (1966b) are shown re-plotted in Fig. 4.1. Each line represents the line of best fit to the experimental points of a single run. The withdrawal layer thickness has been reduced by 0.9, from that used by Koh (1966b), to correspond to the definition used in this report. It is seen that the two cases, salt and heat stratification, fall roughly into two separate lines on the graph. For the heat stratified mixture, the results show little scatter and good agreement with the theoretical predictions. However, when salt is used, although the agreement is reasonable for small values of x/x_c, the data diverges somewhat for larger values. The explanation for this is probably twofold.

(a) The data for large $(x/x_c)^{1/3}$ are from the rear of the tank, where end effects are probably affecting the data. This suspicion is reinforced by the fact that q_f, the forward discharge, varied considerably from one station to the next for the same run.

(b) The definition of δ as that point where the velocity is zero is very difficult to measure (Section 5.1). This is especially so for larger values of $(x/x_c)^{1/3}$ where the velocities are very slow. This could account for some of the scatter.

Experimental Objectives

In view of the above, an experimental program was carried out in a facility much larger than that used by Koh (1966b) to repeat and extend his data. In this way the transient effects due to a finite sized tank were kept to a minimum. All the experiments were conducted in a salt stratified solution, rather than one with a temperature gradient, to avoid the side walls induced convection boundary layers. A perfectly still reservoir is essential, since the velocities in the withdrawal layers are extremely small. All the experiments were carried out in the same 42' long glass tank. For each stratification about six to nine runs at different discharges could be made before the dye contamination affected visibility. Four different stratifications were used.

The Experimental Tank

The experiments were performed in a 42 foot long by 4.0 foot deep by $1\frac{1}{2}$ foot wide tank of the University of California Richmond Field

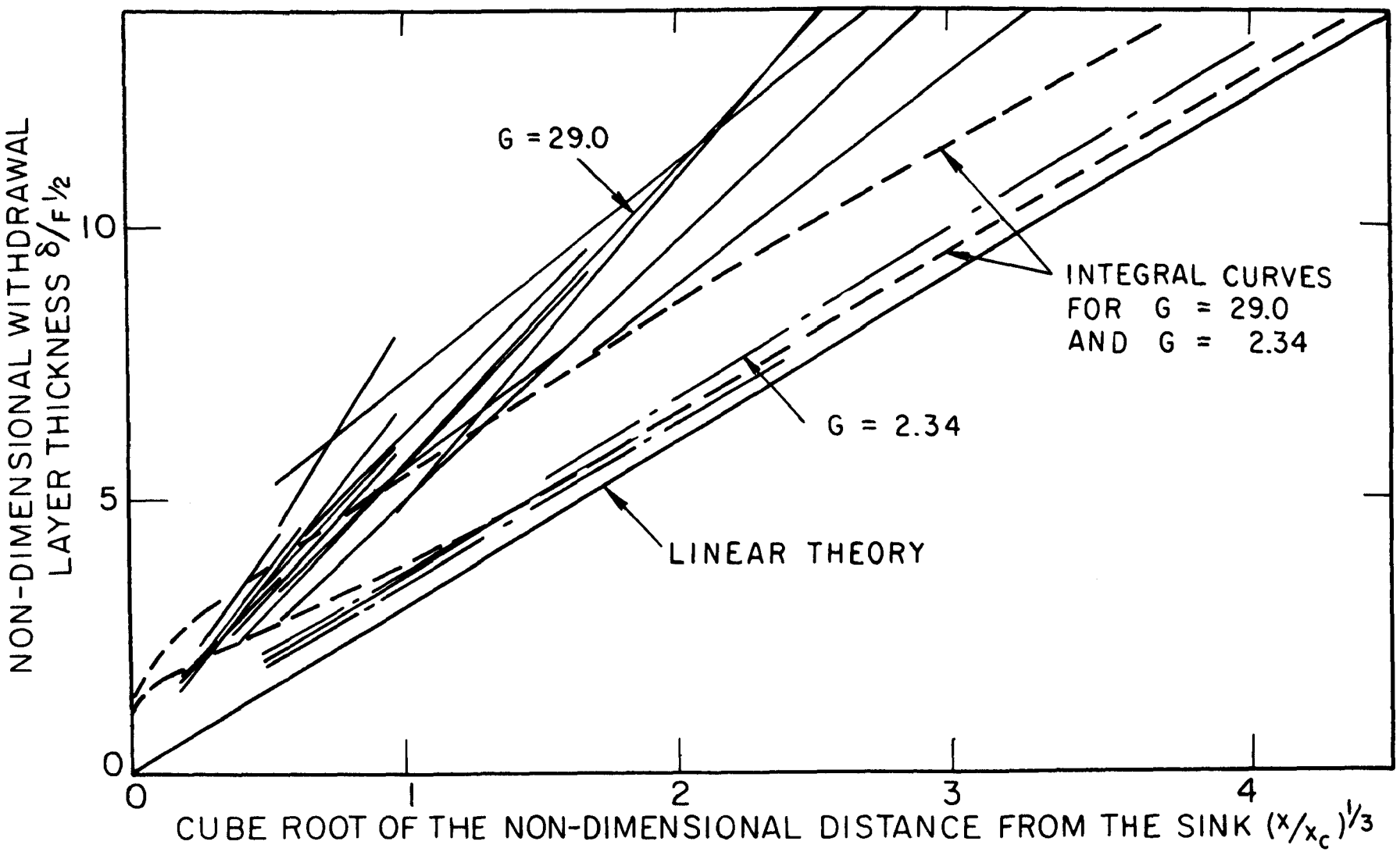

FIG 4.1 EXPERIMENTAL DATA AFTER KOH 1966b.

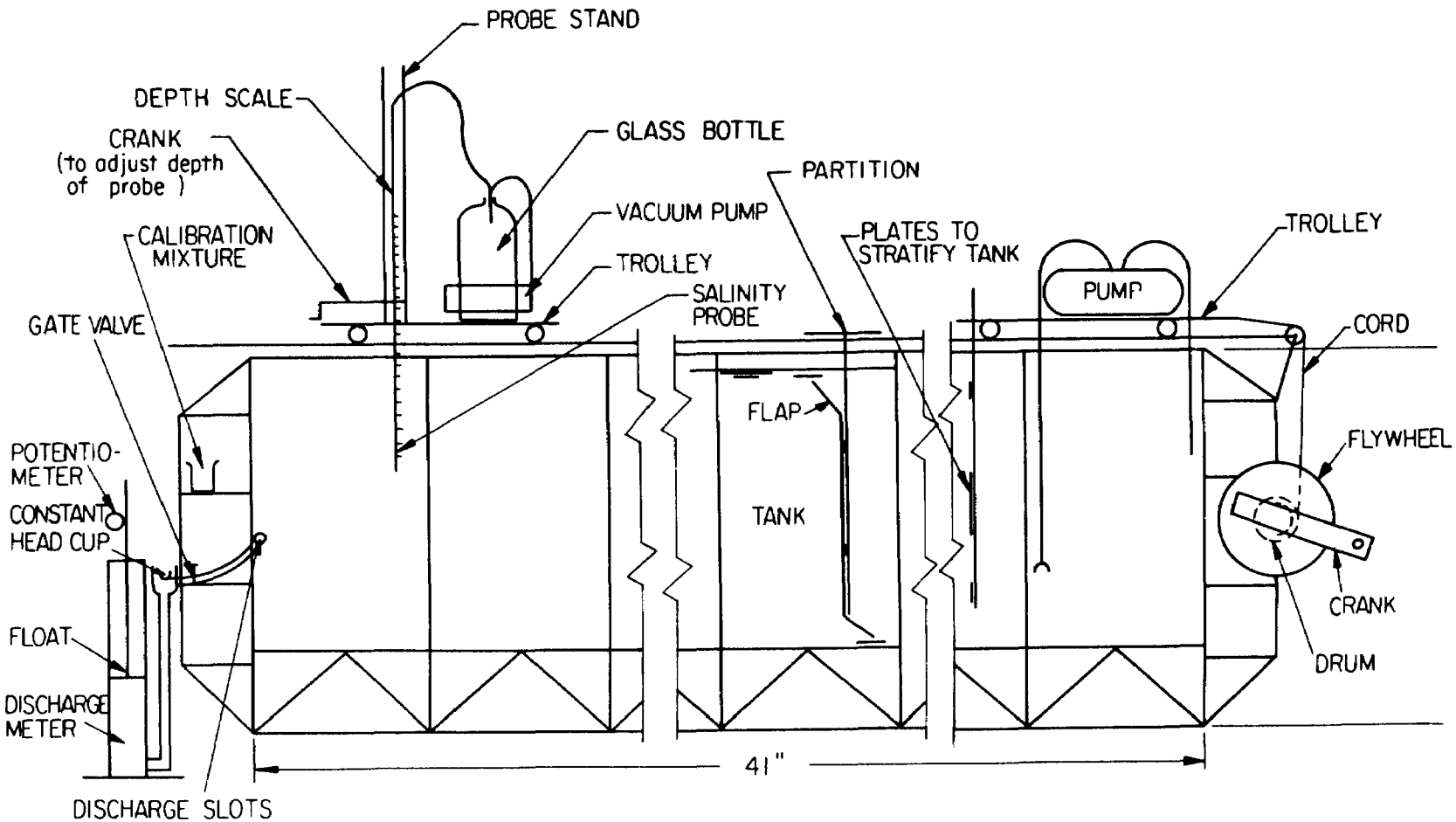

FIG. 4.2 GENERAL LAYOUT OF EXPERIMENTAL TANK

Station. The walls and bottom were constructed of tempered plate glass. The tank is shown schematically in Fig. 4.2 and a photograph of the general layout is given in Fig. 4.3.

Two trolleys were placed on rails on top of the tank. One served as a mounting platform for the stratifier while the other held the salinity probe and the associated vacuum pump. The discharge facility was located at one end. Mounting the salinity probe on the trolley allowed the same probe to be used to measure the density gradients throughout the channel, and the salinity of the discharging water.

The Salinity Probe

To measure the concentration of salinity a conductivity probe was built and mounted on one of the trolleys. The design of the probe was similar to those used successfully at the Delf Hydraulics Laboratory, as observed by the second author during a visit in 1968. The probe was used to measure the background near linear salinity profile. The salt used was an ordinary kiln dried commercial product. No attempt was made to measure the very small deviations of salinity due to the motion.

The probe and its associated circuit are shown in Fig. 4.4. A photograph of its mounting on the trolley is given in Fig. 4.3(a). The probe was constructed from a thin plastic tube, which was closed to a fine hole of a diameter 0.040" at one end, after the electrodes had been inserted. The two platinum electrodes, one on the inside, one around the outside of the tube, created an electric field which had all its field lines passing through the fine hole at the tip of the probe (Fig. 4.3(b)). The other end of the 4' tube was connected to a small vacuum pump which sucked fluid through the small opening at the tip. The actual volume sucked in amounted to a few drops per second, but the velocity induced within the contraction was quite high. In this way the fluid is replaced almost instantaneously in the contracted opening as the density fluctuates in front of the probe. The fact that the electric field is concentrated in the opening, as well means that the probe measures the salinity of the water in the opening only, and the rapid change of fluid there makes the probe respond very quickly to any density change. The profiles could therefore be obtained quite rapidly.

To calibrate the probe, a large bottle was filled with water and salt was added to make a mixture of a concentration corresponding to the maximum salinity anticipated. This served as the stock solution. The specific gravity of the mixture was then measured with a hydrometer. This method proved to be much more accurate than weighing out a certain amount of salt, adding it to water and then neglecting the volume of the salt. After the tank had been stratified a series of 5 dilutions of the stock solution were prepared so that their specific gravity covered the range of the tank stratification. These solutions

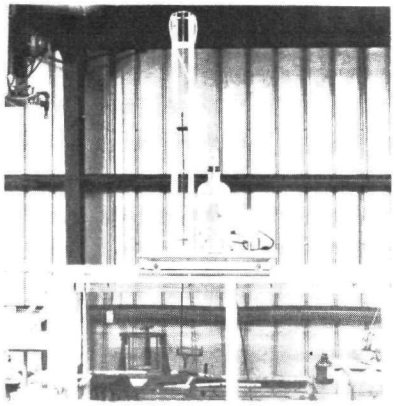

(a)

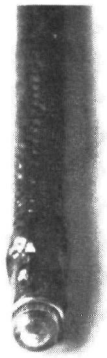

(b)

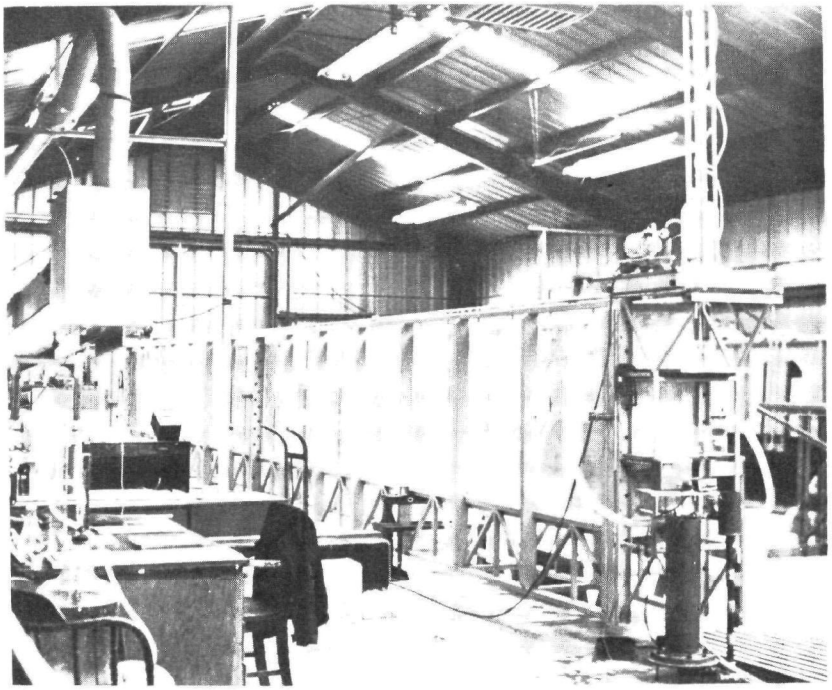

(c)

Fig. 4.3 Photographs of Experimental Equipment

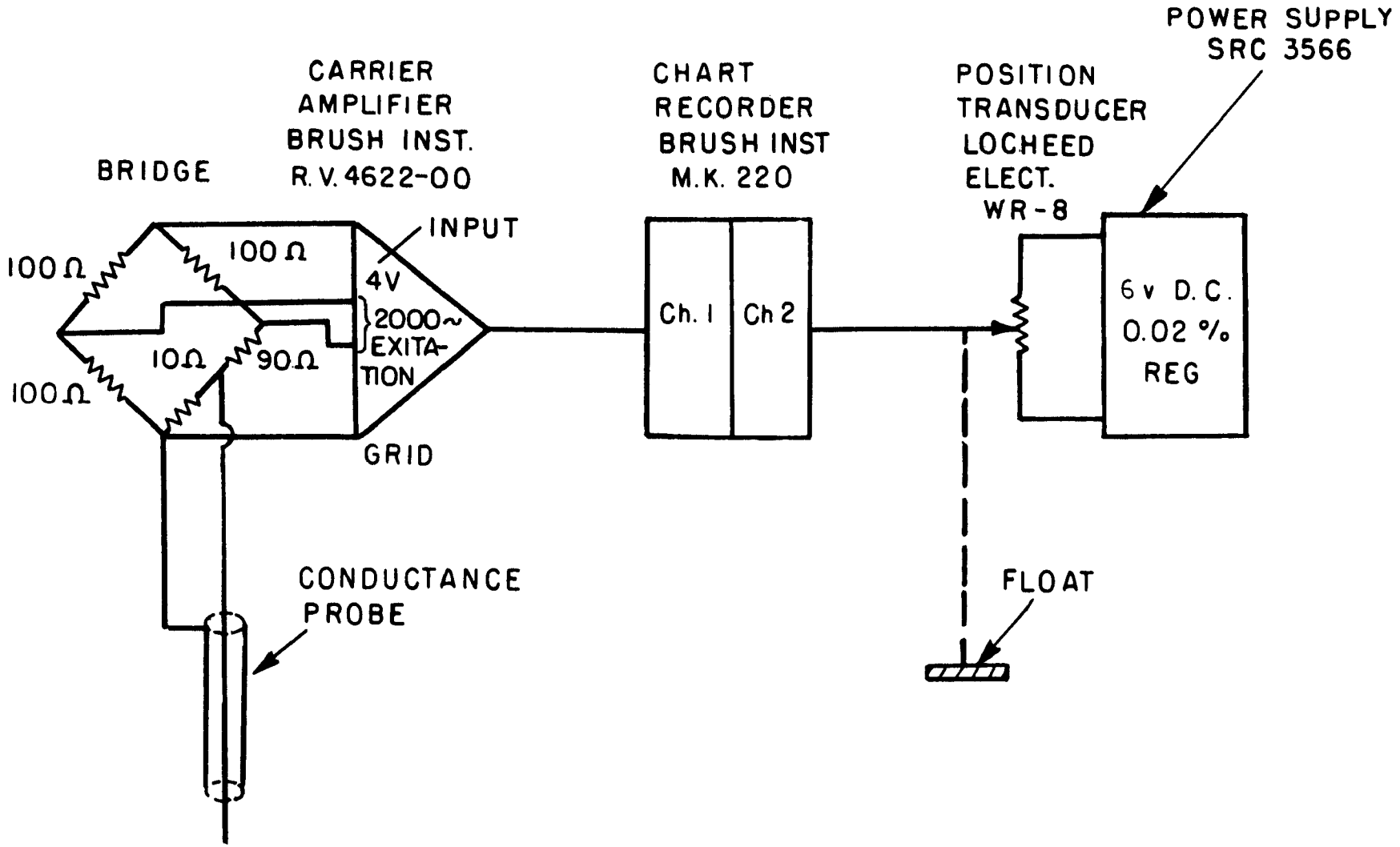

FIG 4-4 CONDUCTANCE PROBE
AND FLOAT CIRCUIT

were then used to calibrate the probe after they had reached the temperature of the water in the tank.

The difference of the temperature of tank water and the temperature at which the specific gravity was measured was always small, and since only the density gradient of the tank water is required, no compensation was made for this temperature difference. The calibration curves were nearly linear, with a slight decrease in sensitivity for the larger concentrations. Figure 4.5(a) shows a typical calibration curve. Over a day no drift was noticed. The probe was, however, recalibrated directly before a density profile was taken.

Establishment of a Linear Density Profile

The aim was to stratify the tank water so that the density of the salt water mixture varied linearly with depth. The technique used is essentially that reported by Clark et al., (1967).

The whole tank was filled with fresh water, which was allowed to come to room temperature. A little detergent was added to reduce the formation of bubbles on the side of the glass which would otherwise hamper the visibility. A gated partition was then introduced vertically into the center of the tank. The partition consisted of a piece of plywood with 9" hinged flaps at the bottom and top (Fig. 4.2). The partition was sealed to the glass walls with a soft rubber spacer. This was sufficient to stop any transfer of water from one side to the other.

The appropriate amount of salt was then stirred into one half of the partition tank. To facilitate mixing the water was pumped from the bottom to the top. Once the mixture was uniform it was allowed to come to rest. The flaps of the partition were then opened very slightly to allow the salty water to flow beneath the fresh water and the fresh water to flow over the salty water. About 1/2 hour elapsed before the whole tank had a two layer stratification in it. The partition was then carefully removed.

To obtain a linear profile, a series of three plates, mounted on the trolley, were then briskly moved through the interface with a crank and pulley arrangement at the end of the tank. The largest plate moved directly through the interface while the two smaller ones stirred up the top and bottom layers. The wakes behind the plates created sufficient turbulence to allow mixing. The mixing smoothed out the interface, and after some adjustment of the position of the plates a very linear profile was obtained throughout the whole depth. Figure 4.2 shows the general layout of the pulley, trolley and the mounted plates. A typical density profile is given in Fig. 4.5(b), showing how the linearity holds right to the bottom and the free surface.

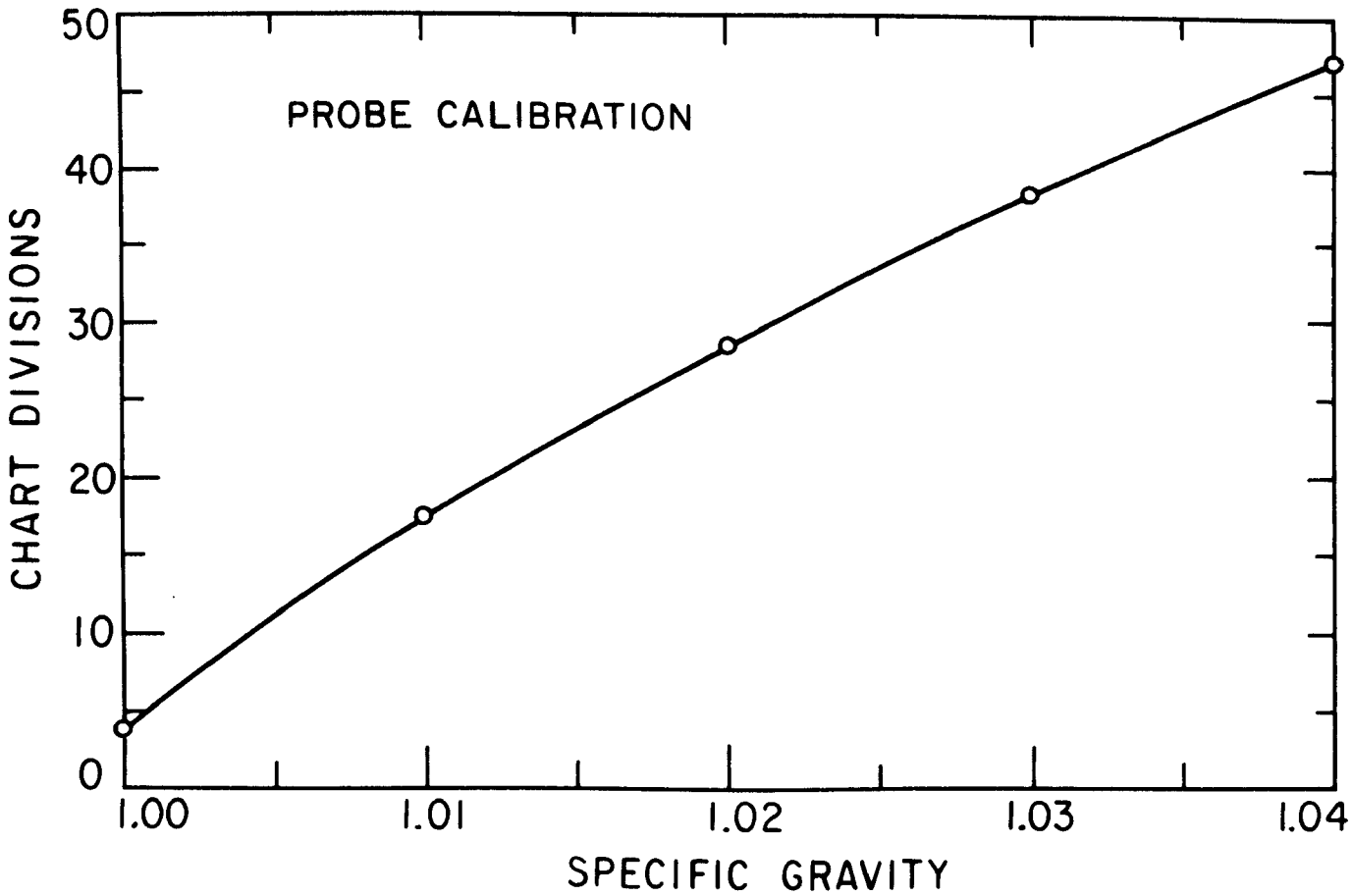

FIG. 4.5a EXAMPLE OF THE PROBE CALIBRATION

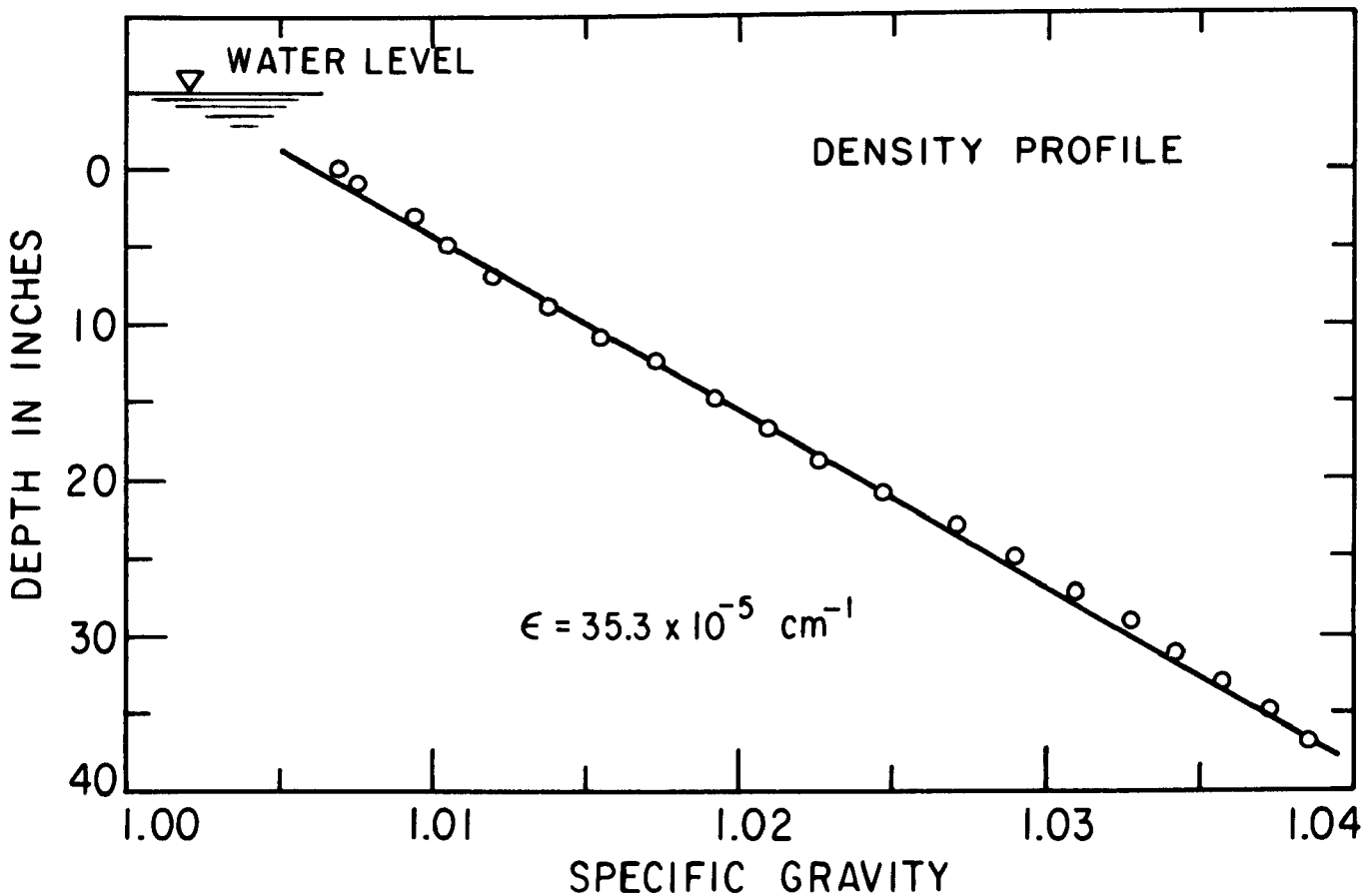

FIG. 4.5b EXAMPLE OF THE DENSITY PROFILE

The linear profile was very stable and would last unaffected for up to two weeks. Only at the surface and bottom was there a slight degeneration of the profile. At these extremes a layer of uniform density formed, the thickness of which increased with time. Most probably this was a temperature induced thermocline formation, as the room air conditioning did not accurately regulate the air temperature.

The Discharge Meter

To ensure constant monitoring of the discharge flowing out through the sink, a float type discharge meter was installed. This provided a means of adjusting the flow rate at a desired value and also to check its constancy as the experiment proceeded. The actual discharge used in the reduction of the data was, however, obtained by integrating the velocity profiles. The procedure used is explained in Section 5.

The flow from the slotted discharge tube was drained off from both sides of the tank into two plastic tubes. The two tubes were joined with a T section and the flow entered the discharge meter through a gate valve behind the T. The general layout is shown in Fig. 4.6 and the circuit used is depicted in Fig. 4.4. On entering the meter the water spilled over a cup down a pipe into the float chamber. The float motion activated a pully arrangement which in turn was monitored by a potentiometer.

The Dye Particles

The velocities induced by the fluid withdrawal are very small. The magnitudes are of the order of a few centimeters per minute. For such low velocities the only suitable method of measurement appears to be that of dyeing parts of the fluid and taking photographs of the deformation of the dye lines. The method used was to drop crystals of dye into the center of the tank at incremented distances from the sink. The purple streaks left in the wake of the falling crystals were then photographed repeatedly.

Of the dyes available, it was found that potassium permanganate was the most suitable for the present experiment. In contrast to organic dyes, this has the great advantage that it forms very fine intense streaks, the lifetime of which are only about 1/4 hour. Their rapid decay, which is due to oxidation, allows experiments to be repeated quite quickly.

The crystals used were about 1/4 - 1/2 mm. in diameter and care was taken to choose the most spherical ones only. Elongated or plate-like crystals form spiral paths which makes the velocity measurement more tedious. A razor blade was used to split larger crystals down to the required size and shape. The cutting of larger crystals also exposed fresh permanganate and much more intense streaks could be

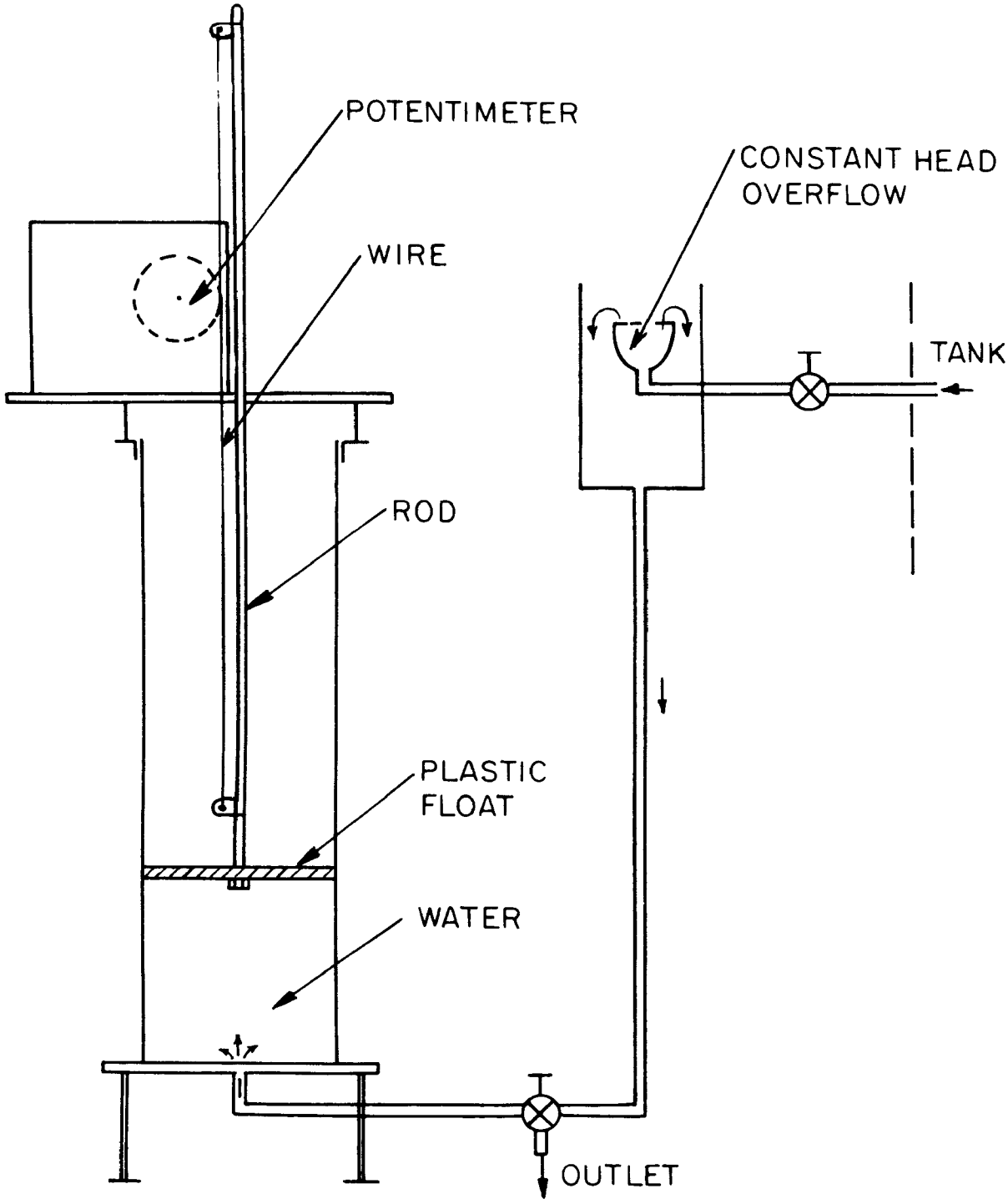

FIG 4.6 DISCHARGE METER

obtained. The crystals were placed, after cutting, into a small recess in a wooden dowling at a spacing of about 10 cm. This wooden bar was then placed on top of the tank. To introduce the crystals into the water, the bar was turned through 180°.

Photography and Timing

The motion of the dye streaks was recorded photographically. The time between photographs was fixed by tripping the camera shutter and the event marker on the recorder, simultaneously.

A Rolleflex S.L. 66 with an 80 mm lens was used throughout the experiments. The camera was fixed at one of two predetermined positions on a sturdy bench. The positions were so chosen that two photographs covered dye lines ranging in distance from 0 to 160 cm from the sink. The film used was Plus x professional and this was developed in D 76 to a characteristic value of .65. The negatives were then enlarged to 1/2 full scale on 11" x 14" Resisto-Rapid photographic paper. The plastic base of this paper makes it dimensionally stable. Successive photographs were aligned over each other, by aligning the images of a series of marks on the glass walls of the tank. The profiles were then pricked through with a sharp needle. A typical dye profile is shown in Fig. 4.7.

To fix the scale of the photographs a 200 cm measuring scale was held into the water at the center of the tank, where the dye lines normally are. This was then photographed. As the position of the bench and the tank remained fixed, this calibration had to be done only once. Also in this way parallax errors do not occur. The scale negative was used to set the enlarger to 1/2 full scale. The alignment marks on the side of the tank offered spot checks on the scale of each photograph.

The camera shutter was released with an electric relay, which also activated the event marker on the Brush recorder. The time between successive photographs was thus displayed by the distance between marks on the chart. Times from 10 to 200 sec. were typical. The accuracy, estimated by comparison with measurements with a stop watch, was near 0.3 sec.

Experimental Procedure

After the tank had been filled with tap water and allowed to stand for a day or so, the procedure for each experimental run was identical and may be summarized as follows:

(a) A small amount of Photoflo detergent was added and the tank water was stirred.

(b) The temperature of the room and the water was measured. The difference was kept less than 2°C.

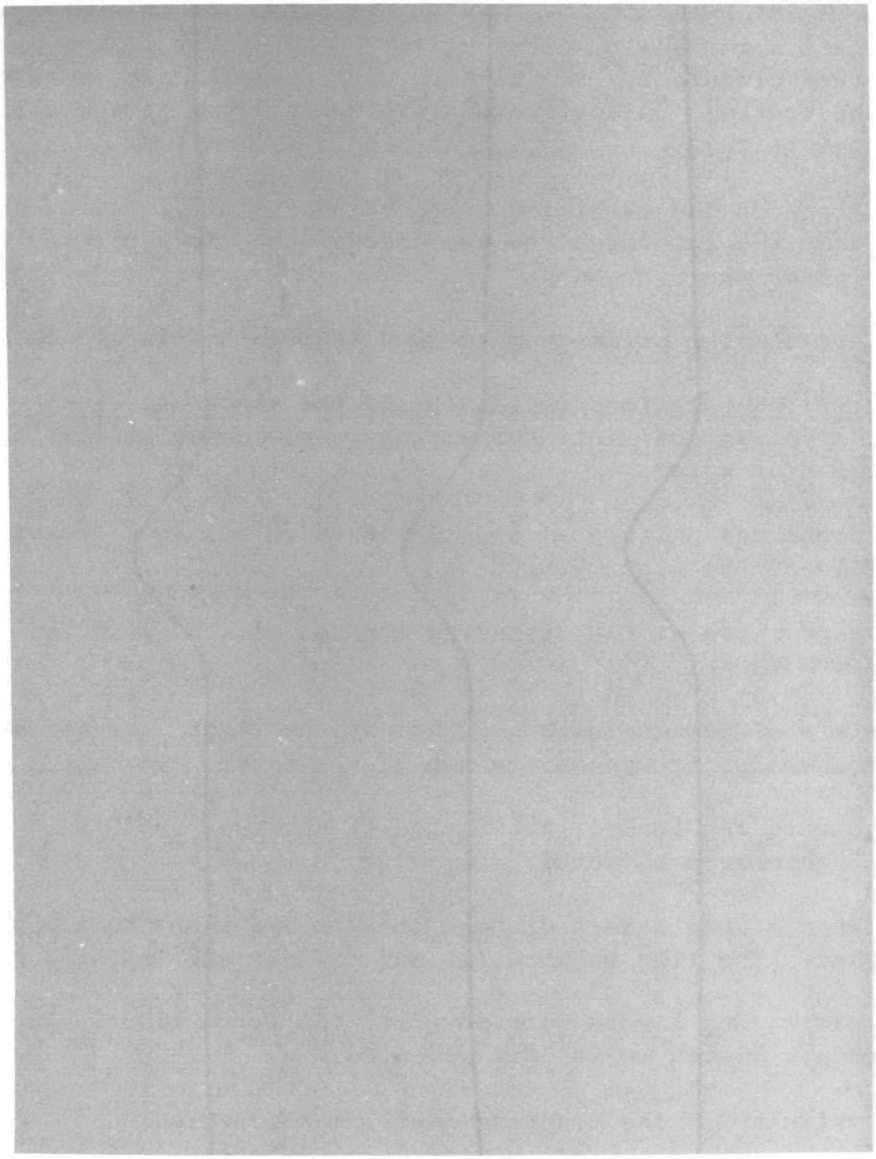

Fig. 4.7 Example of Dye Traces

(c) The wooden partition was inserted at the center of the tank.

(d) The required amount of salt was dumped into one side.

(e) The salt was mixed by first agitating the water with a broom and then circulating the mixture with a small pump, mounted on the trolley. After the mixture was uniform it was allowed to come to rest.

(f) The flaps on the partition were opened about 1". After about 1/2 hour the interface was continuous past the partition and the latter was removed.

(g) The stratifying plates were pulled through the interface.

(h) Calibration solutions (dilutions of the stock solution) were prepared and their temperature was checked against that of the tank water.

(i) The probe was calibrated and then used to obtain a density profile of the tank water.

(j) The gate valve at the discharge end was set to yield the required flow.

(k) Crystals of permanganate were cut to the right size and placed on the wooden trough on the top of the tank.

(l) The camera was loaded and mounted in the rear position. The lights were adjusted.

(m) The rear crystals were dropped and the dye lines were photographed. The time between (j) and (m) was at least 1/2 an hour.

(n) The camera and lights were moved to the front window and the procedure listed in (m) was repeated.

(o) The salinity of the discharge water was measured.

(p) The gate valve was reset to a new flow rate and the procedure was begun at (j) again.

Experimental Program and Data

The experimental program is summarized in Table 4.1. All the data, giving the withdrawal layer thicknesses at different distances from the sink, are reproduced in Appendix I. The aim was to vary ϵ and q to yield a good variation of x_c. The effect of different viscosities or diffusivities was not investigated. The specific gravity of the discharge water was always equal to that corresponding to the specific gravity of the tank water at the level of the sink and it is therefore not included in the table.

TABLE 4.1. EXPERIMENTAL PROGRAM (Key to table on following page)

Exp. No.	T_W °C	ν 10^{-5} cm^2 sec^{-1}	D 10^{-5} cm^2 sec^{-1}	ϵ 10^{-5} cm^{-1}	q cm^2 sec^{-1}	q_m cm^2 sec^{-1}	G approx.	F_m cm^2	α_o^3 10^3 cm^{-2}	x_c cm
1-1	14°C	1120	1.25	2.98	.210	.225	29	1.31	.458	688
1-2	14°	1120	1.25	2.98	.320	.366	29	2.14	.458	1439
1-3	14°	1120	1.25	2.98	.454	.496	29	2.90	.458	2260
2-1	20°	1000	1.25	25.7	.006	.012	29	.024	1.46	5.4
2-2	20°	1000	1.25	25.7	?	.062	29	.124	1.46	64.3
2-3	20°	1000	1.25	25.7	?	.272	29	.543	1.46	584.0
3-1	14°	1120	1.25	29.9	.005	.007	29	.013	1.45	2.18
3-2	15°	1100	1.25	29.9	.013	.014	29	.026	1.46	6.43
3-3	15°	1100	1.25	29.9	.031	.033	29	.062	1.46	22.8
3-4	18°	1040	1.25	29.9	.064	.073	29	.136	1.50	25.0
3-5	18°	1040	1.25	29.9	.118	.143	29	.264	1.50	204.0
3-6	18°	1040	1.25	29.9	.185	.233	29	.429	1.50	420.0
4-1	14°	1120	1.25	35.3	.006	.007	29	.012	1.57	2.14
4-2	14°	1120	1.25	35.3	.005	.007	29	.012	1.57	2.22
4-3	16°	1080	1.75	35.3	.007	.010	29	.017	1.60	3.81
4-5	16°	1080	1.25	35.3	.009	.011	29	.019	1.60	4.38
4-6	16°	1080	1.25	35.3	.012	.013	29	.022	1.60	5.85
4-7	14°	1120	1.25	35.3	.017	.020	29	.034	1.57	9.90
4-8	14°	1120	1.75	35.3	.022	.024	29	.041	1.57	13.40
4-9	14°	1120	1.25	35.3	.037	.044	29	.075	1.57	32.2

Column 1: The first number corresponds to the density stratification, while the second designates the run number for that stratification.

Column 2: T_w is the temperature of the water in degrees centigrade.

Column 3: ν is the kinematic viscosity. The values are those of pure water at T_w°C.

Column 4: D is the molecular diffusivity of salt in water.

Column 5: $\varepsilon = \frac{1}{\rho_o} \frac{d\rho_e}{dz}$, computed by the formula.

$$\varepsilon = \frac{\text{Sp. Gravity at } z_1 - \text{Sp. Gravity at } z_2}{(z_1 - z_2)}$$

Column 6: q is the discharge measured with the discharge meter divided by the width of the channel.

Column 7: q_m is the forward discharge obtained by integration of the velocity profiles (Section 4.2).

Column 8: G is the mean value of $(\nu/D)^{1/2}$ for all the runs.

Column 9: F_m is the Froude number $q_m/\sqrt{\varepsilon g}$.

Column 10: α_o^3 is the inverse of the Rayleigh number. This is used to facilitate comparison with Koh's 1966b data $(\varepsilon g/\nu D)^{\frac{1}{2}}$

Column 11: x_c is the critical distance below which inertial effects become important. $(F_m^{3/2}\ \alpha_o^3)$

5. ANALYSIS AND DISCUSSION OF EXPERIMENTAL RESULTS

Analysis of Data

The half scale photographs of the dye lines at consecutive times formed the unprocessed velocity data. The time between photographs was obtained by measuring the length of chart between notches at the event marker trace. The reduction of this data may be divided into three parts.

(a) Discharge calculations: The no slip condition on the side walls forced the layer to have a parabolic velocity variation across the width of the tank, rather than a uniform distribution as assumed in the theory. For this reason the local discharge q_m, obtained by integrating the velocity profile, was used in the reduction of the data. To obtain q_m, successive photographs were aligned and the top profile was pricked through onto the other photograph. The area between the two curves of 6 roughly equally spaced profiles was then measured with a planimeter. The total net area was used rather than just the forward flowing part. To within 10% the areas were the same and the mean of the 6 areas was used to calculate the discharge by the formula

$$q_m = \text{mean area} \div \text{time between photographs.}$$

(b) Withdrawal layer thickness δ: In the integral solution δ was defined by the velocity profile

$$u = \frac{a(x)}{\pi} \frac{1-kz^2\delta^{-2}}{(1+z^2\delta^{-2})^3}$$

when $z = \delta$

$$\frac{u}{u_{max}} = \frac{1}{12}$$

hence a convenient definition for δ in the experimental data is that width at which the velocity has dropped to 1/12 the center line value. This value of δ was also much better defined on the photographs than the point where the velocity is zero. The profile had a large non-zero slope here, and it formed a definite intersection with the constant line of $u = \frac{1}{12} u_{max}$. The values of δ, measured as described, and the above value of q_m were then used to set up a table as shown in Appendix I. The actual quantities plotted on Fig. 5.1 are:

$$\frac{\delta}{F_m^{1/2}} \text{ versus } \left(\frac{x}{x_c}\right)^{1/3}, \quad \text{where } x_c = F_m^{3/2} \left(\frac{\epsilon g}{\nu D}\right)^{1/2}.$$

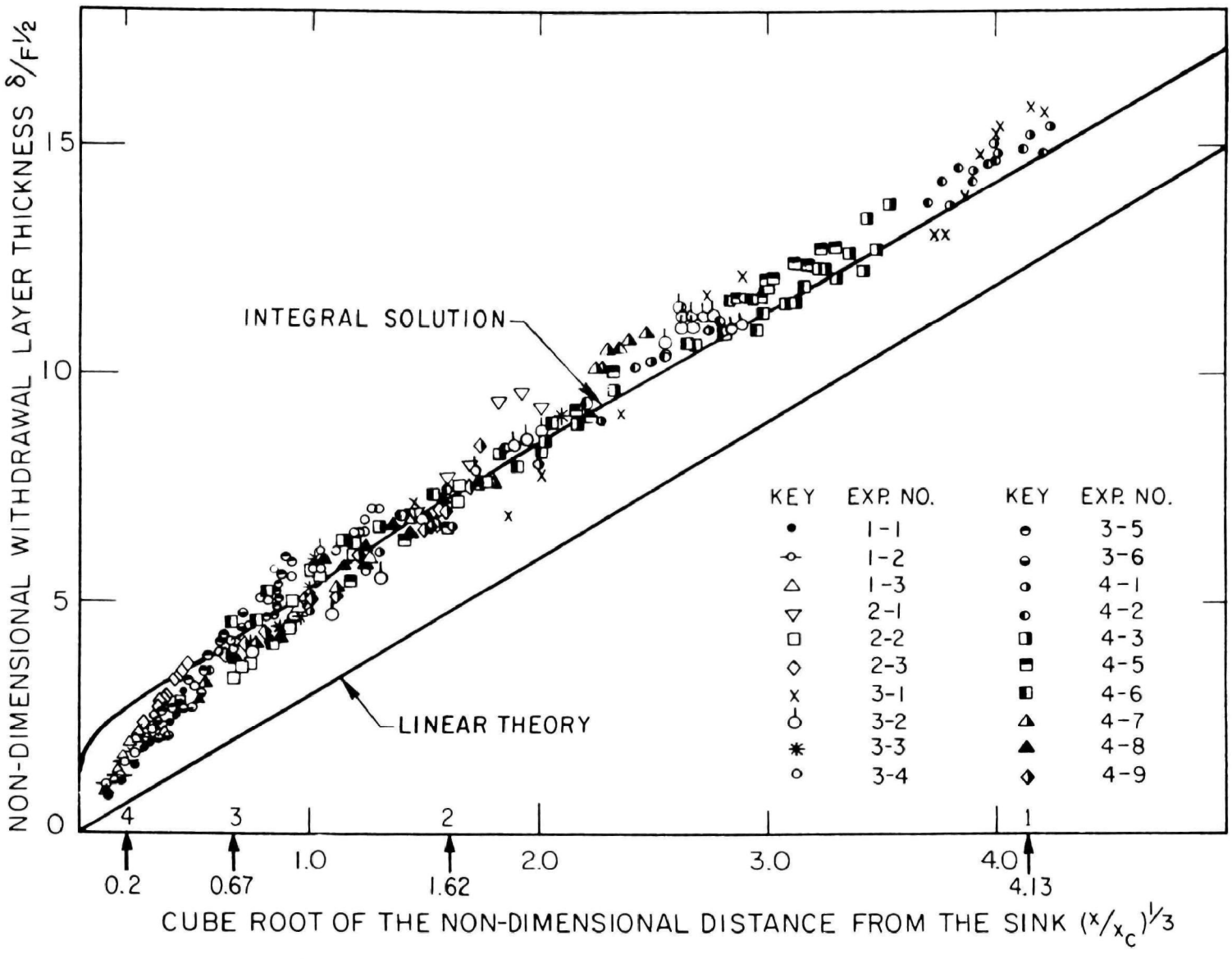

FIG. 5.1 EXPERIMENTAL WITHDRAWAL LAYER THICKNESS: G = 29.0

(c) Velocity Profiles: At four values of $(x/x_c)^{1/3}$ the actual velocity profiles were reduced. To obtain the velocity profile, the image of the dye lines was transferred onto a transparent graph paper. From this the ordinates were read off and divided by the time between photographs to yield velocities. The above velocity profiles were all plotted on a single graph by normalizing the maximum velocity and the discharge to 1. This is shown in Fig. 5.2. The solid line again corresponds to the integral velocity distribution. Rewritten to have u/u_{max} as the ordinant and zu_{max} as the abscissa this reads:

$$\frac{u}{u_{max}} = \frac{1 - .367(zu_{max})^2}{(1 + 1.1(zu_{max})^2)^3}$$

Effects of the Finite Size of the Tank

Figures 5.1 and 5.2 show little scatter, indicating that random errors due to parallax, enlarging, and aligning of photographs are quite small. Systematic errors are, however, possible as the tank has a finite width and a finite length. The possibility of a systematic error of this sort is now assessed.

The finite width introduces a parabolic profile in the y direction. Koh (1966b) has made a detailed analysis of the effects of the parabolic profile on the withdrawal layer thickness. As long as the scale in the vertical direction, 2δ, is smaller than the width, and provided the local centerline discharge q_m is used, the error introduced will be small. In the present experiments the ratio of thickness to width of the layer was kept to less than 0.1 by taking data only in the first 6 feet of the tank.

The tank was long enough so that the measured discharges in the test section were independent of the distance from the sink. This means that the layer spread sufficiently to prevent any influence of the back wall. To ensure that the layer far upstream was inertia free, the discharge q was limited to make x_c less than the length of the tank. In the experiments x_c was kept, with one exception, to below 1/6 of the tank length.

With the above precautions, it is reasonable to assume that the data is a true representation of flow in a long reservoir.

Comparison With The Theoretical Results And Previous Experiments

The present experimental results have been summarized on Figs. 5.1 and 5.2. The data from Koh (1966b) was replotted to conform with theoretical scaling as shown in Fig. 4.1. Comparison shows excellent agreement up to $(x/x_c)^{1/3}$ of approximately 2. For larger values of this parameter Koh (1966b) found values of δ slightly larger than

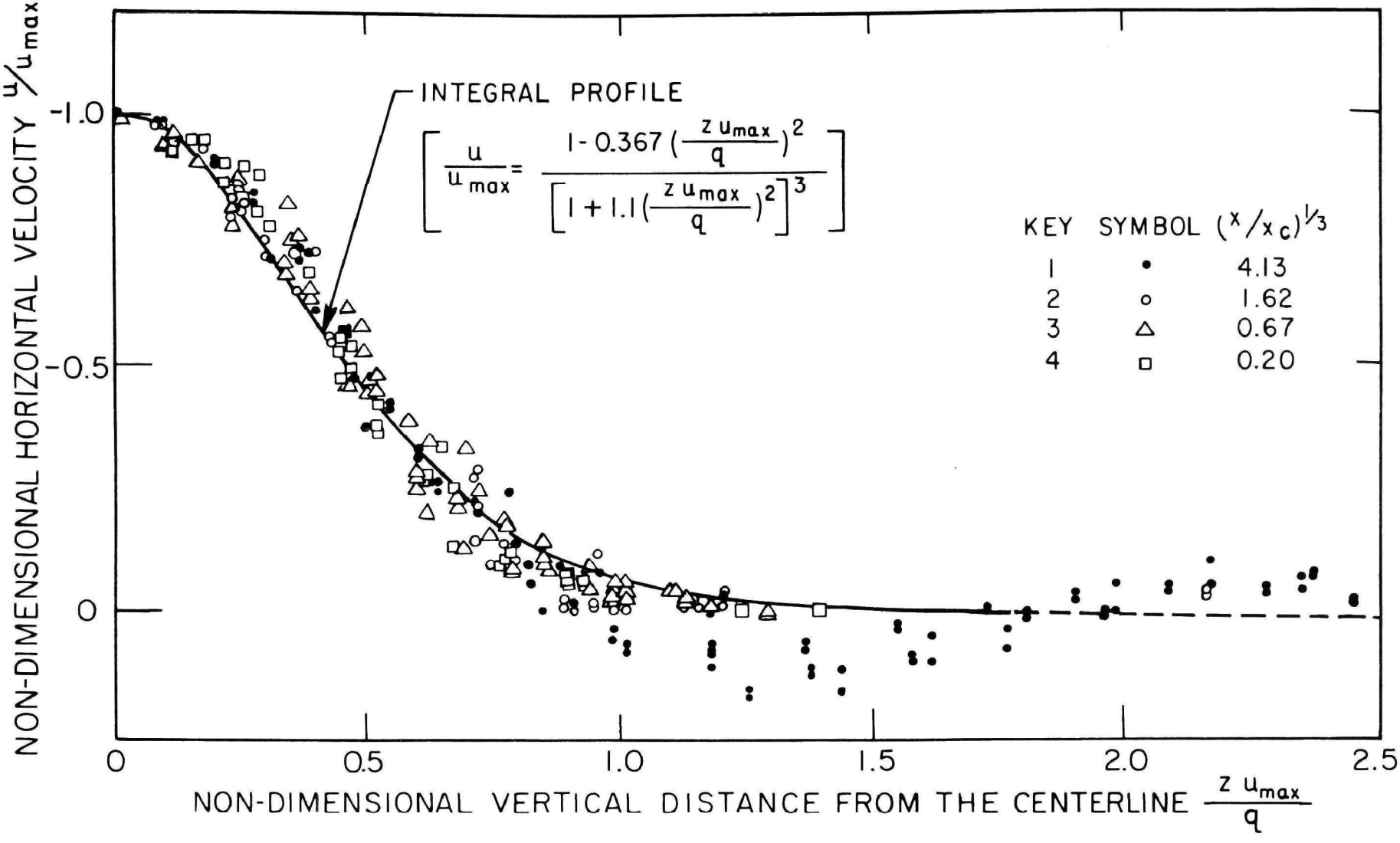

FIG 5.2 EXPERIMENTAL VELOCITY PROFILES: G = 29.0

those measured by the author. However, as already pointed out, this difference is not significant as it is most probably due to end wall effects in the former's experiments.

Theory showed that the flow should be independent of any parameter except G, when the x and z coordinates are scaled correctly. This is verified in Figs. 5.1 and 4.1 where the data is seen to fall all onto one curve for a particular G. The above observation is equally true for the salt stratification where G is quite large, even though the theory was developed for G of order one. This may be explained by noting that the inner Eqs. (3.46) - (3.48) are merely a boundary layer type simplification of the full equations and therefore still contain a representation of all the forces. Thus even if there are for large G, regions in which diffusion is absent, the governing equations there would be special cases of the more general Eqs. (3.46) - (3.48).

For the same reason a large value of G does not invalidate the integral solution results. A comparison between the theory and experiment is shown in Fig. 5.1 and it can be considered good, everywhere except near the sink. The difficulty here results from the still unknown behavior of the flow very near the sink. There is a temptation to adjust K_3, the floating upstream constant, to improve the fit near the origin. Figure 5.3 shows curves for different values of K_3 and it is seen that the integral curve for $K_3 = -82.2$ fits the data better than the originally adopted curve, which has $K_3 = -81.8$. This is an encouraging flexibility of the method, but the original choice of K_3 remains the only theoretically justifiable one until a more definite solution for the flow very close to the sink is obtained, to which the integral solution may be matched.

The depth of the experimental tank was 4 feet, which was large compared with the values of $F_m^{1/2}$ used, so that the top and bottom boundaries did not influence the flow for the experimental values of (x/x_c). This meant that the linear or outer solution, as derived in Section 3.3 and included in Fig. 5.1, was identical with Koh's (1966b) solution. Inspection of Fig. 5.1 shows that the integral solution, which reflects the effects of the inertial terms in the equations of motion, predicts layer thicknesses more in agreement with the experimental data than either the solution of Koh (1966b) or the solution $\delta/F_m^{1/2} = 1.35$ found by Kao (1970).

By examining Koh's (1966b) data Brooks and Koh (1969) anticipated to some extent the theoretical scaling. In Fig. 9 of that reference Koh's (1966b) data is replotted in terms of

$$\frac{\alpha}{\alpha_o} \quad \text{versus} \quad \frac{q}{D\alpha_o x^{2/3}} \ .$$

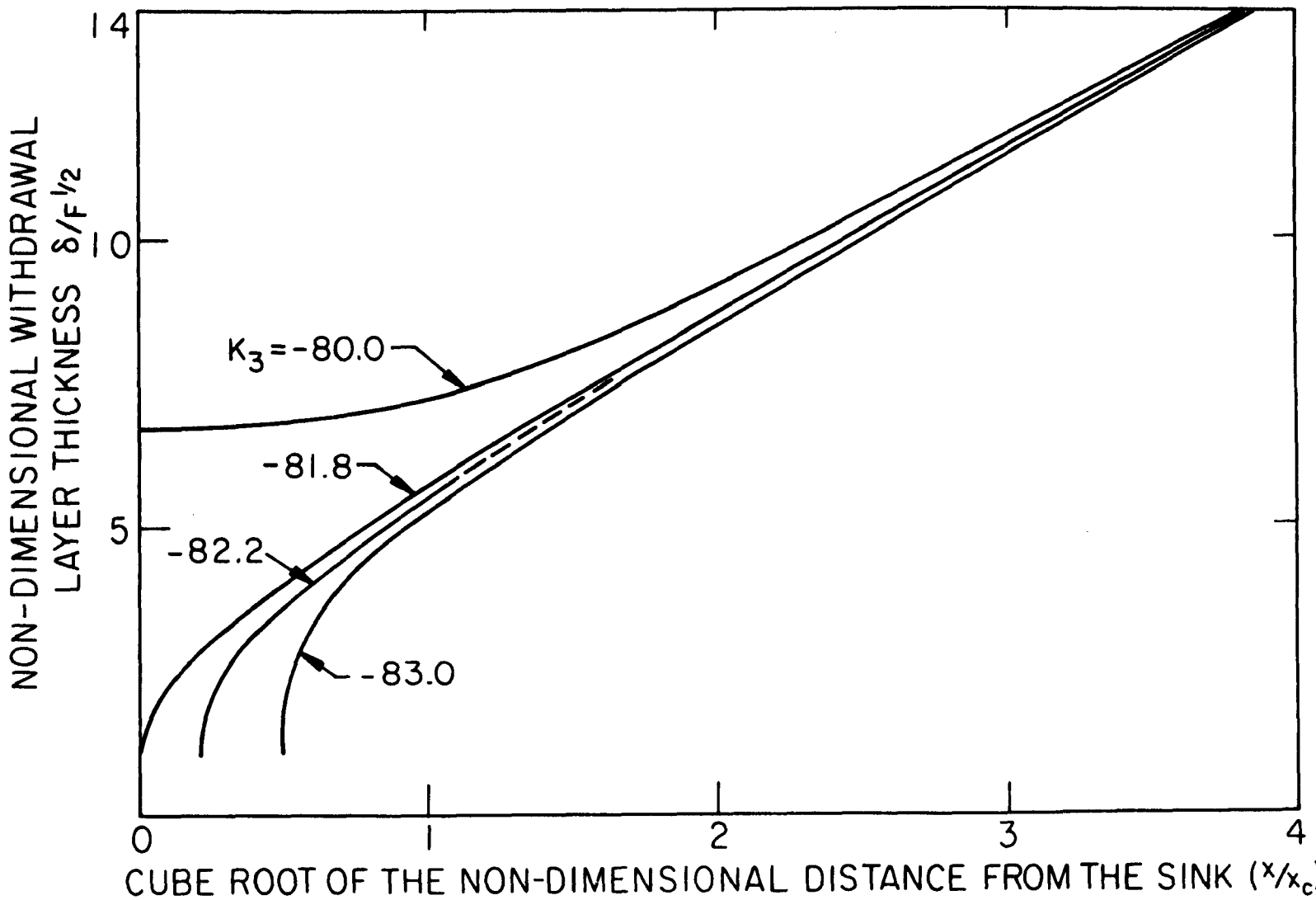

FIG. 5.3 VARIATION OF THE INTEGRAL SOLUTION WITH K_3

A little rearranging shows that this is in the present notation

$$3.57\ \frac{F_m^{1/2}}{\delta}\left(\frac{x}{x_c}\right)^{1/3} \quad \text{versus} \quad \left(\frac{x_c}{x}\right)^{2/3} F\ .$$

The only real difference between the above and that established in Section 3 is the factor $(x/x_c)^{1/3}$ in the ordinant.

It was hoped that the velocity profile measurements would indicate some of the structure changes very close to the sink, and clarified the nature of the inviscid core. Figure 5.2 shows, however, that even for x of the order of $F^{1/2}$ the velocity profiles are self similar to those for large (x/x_c). The only change is that the back flow velocity decreases, in relation to the center line velocity, as x is decreased or, equivalently, as q is increased. Further work is needed both experimentally and theoretically to describe the flow close to the sink.

6. COMPARISON WITH FIELD DATA

The tests conducted by the Tennessee Valley Authority on some of their reservoirs appears to be the only source of actual reservoir data. The work summarized in the T.V.A. reports (1969(a),(b)) is concerned with the measurement of the velocity, temperature, and water oxygen content distribution in a reservoir from which water is being drained. The investigations involved the Fontana and Cherokee Reservoirs with further work in progress in the Douglas and Barron-Nolin Reservoirs.

The difficulty of measuring velocities is compounded by the unsteady nature of the operating discharge and the irregular geometry of most reservoirs. Over the first 20 miles the Cherokee Reservoir is in the form of a 1 mile wide trough making it the most suitable example for a comparison with the simplified geometry of the theory. Altogether, there are data from 5 steady runs, 4 from the Cherokee and one from the Fontana reservoir. The complete data is summarized in Table 5.1. The investigations dealing with the transient response are still very limited; only one complete run has been published.

Unsteady Withdrawal

In Section 3 it was shown that the time scale of the reservoir response, to an increase in turbine discharge, was of the order of $1/\sqrt{\varepsilon g}$. The actual time it will take to form a withdrawal layer of thickness δ_s at a distance x from the sink was found to be given by

$$t = \frac{1}{\sqrt{g\varepsilon}} \frac{\pi x}{\delta_s} .$$

The value of δ_s is obtained from the composite solution given in Fig. 3.7. The turbine response for the two partial tests given was very close to a step function, and the time taken to reach steady state, at the station corresponding to the data 8-16-67, was of the order of 12 hours. By comparison the theoretical value yields

$$t = \frac{1}{\sqrt{3.8 \times 10^{-4}}} \pi \frac{8980}{18.6 \times 1.60} \frac{1}{3600} = 13.6 \text{ hrs.}$$

The agreement is rather encouraging.

Steady Withdrawal

Figure 6.1 shows the available prototype data, plotted non-dimensionally with respect to molecular transport properties, as described in Section 3. The half layer thickness chosen was that which corresponded to a velocity 1/12 the maximum velocity. The theoretical curve is shown for comparison. The prototype values are seen to be 50-100% larger than those predicted. This is especially noticeable since the experimental results in Fig. 5.1 are always a little smaller

TABLE 6.1. PROTOTYPE DATA FROM T.V.A. (1969(a) & (b)

Date	T°C	ν 10^{-5} ft^2 sec^{-1}	D 10^{-5} ft^2 sec^{-1}	G 10^{-5} ft^{-1}	εg 10^{-1} sec^{-1}	α_o^3 10^3 ft^{-2}	g ft^2 sec^{-1}	F_m ft^2	$F_m^{\frac{1}{2}}$ ft.	x_c 10^6 ft	δ ft	$\delta / F_m^{\frac{1}{2}}$	x ft	$(x/x_c)^{1/3}$	2ℓ ft	$2\ell / F_m^{\frac{1}{2}}$
Cherokee																
8-17-57	25	0.900	0.144	12	3.8	5.2	5.6	288	17.0	25.5	40	2.4	2,100	.049	150	8.9
9-20-67	20	0.980	0.144	0.36	1.1	2.8	5.2	495	22.2	30.8	40	1.8	2,100	.041	140	6.3
8-16-67	20	0.980	0.144	1.2	3.8	5.2	6.75	346	18.6	33.3	40	2.2	8,980	.065	140	7.5
8-24-67	Extraneous currents.															
9-14-67	20	0.980	0.144	1.65	5.3	6.1	3.8	165	12.8	12.8	30	2.3	52,800	.16	120	9.4
Fontana																
9-9-66	20	.980	.144	1.11	3.6	5.1	7.6	400	20	30.6	45	2.3	3,430	.022	330	16.5

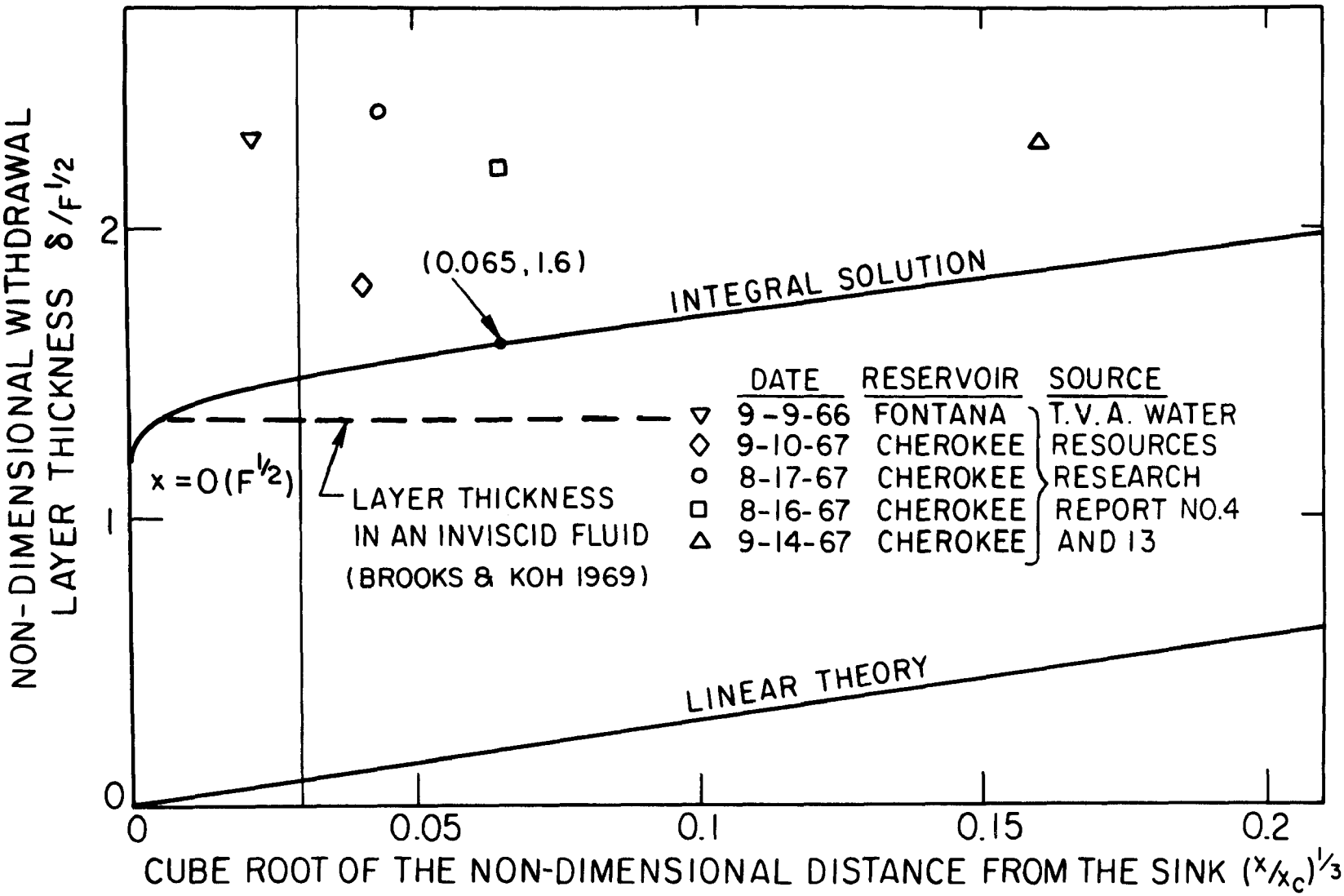

FIG. 6.1 PROTOTYPE EXPERIMENTAL DATA

than the integral curve for such small values of (x/x_c).

Column 11 of Table 6.1 shows that for molecular transport coefficients, the corresponding values of x_c for both the Cherokee and Fontana data are about 10-100 times larger than the length of the reservoirs. This means that the inertial region III of Fig. 3.6 extends over the whole reservoir. Consequently the outer solution is valid nowhere in the reservoir. Brooks and Koh (1969), in an effort to explain the difference between the observed withdrawal layer thickness and that predicted by Koh (1966b), postulated eddy transport coefficients much larger than their molecular counterparts. The use of Koh's (1966b) solution is now seen to be incorrect, but a similar procedure can be used for the present theory. An increase in ν and D, decreases x_c and this moves the data points to the right in Fig. 6.1. With the assumption that $\nu = D$, a typical value of the eddy transport values, sufficient to move the data onto the theoretical curve is 10^{-3} ft^2 sec^{-1}. This is an increase over the molecular values of 10^2, considerably less than the 10^3 postulated by Brooks and Koh (1969) on the basis of Koh's (1966b) theory. The value of x_c, corresponding to such transport coefficients and the mean of the data for the first three runs listed in Table 6.1, is approximately 23 miles, which is roughly the length of the reservoir. This means therefore that the use of the higher transport coefficients still requires the inclusion of inertial effects.

The weakness of the above procedure is that as yet, there is no explanation of a mechanism which could sustain these larger eddy transport coefficients. Measurements (T.V.A. 1969b) of the local Richardson number with depth, for a typical run indicate that this varies between 10 and 10,000; values much higher than required for local shear instability.

The large values of x_c encountered in reservoirs with peak discharges means that the end walls cannot be neglected and these could have 1st order effects on the thickness of the layer. An end wall stops the withdrawal layer and much larger reverse flows are induced. A large discharge could cause a vigorous layer to extend to the rear wall and this would induce a reverse layer above and below the center layer. Schiff (1966) has found, in a related problem, that this induced snaking of the flow with possible mixing at the boundaries leads to increased diffusion of the species.

In summary it can be said that the theory, although yielding good agreement with laboratory experiments, is still not able to completely explain prototype behavior. However, it does yield a rational basis from which to proceed to include the effects of larger eddy transport coefficients and end wall effects.

ACKNOWLEDGEMENTS

The authors would like to thank Dr. G. Corcos and Dr. A. Lewy for reading the manuscript and offering their valuable suggestions. Appreciation is also due to Mr. K. Bremel who designed and supervised the construction of the experimental tank; Mr. E. Parscale, who built most of the experimental equipment; Mr. W. Kot, who prepared the drawings; and Mrs. D. Aoki and Mrs. D. Haasarud, who typed the manuscript.

The first writer wishes to thank the Robert and Maude Gledden Fund of the University of Western Australia for making it possible for him to come to Berkeley by providing a fellowship for two years. Furthermore, he would like to thank the University of California for providing him with a Science Fellowship in the third year.

The initial portion of the research was supported by funds from the Water Resources Center of the University of California under project W-204. The support of the project by the Environmental Protection Agency and the help provided by Mr. Phillip C. Woods, Grant Project Officer, is acknowledged with sincere thanks.

REFERENCES

Beard, L., and Wiley, 1970. An approach to reservoir temperature analysis, Water Resources Research (in press).

Bellman, R., 1953. Stability theory of differential equations. McGraw-Hill, New York.

Brooks, N. H., and Koh, R. C. Y., 1969. Selective withdrawal from density-stratified reservoirs. Journal of the Hydraulics Div., Proc. ASCE, Vol. 95, HY4, pp. 1369-1400.

Childress, S., 1966. Solutions of Euler's equations containing finite eddies. The Physics of Fluids, Vol. 9, No. 5, pp. 860-872.

Clark, C. B., Stockhausen, P. J., and Kennedy, J. F., 1967. A method for generating linear density profiles in laboratory tanks. Journal of Geophysical Research, Vol. 72, No. 4, pp. 1393-1395.

Debler, W. R., 1959. Stratified flow into a line sink. Journal Eng. Mech. Div., Proc. ASCE, Vol. 85, pp. 673-695.

Fraenkel, L. E., 1961. On corner eddies in plane inviscid shear flow. Journal of Fluid Mechanics, Vol. 11, Pt. 3, pp. 400-406.

Gelhar, L. W., and Mascolo, D. M., 1966. Non-diffusive characteristics of slow viscous stratified flow towards a line sink. M.I.T. Hydrodynamics Laboratory Report No. 88, pp. 1-39.

Gill, A. E., and Smith, R. K., 1970. On similarity solutions of the differential equation $\psi_{zzzz} + \psi_x = 0$. Proc. Camb. Phil. Soc., Vol. 67, pp. 163-171.

Green, A. E., and Naghdi, P. M., 1969. On basic equations for mixtures. Univ. of Calif. College of Eng. Report No. AM-69-4, pp. 1-19.

Imberger, J., 1970. Selective withdrawal from a stratified reservoir. Ph.D. Thesis, Univ. of Calif., Berkeley, Dec. 1970.

Kao, T. W., 1965. A free-streamline solution for stratified flow into a line sink. Journal of Fluid Mechanics, Vol. 21, Pt. 3, pp. 535-543.

Kao, T. W., 1970. A free-streamline theory for inviscid stratified flow. Physics of Fluids, Vol. 13, No. 3, pp. 558-564.

Koh, R. C. Y., 1964. Karman integral solution to the problem of selective withdrawal. California Institute of Tech., W. M. Keck Laboratory Tech. Memo. 64-14, pp. 1-16.

Koh, R. C. Y., 1966a. Unsteady stratified flow into a line sink. Journal of Hydraulic Research, Vol. 4, No. 2, pp. 21-34.

Koh, R. C. Y., 1966b. Viscous stratified flow towards a sink. Journal of Fluid Mechanics, Vol. 24, Pt. 3, pp. 555-575.

Krenkel, P. A., Thackston, E. L., and Parker, F. L., 1969. Impoundment and temperature effect on waste assimilation, Journal of the Sanitary Eng. Div., Proc. A.S.C.E., Vol. 95, No. SA1, pp. 37-64.

List, E. J., 1968. A two-dimensional sink in a density-stratified porous medium. Journal of Fluid Mechanics, Vol. 33, Pt. 3, pp. 529-543.

List, E. J., 1970. Private communication.

Long, R. R., 1959. The motion of fluids with density stratification. Journal Geophys. Res., Vol. 64, pp. 2151-2163.

Lorence, K. Z., 1952. King Solomon's Ring. Thomas Y. Crowell Company, New York.

Miles, J. W., 1961. On the stability of heterogeneous shear flows. Journal of Fluid Mechanics, Vol. 10, Pt. 4, pp. 496-508.

Müller, I., 1968. A thermodynamic theory of mixtures of fluids Arch. Rational Mech. Anal., Vol. 28, pp. 1-39.

Orlob, G. T., and Selna, L. G., 1970. Temperature variations in deep reservoirs. Journal of the Hydraulics Div., Proc. ASCE, Vol. 96, HY2, pp. 391-410.

Redekopp, L. G., 1969. Theoretical analysis of boundary layer regions in stratified flow. Univ. of Calif. Los Angeles, School of Eng. and App. Sc. Report No. 69-23, pp. 1-156.

Redekopp, L. G., 1970. The development of horizontal boundary layers in stratified flow. Journal Fluid Mechanics, Vol. 42, Pt. 3, pp. 513-527.

Schiff, L. I., 1966. Lateral boundary mixing in a simple model of ocean convection. Deep Sea Research, Vol. 13, pp. 621-626.

Segur, H., 1970. Private communication.

Stotta, L. S., Elwin, E. H., Mercier, H. T., and Terry, M.D., 1969. Stratified Reservoir Currents. Oregon State Univ. Eng. Exp. Station, Bull. No. 44.

Smith, R. K., 1969. On the effects of vorticity entrainment in zonal jet flows. Journal of Atmospheric Sciences, Vol. 26, No. 6, pp. 1233-1237.

Spiegel, E. A. and Veronis, G., 1960. On the Boussinesq approximation for a compressible fluid. Astrophysical Journal, Vol. 131, pp. 442-447.

Tennessee Valley Authority, 1969. The prediction of withdrawal layer thickness in density stratified reservoirs. Water Resources Research Lab. Report, No. 4, pp. 1-8.

Tennessee Valley Authority, 1969. Cherokee Reservoir selective withdrawal. Water Resources Research Lab. Report No. 13, pp. 1-30.

Trustrum, K., 1964. Rotating and stratified flow. Journal of Fluid Mechanics, Vol. 19, Pt. 2, pp. 415-432.

Yih, C. S., 1965. Dynamics of Nonhomogeneous Fluids. The MacMillan Co., New York.

GLOSSARY OF TERMS

D = Molecular diffusion coefficient of salt or heat

F, F_m = Densimetric Froude number $\dfrac{q}{\sqrt{\epsilon g}\, \ell^2}$, $\dfrac{q_m}{\sqrt{\epsilon g}}$

G = Square root of the Schmidt number $\left((\nu/D)^{\frac{1}{2}}\right)$

g = Acceleration due to gravity

J = Momentum flux

K_i = Coefficients in the asymptotic expansion of the withdrawal layer thickness

L = A typical length scale of the motion

ℓ = Half depth of the reservoir

P = Scale of the pressure perturbation

p_T = Total pressure

p_e = Hydrostatic pressure

p = Pressure due to the motion

q, q_m = Discharge into the sink from the right; measured q

R = Rayleigh number $\left(\dfrac{\nu D}{\epsilon g}\right)^{\frac{1}{2}} \cdot \dfrac{1}{L^2}$ or $\left(\dfrac{\nu D}{\epsilon g}\right)^{\frac{1}{2}} \cdot \dfrac{1}{\ell^2}$

R_e = Reynolds number $\left(\dfrac{q}{\nu}\right)$

r = Radius vector $\left((x^2 + z^2)^{\frac{1}{2}}\right)$

T = Brunt Väisälä period $\left(1/(\epsilon g)^{\frac{1}{2}}\right)$

t = Time

$\vec{u}$ = Velocity vector $\left((u, v, w)\right)$

x = Horizontal distance from the sink

x^* = Scaled horizontal distance from the sink $\left(\dfrac{x}{\ell}\right)$

x^{**} = Scaled horizontal distance from the sink $\left(\dfrac{x^*}{x^*_c}\right)$

x^{***} = Scaled horizontal distance from the sink $\left(\frac{F}{R}\, x^{**}\right)$

x_c^*, x_c = Length of the non-uniformity $\left(\frac{F^{3/2}}{R}\right)$, $\left(F_m^{3/2}\ \alpha_o^3\right)$

z = Vertical distance from the sink

z^* = Scaled vertical distance from the sink $\left(\frac{z}{\ell}\right)$

z^{**} = Scaled vertical distance from the sink $\left(\frac{z^*}{R^{1/3}}\right)$

z^{***} = Scaled vertical distance from the sink $\left(\frac{R^{1/3}\ z^{**}}{F^{1/2}}\right)$

α_o = $(\epsilon g/\nu D)^{1/6}$

δ = Withdrawal layer half thickness

ϵ = Normalized background density gradient $\left(\frac{1}{\rho_o}\,\frac{d\rho_e}{dz}\right)$

Λ = Scale of the density perturbation

μ = Molecular viscosity

ν = Kinematic molecular viscosity $\left(\frac{\mu}{\rho_o}\right)$

ρ_T = Total value of the density of the water

ρ_o = Mean of the density of the water over the depth

ρ_e = Background density

ρ = Density perturbation due to the motion

ρ^* = Scaled density $\left(\frac{\rho}{\Lambda}\right)$

ρ^{**} = Scaled density $(R^{1/3}\ \rho^*)$

ρ^{***} = Scaled density $\left(\frac{F^{1/2}}{R^{1/3}}\ \rho^{**}\right)$

τ = Surface stress

ψ = Stream function

ψ^* = Scaled stream function $\left(\frac{\psi}{q}\right)$

APPENDIX I

EXPERIMENTAL WITHDRAWAL LAYER THICKNESS DATA

Exp. No.	ϵ 10^{-5} cm^{-1}	α_o^3 10^3 cm^{-2}	$F_m^{\frac{1}{2}}$ cm	x_c cm	δ cm	$\delta/F_m^{\frac{1}{2}}$	x cm	$(x/x_c)^{1/3}$
1-1	2.98	0.458	1.145	688	1.0	0.87	1.0	0.113
					1.3	1.14	3.4	0.170
					1.5	1.31	6.0	0.206
					1.7	1.49	8.3	0.229
					2.0	1.75	13.6	0.270
					2.1	1.83	15.2	0.280
					2.3	2.00	20.8	0.315
					2.7	2.36	29.0	0.348
					2.8	2.44	37.4	0.378
					2.9	2.54	43.4	0.398
					3.3	2.88	52.0	0.422
					3.5	3.06	60.8	0.445
1-2	2.98	0.458	1.46	1439	1.6	1.10	2.6	0.106
					1.8	1.23	7.0	0.169
					2.3	1.57	10.8	0.196
					2.4	1.64	12.6	0.206

Exp. No.	ϵ 10^{-5} cm^{-1}	α_o^3 10^3 cm^{-2}	$F_m^{\frac{1}{2}}$ cm	x_c cm	δ cm	$\delta/F_m^{\frac{1}{2}}$	x cm	$(x/x_c)^{1/3}$
					2.4	1.64	13.6	0.215
					2.6	1.78	17.4	0.230
					2.9	1.99	24.4	0.255
					3.0	2.06	30.8	0.278
					3.3	2.26	38.0	0.298
					3.3	2.26	47.0	0.319
					3.5	2.40	53.6	0.333
1-3	2.98	0.458	1.70	2260	1.6	0.94	2.6	0.105
					1.9	1.12	4.0	0.121
					2.3	1.35	8.0	0.152
					2.8	1.65	16.4	0.194
					3.4	2.00	22.6	0.215
					3.5	2.06	30.2	0.237
					3.5	2.06	39.4	0.259
					3.7	2.18	47.0	0.275
					3.8	2.24	57.1	0.294

Exp. No.	ϵ 10^{-5} cm^{-1}	α_o^3 10^3 cm^{-2}	$F_m^{\frac{1}{2}}$ cm	x_c cm	δ cm	$\delta/F_m^{\frac{1}{2}}$	x cm	$(x/x_c)^{1/3}$
2-1	25.7	1.46	0.16	5.4	1.10	7.10	16.8	1.46
					1.2	7.75	22.0	1.59
					1.25	8.07	26.1	1.69
					1.47	9.49	32.9	1.82
					1.50	9.68	37.6	1.91
					1.45	9.37	43.5	2.00
2-2	25.7	1.46	0.35	64.3	1.02	2.90	4.6	0.424
					1.20	3.41	16.8	0.644
					1.28	3.64	21.4	0.693
					1.34	3.80	24.0	0.720
					1.58	4.48	44.6	0.886
					1.80	5.11	47.3	0.902
2-3	25.7	1.46	0.74	584.0	1.53	2.08	4.6	0.200
					1.64	2.22	9.4	0.252
					1.77	2.40	13.0	0.280
					1.93	2.69	17.6	0.310

Exp. No.	ϵ 10^{-5} cm^{-1}	α_o^3 10^3 cm^{-2}	$F_m^{\frac{1}{2}}$ cm	x_c cm	δ cm	$\delta/F_m^{\frac{1}{2}}$	x cm	$(x/x_c)^{1/3}$
					2.07	2.82	20.4	0.327
					2.17	2.94	25.2	0.350
					2.20	2.98	27.0	0.353
					2.21	3.00	30.2	0.373
					2.46	3.34	37.0	0.398
					2.46	3.34	39.6	0.408
					2.70	3.66	44.4	0.424
					2.80	3.79	46.0	0.429
3-1	29.9	1.45	0.11	2.18	0.83	7.30	6.8	1.46
					0.80	7.01	14.2	1.87
					0.90	7.92	19.4	2.07
					1.05	9.22	28.4	2.36
					1.20	10.56	33.8	2.49
					1.35	11.80	44.4	2.73
					1.40	12.21	52.2	2.88
					1.50	13.11	111.4	3.74

Exp. No.	ϵ 10^{-5} cm^{-1}	α_o^3 10^3 cm^{-2}	$F_m^{\frac{1}{2}}$ cm	x_c cm	δ cm	$\delta/F_m^{\frac{1}{2}}$	x cm	$(x/x_c)^{1/3}$
					1.50	13.11	118.4	3.78
					1.60	14.00	125.4	3.86
					1.70	14.92	132.4	3.93
					1.75	15.31	141.0	4.00
					1.79	15.64	148.2	4.09
					1.82	15.89	156.0	4.15
					1.80	15.80	163.0	4.21
3-2	29.9	1.46	0.16	6.43	0.65	3.99	2.8	0.76
					0.77	4.72	8.6	1.10
					0.92	5.64	14.6	1.31
					1.12	6.87	21.4	1.49
					1.20	7.36	28.4	1.64
					1.30	7.98	33.0	1.72
					1.38	8.46	43.4	1.89
					1.40	8.60	47.0	1.94
					1.45	8.87	53.2	2.02

Exp. No.	ϵ 10^{-5} cm^{-1}	α_o^3 10^3 cm^{-2}	$F_m^{\frac{1}{2}}$ cm	x_c cm	δ cm	$\delta/F_m^{\frac{1}{2}}$	x cm	$(x/x_c)^{1/3}$
					1.50	9.20	60.6	2.11
					1.75	10.71	108.2	2.56
					1.86	11.41	115.1	2.62
					1.82	11.12	119.4	2.64
					1.82	11.12	125.3	2.69
					1.85	11.31	130.0	2.72
					1.85	11.31	136.2	2.76
					1.85	11.31	142.4	2.79
					1.80	11.00	148.0	2.84
					2.00	12.22	156.0	2.89
					2.00	12.22	160.0	2.92
3-3	29.9	1.46	0.25	22.8	1.00	4.00	7.0	0.67
					1.15	4.62	14.6	0.86
					1.20	4.80	19.8	0.95
					1.35	5.44	25.6	1.04
					1.40	5.62	29.0	1.08

Exp. No.	ϵ 10^{-5} cm^{-1}	α_o^3 10^3 cm^{-2}	$F_m^{\frac{1}{2}}$ cm	x_c cm	δ cm	$\delta/F_m^{\frac{1}{2}}$	x cm	$(x/xc)^{1/3}$
					1.50	6.00	38.0	1.19
					1.50	6.00	41.8	1.23
					1.61	6.42	50.8	1.31
3-4	29.9	1.50	0.37	75.0	0.98	2.66	2.4	0.32
					1.20	3.25	8.8	0.49
					1.46	3.95	15.8	0.60
					1.62	4.39	21.6	0.66
					1.70	4.61	29.1	0.73
					1.92	5.20	38.4	0.80
					1.90	5.15	42.4	0.83
					2.12	5.75	52.4	0.89
					2.10	5.69	59.6	0.93
					2.30	6.24	106.9	1.12
					2.35	6.36	116.0	1.16
					2.38	6.45	119.0	1.17
					2.40	6.50	124.6	1.18

Exp. No.	ϵ 10^{-5} cm^{-1}	α_o^3 10^3 cm^{-2}	$F_m^{\frac{1}{2}}$ cm	x_c cm	δ cm	$\delta/F_m^{\frac{1}{2}}$	x cm	$(x/x_c)^{1/3}$
					2.45	6.64	130.4	1.20
					2.40	6.50	132.0	1.20
					2.40	6.50	141.6	1.24
					2.55	6.90	149.0	1.26
					2.65	7.16	155.0	1.27
					2.65	7.16	165.0	1.30
3-5	29.9	1.50	0.51	204.0	0.65	1.27	0.6	0.14
					1.00	1.95	3.8	0.27
					1.20	2.34	7.0	0.32
					1.35	2.64	9.0	0.35
					1.40	2.73	13.2	0.40
					1.70	3.32	21.8	0.47
					1.80	3.51	31.8	0.54
					2.00	3.90	36.4	0.56
					2.20	4.29	45.8	0.61
					2.25	4.39	52.0	0.63

Exp. No.	ϵ 10^{-5} cm^{-1}	α_o^3 10^3 cm^{-2}	$F_m^{\frac{1}{2}}$ cm	x_c cm	δ cm	$\delta/F_m^{\frac{1}{2}}$	x cm	$(x/x_c)^{1/3}$
					2.25	4.39	61.0	0.67
					2.45	4.78	111.6	0.82
					2.45	4.78	117.4	0.83
					2.55	4.97	124.0	0.85
					2.70	5.26	130.4	0.86
					2.75	5.36	133.6	0.87
					2.80	5.47	140.4	0.82
					2.90	5.65	147.8	0.90
					3.20	6.24	156.2	0.91
					3.10	6.04	160.5	0.92
3-6	29.9	1.50	0.65	420.0	1.00	1.53	3.2	0.20
					1.00	1.53	4.8	0.23
					1.20	1.84	10.0	0.29
					1.30	1.99	12.6	0.31
					1.35	2.06	16.4	0.34
					1.40	2.14	20.6	0.37

Exp. No.	ε 10^{-5} cm^{-1}	α_o^3 10^3 cm^{-2}	$F_m^{\frac{1}{2}}$ cm	x_c cm	δ cm	$\delta/F_m^{\frac{1}{2}}$	x cm	$(x/x_c)^{1/3}$
					1.65	2.52	28.6	0.41
					1.65	2.52	33.6	0.43
					1.75	2.68	40.4	0.46
					1.80	2.75	48.4	0.49
					2.00	3.06	60.0	0.52
					2.70	4.13	109.4	0.64
					2.70	4.13	115.0	0.65
					2.80	4.29	123.2	0.66
					2.90	4.44	132.8	0.68
					3.00	4.59	141.4	0.70
					3.00	4.59	148.3	0.71
					3.20	4.89	158.0	0.72
4-1	35.3	1.57	0.11	2.14	0.55	4.96	2.3	1.04
					0.68	6.15	4.9	1.32
					0.75	6.78	9.0	1.61
					0.90	8.13	17.0	1.99

Exp. No.	ϵ	α_o^3	$F_m^{\frac{1}{2}}$	x_c	δ	$\delta/F_m^{\frac{1}{2}}$	x	$(x/x_c)^{1/3}$
	10^{-5} cm^{-1}	10^3 cm^{-2}	cm	cm	cm		cm	
					1.00	9.03	24.8	2.26
					1.15	10.41	32.8	2.48
					1.22	11.00	44.2	2.74
					1.30	11.72	52.8	2.91
					1.52	13.72	116.0	3.79
					1.61	14.53	124.8	3.90
					1.68	15.18	135.1	3.98
					1.65	14.90	143.6	4.06
					1.70	15.35	153.6	4.15
					1.72	15.50	163.4	4.24
4-2	35.3	1.57	0.11	2.22	0.40	3.57	0.4	0.56
					0.65	5.80	4.4	1.25
					0.78	6.96	6.1	1.40
					0.84	7.50	9.0	1.59
					0.93	8.30	14.4	1.86
					1.05	9.40	23.6	2.20

Exp. No.	ϵ 10^{-5} cm^{-1}	α_o^3 10^3 cm^{-2}	$F_m^{\frac{1}{2}}$ cm	x_c cm	δ cm	$\delta/F_m^{\frac{1}{2}}$	x cm	$(x/x_c)^{1/3}$
					1.14	10.20	31.4	2.42
					1.19	10.61	37.0	2.55
					1.25	11.22	48.2	2.79
					1.55	13.83	112.4	3.70
					1.60	14.31	119.0	3.77
					1.64	14.61	124.8	3.83
					1.60	14.30	131.3	3.90
					1.65	14.70	137.6	3.96
					1.66	14.82	143.7	4.01
					1.68	15.00	154.0	4.11
					1.67	14.93	165.0	4.20
4-3	35.3	1.60	0.13	3.81	0.75	5.63	4.3	1.04
					0.85	6.36	5.3	1.12
					0.85	6.36	6.9	1.22
					0.90	6.75	8.2	1.29
					1.00	7.50	17.1	1.64

Exp. No.	ϵ 10^{-5} cm^{-1}	α_o^3 10^3 cm^{-2}	$F_m^{\frac{1}{2}}$ cm	x_c cm	δ cm	$\delta/F_m^{\frac{1}{2}}$	x cm	$(x/x_c)^{1/3}$
					1.10	8.25	23.8	1.84
					1.15	8.60	31.1	2.01
					1.20	9.00	39.2	2.17
					1.30	9.75	48.0	2.32
					1.55	11.60	110.7	3.07
					1.55	11.60	115.4	3.12
					1.60	12.00	119.5	3.15
					1.65	12.41	126.2	3.21
					1.65	12.41	130.5	3.24
					1.62	12.20	137.3	3.30
					1.70	12.75	143.7	3.35
					1.65	12.41	151.2	3.41
					1.80	13.55	154.8	3.44
					1.70	12.75	161.2	3.48
					1.85	13.81	166.9	3.52
4-4	35.3	1.60	0.14	4.38	0.60	4.20	2.6	0.84

Exp. No.	ϵ 10^{-5} cm^{-1}	α_o^3 10^3 cm^{-2}	$F_m^{\frac{1}{2}}$ cm	x_c cm	δ cm	$\delta/F_m^{\frac{1}{2}}$	x cm	$(x/x_c)^{1/3}$
					0.63	4.60	3.2	0.91
					0.77	5.55	6.9	1.16
					0.90	6.45	12.0	1.40
					0.93	6.72	18.0	1.60
					1.30	9.30	43.5	2.15
					1.28	9.17	48.3	2.22
					1.43	10.20	53.9	2.31
					1.65	11.80	107.7	2.90
					1.65	11.80	116.4	2.98
					1.70	12.21	117.2	2.99
					1.70	12.21	126.5	3.06
					1.75	12.52	131.4	3.10
					1.75	12.52	136.2	3.14
					1.75	12.52	141.2	3.18
					1.80	12.91	146.5	3.22
					1.80	12.91	156.0	3.29

Exp. No.	ϵ 10^{-5} cm^{-1}	α_o^3 10^3 cm^{-2}	$F_m^{\frac{1}{2}}$ cm	x_c cm	δ cm	$\delta/F_m^{\frac{1}{2}}$	x cm	$(x/x_c)^{1/3}$
4-5	35.3	1.60	0.15	5.85	0.68	4.60	1.8	0.68
					0.70	4.70	2.8	0.78
					0.80	5.30	3.4	0.83
					0.85	5.70	7.0	1.06
					0.95	6.35	10.8	1.22
					1.05	7.00	17.2	1.43
					1.10	7.38	21.6	1.54
					1.15	7.70	32.3	1.77
					1.20	8.04	39.4	1.89
					1.25	8.36	47.1	2.00
					1.35	9.00	51.4	2.05
					1.60	10.71	108.1	2.64
					1.60	10.71	114.0	2.69
					1.65	11.00	128.9	2.80
					1.75	11.72	133.0	2.84
					1.75	11.72	145.0	2.92

Exp. No.	ϵ 10^{-5} cm^{-1}	α_o^3 10^3 cm^{-2}	$F_m^{\frac{1}{2}}$ cm	x_c cm	δ cm	$\delta/F_m^{\frac{1}{2}}$	x cm	$(x/x_c)^{1/3}$
					1.65	11.00	148.9	2.94
					1.70	11.40	155.1	2.98
					1.80	12.00	159.1	3.00
4-6	35.3	1.57	0.18	9.90	0.60	3.30	1.6	0.55
					0.78	4.20	4.8	0.78
					0.92	5.00	8.4	0.95
					1.00	5.40	14.1	1.13
					1.10	6.00	20.8	1.28
					1.22	6.60	29.8	1.44
					1.35	7.30	41.6	1.61
					1.40	7.60	49.6	1.71
					1.42	7.70	57.4	1.80
					1.88	10.21	111.1	2.24
					1.88	10.21	116.2	2.27
					2.00	10.81	121.4	2.31
					1.95	10.62	127.2	2.34

Exp. No.	ϵ 10^{-5} cm^{-1}	α_o^3 10^3 cm^{-2}	$F_m^{\frac{1}{2}}$ cm	x_c cm	δ cm	$\delta/F_m^{\frac{1}{2}}$	x cm	$(x/x_c)^{1/3}$
					1.98	10.71	136.0	2.39
					2.00	10.83	142.3	2.43
					2.02	10.90	148.6	2.46
					2.05	11.10	161.8	2.54
					2.05	11.10	164.8	2.56
4-7	35.3	1.57	0.20	13.40	0.60	2.94	1.8	0.51
					0.78	3.83	4.4	0.69
					0.87	4.27	7.0	0.81
					0.90	4.41	9.4	0.89
					1.25	6.14	15.6	1.05
					1.20	5.89	20.3	1.15
					1.30	6.38	26.8	1.26
					1.38	6.77	33.4	1.35
					1.42	6.97	40.9	1.45
					1.40	6.90	46.0	1.51
					1.50	7.35	51.6	1.57

Exp. No.	ϵ 10^{-5} cm^{-1}	α_o^3 10^3 cm^{-2}	$F_m^{\frac{1}{2}}$ cm	xc cm	δ cm	$\delta/F_m^{\frac{1}{2}}$	x cm	$(x/x_c)^{1/3}$
					1.50	7.35	57.0	1.62
4-8	35.3	1.57	0.27	32.20	0.70	2.56	2.3	0.41
					1.10	4.02	8.8	0.65
					1.15	4.20	14.3	0.76
					1.20	4.38	16.6	0.80
					1.30	4.75	25.0	0.92
					1.38	5.04	31.0	0.99
					1.40	5.10	36.3	1.04
					1.45	5.28	45.4	1.12
					1.70	6.20	58.3	1.22
					1.85	6.75	106.8	1.50
					1.85	6.75	112.7	1.52
					1.90	6.84	119.5	1.55
					1.95	7.12	127.4	1.58
					1.95	7.12	130.9	1.59
					2.00	7.30	136.7	1.62

Exp. No.	ϵ 10^{-5} cm^{-1}	α_o^3 10^3 cm^{-2}	$F_m^{\frac{1}{2}}$ cm	x_c cm	δ cm	$\delta/F_m^{\frac{1}{2}}$	x cm	$(x/x_c)^{1/3}$
					2.05	7.50	144.8	1.65
					2.05	7.50	150.7	1.67
					2.05	7.50	157.3	1.70
					2.35	8.57	166.8	1.73